A DYNAMIC PHANTOM MODEL

FOR 2450 MHZ MICROWAVE HYPERTHERMIA

A Thesis Report

by

Antonia G. Tsoukatos

Submitted to the Faculty of
Graduate Studies of
The University of Manitoba
in partial fulfillment of the
requirements for the degree
of Master of Science.

 August, 1986

Winnipeg, Manitoba

ISBN 0-315-37166-8

A DYNAMIC PHANTOM MODEL FOR 2450 MHZ MICROWAVE HYPERTHERMIA

BY

ANTONIA G. TSOUKATOS

A thesis submitted to the Faculty of Graduate Studies of
the University of Manitoba in partial fulfillment of the requirements
of the degree of

MASTER OF SCIENCE

TABLE OF CONTENTS

ACKNOWLEDGEMENTS

I would like to thank my supervisor, Dr. P. B. Dunscombe, for introducing me to this project and also for his continuous support and encouragement while I was working on this project.

I would also like to thank Dr. G. Froese for providing some of the equipment that was required for this work. Special thanks are also due to Mr. J. McLellan for his Hyperthermia Computer Programs and Mr. T. Constable for the fruitful discussions on our projects.

The assistance of both the Machine and Electronics shops staff is also gratefully acknowledged.

Finally, I would like to thank my husband for his support and help during the course of this work.

ABSTRACT

The successful clinical application of microwave hyperthermia requires accurate knowledge of the temperature fields throughout the heated volume. However, this is one of the major problems in clinical hyperthermia due to the fact that hyperthermia thermometry is invasive and thus the number of sites at which temperature can be measured is limited. One way to make progress in this area is through the development of physical models that can be used to quantify the effects of heat treatments using clinical applicators.

The theoretical basis, the practical design, the testing and assessment of a dynamic (perfused) phantom intended for the study of 2450 MHz microwave hyperthermia of muscle tissues are discussed in the course of this report. The study on the prediction of blood flow rates from thermal clearance measurements is also discussed, with reference to relatively low temperature gradients at the measurement sites.

1.1 CANCER TREATMENT

1.1.1 CONVENTIONAL METHODS FOR CANCER THERAPY

Over the years, there has been extensive effort invested in the study of cancer and the possible treatment modalities. The results of these studies are currently presented in the form of established treatment methods that are routinely used in various treatment centers.

Presently, the conventional methods used for cancer treatment are extending over the three following areas: Surgery, Radiotherapy, and Chemotherapy.

Surgery is a very drastic means of eliminating the malignant growth, that is possible only if the tumor can be removed without damaging vital organs and which can be very traumatic to the patient if it involves the removal of a body part, i.e. breasts, limbs, etc. Furthermore, it is only the primary or localized cancer growth and the surrounding tissue that can be removed, which means that there is an uncertainty as to whether the whole volume of the malignant mass is removed. Radiotherapy is a very effective modality, whether it is used alone or in combination with the other two modalities to locally treat cancer. However, the presence of hypoxic (non-oxygenated) cells in the tumor volume reduces the effectiveness of the ionizing radiations used, since hypoxic cells are resistant to these irradiations.[21,22]

The use of drugs for the treatment of systemic cancer (chemotherapy) can effectively eliminate carcinomas, but, the drug toxicity might be harmful to the normal tissue also.[1]

It can be seen therefore, that conventional cancer treatments however effective in their present form, need further refinement and/or new treatment methods to be developed in order to achieve the desirable recurrence free method for treating the patients. This is the reason that reinforces the continuous research on the subject, aiming for more effective and less traumatic (physically and psychologically) treatments that are to be used alone or in combination with the conventional modalities.

1.2 HYPERTHERMIA

1.2.1 AN OVERVIEW OF THE SUBJECT

The elevation of the temperature of biological materials above their normal temperatures (i.e. normal human: T ~ 37°C) can alter their function at the cellular level and sometimes it can even cause cell killing. This method of increasing body temperatures is called hyperthermia. The applications of various hyperthermia techniques for the treatment of cancer can be traced as far back as the late 1800s.[2,3,4] During the 1930s hyperthermia use declined due to the flourishing of radiotherapy. The interest in hyperthermia was revived after the 1960s because of its promising results as an adjuvant therapy to radiotherapy or chemotherapy. The use of hyperthermia in the treatment of cancer is based on its substantial biological and physiological effects which will be discussed in the following section.

Clinical applications of hyperthermia are divided into three categories: The whole body systemic hyperthermia, the regional

hyperthermia and the local hyperthermia. Whole body systemic hyperthermia is relatively simple regarding its thermometry control. The heating techniques involve heating by immersion of the whole body in a wax bath (Pettigrew technique)[5] or heating in a suit, similar to those used by the astronauts in space.[6]

In regional hyperthermia, it is usually the part of the body that contains the tumor mass (eg. limb) that is heated. A more complicated means of heating is in the form of local hyperthermia (i.e. heating of tumor plus a minimal amount of normal tissue), which is considered in the present work. There exists an appreciable amount of difficulty in its applications, due to the fact that the techniques used for heating the malignant masses are not adequately established in terms of accuracy and precision in the administered dose and the methods of temperature recording.

Local hyperthermia is induced through several different methods which include: 1) hot water baths; 2) shortwave diathermy; 3) RF-induced currents; 4) microwaves; and 5) ultrasound.

In our laboratory local hyperthermia is induced using a 2450 MHZ power generator with a TAG-MED TCA 2450-1 circularly polarized applicator[7], and which is further discussed in Appendix A. At present, the problems associated with local hyperthermia are the production of localized deep heating without excessive heating on the surface and surrounding normal tissue and the temperature monitoring that ideally needs to be noninvasive. To date, it is only the applications of hyperthermia for the treatment of superficial tumors that are quite satisfactory regarding the systems available. It is the treatment of the deep seated tumors that is difficult to perform because of the unavailability of appropriate systems for this purpose.

1.2.2 BIOLOGICAL AND PHYSIOLOGICAL MECHANISMS OF HYPERTHERMIA.

The biomolecular mechanisms which activate cell killing during hyperthermia cannot be attributed to a specific and unanimously accepted theory. This is due to the lack of sufficient information regarding the site of attack in the cell.

Of all the existing theories on the subject, there are three theories that seem to be plausible and have some experimental evidence to their support.

One of the theories considers the mechanism that involves protein thermal damage and eventually cell death. It has been reported that following a heat treatment there is an increase of non-histone proteins which results in a large increase in the protein to DNA ratio.[14,1,3] However, this phenomenon has relatively limited relation to cell death. It is rather connected to the prevention of cell repair from radiation damage as will be discussed in a later section. Furthermore, more protein functions have been reported to be impaired or destroyed, such as the DNA synthesis,[8,9] the RNA synthesis,[10] the protein synthesis,[11] and respiration.[12,13] Another theory on the thermal cell inactivation considers the heat effects on the cell membrane. Hyperthermia affects the cell membrane by altering its composition and permeability and eventually causing the cell to die.[14,15,1] Finally, another process of cell killing considers the heat inactivation of cells through disintegration of the lysosome vesicles in the cytoplasm. The damage is thus caused by the released digestive enzymes which can promote cell death.[16] Cell sensitivity to heat is first specifically observed at temperatures between 42° C and

43° C and depending on the cell line the response range can extend up to 46° C. This can be observed in an Arrhenius plot of the Log of 1/Do as a function of the inverse temperature; where Do is the time required to reduce the fraction of surviving cells to 37% of their previous value, when exposed to a given temperature. An Arrhenius plot is presented in Figure 1.1 for heat inactivation of mammalian cells in culture.[9] The time-temperature relationship indicated from the Arrhenius plot is not necessarily applicable to all cell lines tested. This is due to the fact that different cell lines have different responses to the same heat exposure, which means that their heat sensitivities are different.[17]

Furthermore, malignant cells may be intrinsically more sensitive to heat exposure than normal cells.[2] This differentiated response of neoplastic cells and normal cells may be attributed to the following facts: a) oxygenation, b) nutrition and c) pH level.

All of the above factors emerge from the differential blood flow in the two types of tissues. In neoplastic tissues blood flow is sometimes impaired thus resulting in a slower flow rate and/or occlusion.[4,18] This impaired blood flow is further deteriorated when exposed to hyperthermia and in this manner the differentiation is more prominent between normal and tumor tissues.[18,19,20]

Most tumor cells exist in an acidic environment, under low oxygen tension conditions and are nutritionally deprived due to inefficient blood flow in the tumor. It has been indicated that poorly oxygenated (hypoxic) cells are very succeptible to heat induced death.[21,22] It has also been shown that poor nutrition increases anaerobic glycolysis, thus enhancing the production of lactic acid and causing

Figure 1.1: An Arrhenius plot for heat inactivation of mammalian cells in culture (Reproduced from Ref. 9)

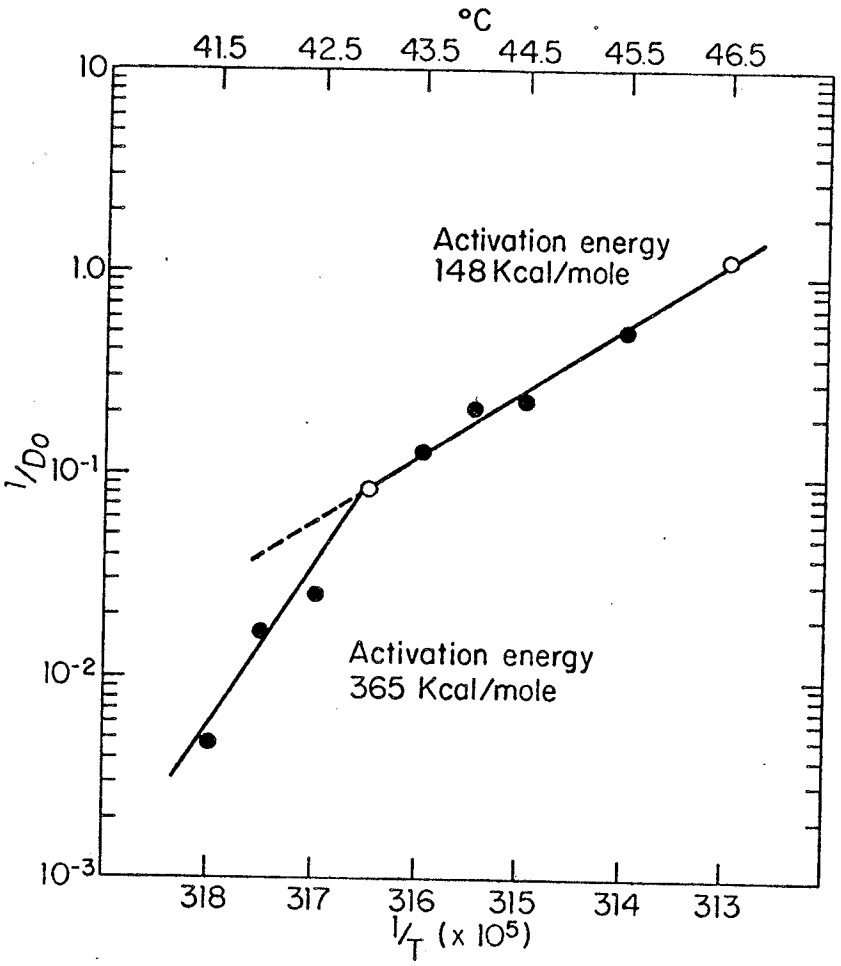
°C
41.5
42.5
43.5
44.5
45.5
46.5
10
1.0
10-1
10-2
10-3
1/D0
Activation energy
148 Kcal/mole
Activation energy
365 Kcal/mole
318
317
316
315
314
313
1/T (x 10^5)

the tumor pH to decrease. Under these conditions heat is very effective in eliminating tumor cells.[23,24,25,26,27] Hyperthermia applications have also been proven very effective for killing cells found in the S-phase of their mitotic cycle.[1,2,3,14]

It was mentioned above that tumor blood flow is a vital factor for its sensitization to hyperthermia. Tumor vasculature however, is not always the same and varies with tumor size, type and site of growth.[4,18] Initially, tumor cells survive using the nutrition supplied by the host vessels. As the tumor grows larger the nutrient demand increases and hence the beginning of neovascularization. That is the development of a new capillary network in the tumor due to induced proliferation of the endothelial cells of host vessels and/or the increase in length and caliber of host vessels. The tumor response to heat is dependent on the type of vasculature that is incorporated in a tumor, because newly formed capillaries respond differently to stress of either physical or chemical origin.[28] That is they are very weak vessels compared to the host vessels. As the tumor size increases, its vasculature collapses and blood flow is very slow and sometimes it is halted temporarily or permanently. This fact renders larger tumors more succeptible to heat exposure due to the slower heat dissipation. The repair from thermal damage is relatively complicated because of the phenomenon occurring right after the first administration of hyperthermia. This phenomenon is referred to as thermotolerance and it may be defined as the decrease in cellular sensitivity to a following heat exposure produced by the initial hyperthermia application and not any kind of genetically induced resistance to heat.[1] The degree of thermal tolerance depends on the

magnitude of the first exposure with respect to temperature and the treatment duration.[29,30] Thermotolerance is not permanent, it lasts for 36 to 72 hours after the cells are returned to 37° C. It has been reported that the rate of decay of thermotolerance depends on the proliferating rate of tissues. That is rapidly proliferating tissues have a short decay from thermotolerance while the slowly proliferating have longer decay times.[32] In general, the mechanism of thermotolerance is not known, but what is known is the fact that it cannot develop unless protein or RNA synthesis occur.[33,34,35] It has also been suggested that the change in slope in the Arrhenius plot is due to thermotolerance.[35,36]

There seem to be a lot of questions to be answered regarding the biological and physiological effects of heat; and great care to be taken when applying in vitro observations to in vivo human responses. Nonetheless, heat exposure is definitely effective in eliminating tumor cells, whether this is in vitro or in vivo, when it is used alone or in combination with other conventional therapies as will be discussed next.

1.2.3 HYPERTHERMIA IN THE TREATMENT OF CANCER

Hyperthermia has been used clinically for the treatment of cancer and its applications have been quite successful in controlling tumors, whether it is applied alone or in combination with other modalities. Heat and radiation are going to be discussed first, in terms of their biological correlation.

It has been observed that heat sensitizes cells to radiation.[9,37]

The fact that heat is extremely effective in radiosensitizing cells in the S-phase of their cycle, which in turn are resistant to radiation alone, is made evident in Figure 1.2. The survival curves of Figure 1.2 indicate the differential response to heat and radiation at the different stages of the cell cycle.[38]

This radiosensitization of the cells is possibly caused by the accumulation of non-histone proteins which bind to the DNA after heat exposure, and prevent the cells from repairing the radiation damage.[14]

As described previously, heat is effectively killing hypoxic, low pH and nutritionally deprived cells. However, when heat is combined with X-irradiation in vitro or in vivo the Oxygen Enhancement Ratio (OER), a specific characteristic of sparsely ionizing radiations, is said to be reduced. This has been reported by several investigators.[1,39] However, there are other conflicting reports that indicate that the decrease in OER is not very significant when the combination takes place in vivo.[40] In addition, these same reports indicate that the response of the tissue (in vivo) is the same regardless of its oxygenation status as long as the treatment temperature is in the high range (i.e. 44.5° C). Furthermore, because the recovery from thermal damage decreases in a nutritionally deprived and low pH environment, there will be more apparent radiosensitization due to heat in an acidic pH than in an alkaline pH.[41]

It has been shown that heat prevents the repair of Potentially Lethal Damage (PLD) from X rays. Since the repair of PLD has been observed in normal tissues exposed to radiation and it presumably does not happen in tumors, it can be expected that heat selectively potentiates tumor radiosensitization more than it does normal tissue

Figure 1.2: The comparison of the fraction of cells that survive heat, + X-rays which are delivered at different phases of the cell cycle. (Reproduced from Ref. 38)

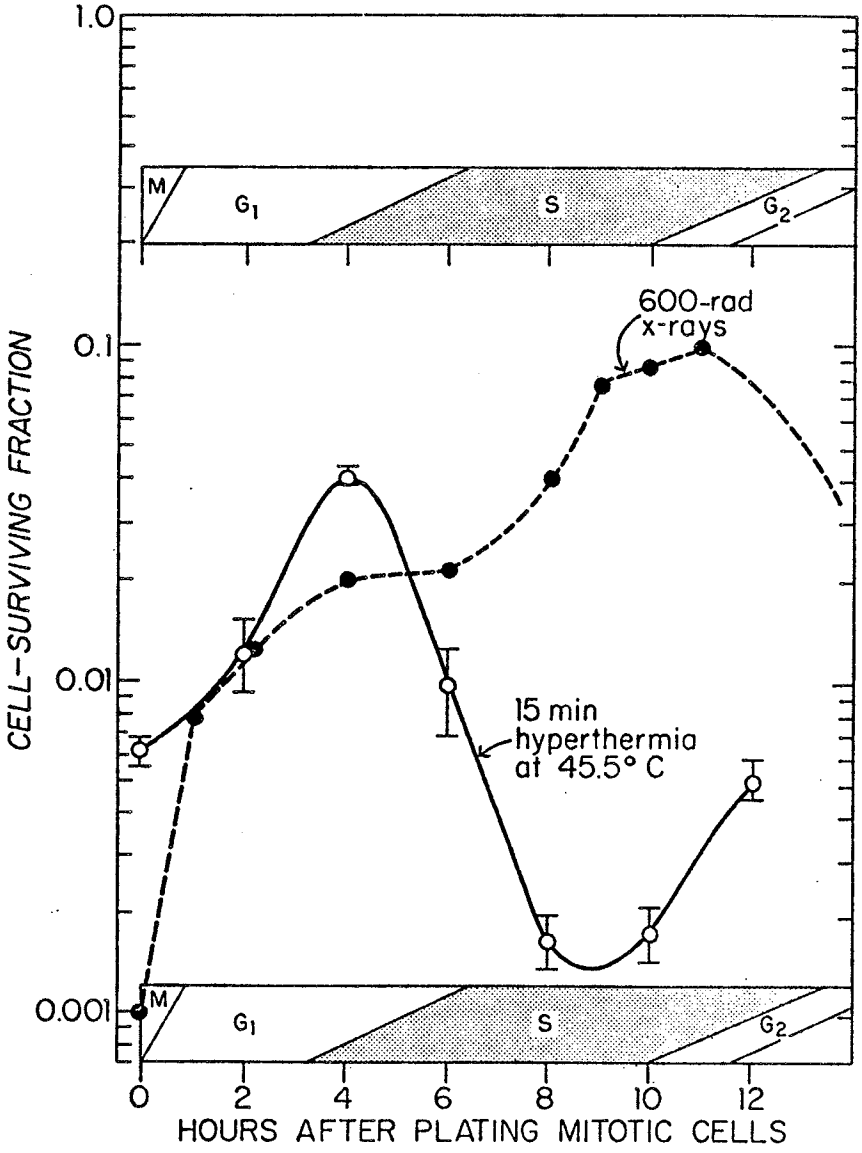
1.0
0.1
0.01
0.001
CELL-SURVIVING FRACTION
M
G1
S
G2
600-rad
x-rays
15 min
hyperthermia
at 45.5° C
0
2
4
6
8
10
12
HOURS AFTER PLATING MITOTIC CELLS

radiosensitization.[1]

The effects of thermal exposure to irradiation response are assessed by the Thermal Enhancement Ratio (TER) which is defined as the ratio of the X ray dose necessary to produce a given level of biological damage without and with the thermal exposure. Successful combination of the two modalities requires a well adjusted sequencing of the two types of treatment, in order to take advantage of their relative effects.[42]

It has been observed that the thermal sensitization of mouse tumors is not greater than that of the respective normal tissue when the heat is administered shortly before or after irradiation.[43] The same study also indicates that it is of therapeutic advantage relative to the skin damage if the heat and the X rays are separated by more than one hour. In vitro studies however, indicate that there is greater cell killing when both radiation and heat are administered together rather than when heat precedes or follows radiation by more than 30 minutes.[44,36,9,42] In vivo applications of fractionated hyperthermia and radiation have been proved superior to single dose applications in developing differential responses in tumor and normal tissues.[45] The sequencing of the two modalities is of vital importance in the resulting response. Clinical trials with cancer patients treated with combined heat and radiation show the response to be as high as 85% when the heat was applied immediately after (<20 minutes) the second daily fraction of irradiation.[46,47] The heating temperatures were set in the range of 42 to 42.5° C which suggests that there may be an optimum temperature for the combined therapy. It is therefore very important to collect this information and

constructively use it for clinical treatments of cancer patients realizing however, that the results collected from in vitro and in vivo studies do not always apply quantitatively to clinical applications.

In the second part of this section the effects of heat and chemotherapy are going to be discussed in relation to cancer therapy. A number of in vitro and clinical studies have shown that the cytotoxic efficiency of certain drugs increases at hyperthermic temperatures.[48]

In vitro experiments have indicated the synergistic effect of hyperthermia when combined with drugs (i.e. bleomycin, adriamycin).[47] The fact that drugs get into the cell more easily at temperatures of around 43° C, can be explained by the changes in the properties of the cell membrane permeability at these temperatures. The use of thermo-chemotherapy is very promising for the treatment of solid tumors, which because of the lack of adequate blood flow, are difficult to be treated. However, the same problem is encountered with thermo-chemotherapy as with heat combined with irradiation. That is, the drugs can be sometimes as toxic for the normal tissues as for the tumors.[1]

Chemotherapy with localized hyperthermia seems to be a combination with good prospects. However, it requires the development of a heating system that would accurately heat the tumor area and more importantly, a thermometry system that would provide accurate thermal mapping of the heated volume. Moreover, thermo-chemotherapy can become a more realistic goal for the treatment of a wide spectrum of tumors.[1]

1.3 HYPERTHERMIA DOSIMETRY

1.3.1 THERMOMETRY SYSTEMS AND TECHNIQUES

Successful hyperthermia applications necessitate the use of an appropriate thermometry system. The ideal thermometry system for hyperthermia would be one that is completely non-invasive, and that provides temperature and spatial resolutions to 0.1° C or better and of 1 cm or less respectively.[49] However, the presently available thermometry systems do not measure up to these standards, because they are completely invasive and their performance is dependent on the heat generating technique. There are several types of thermometers used for hyperthermia temperature measurements but the most commonly used are the miniature thermistors and thermocouple probes. The advantage that thermocouples have over the thermistors is that thermocouples can have multiple sensors per probe as opposed to the latter which have only one sensor per probe. This is also the reason that thermocouples are found to be used in most hyperthermia applications, along with some other factors that are going to be discussed further in a later section (Chapter 3: Section 3.5)

There are three major sources that can cause errors in the temperature recording with the conventional systems (i.e. thermocouples).[50,51,3] Firstly, when the metallic leads are used in the vicinity of the EM field there are possible interference effects if they are not properly aligned with the field. Secondly, self-heating of the thermocouple can cause an over-estimation of the recorded temperature. Finally, there might be selective heating of the tissue surrounding the thermometer due to the field perturbation

by the sensor probe, thus resulting in a non-uniform temperature distribution inside the tumor volume. The problems associated with the perturbation of the field can be avoided if non-perturbing probes are employed. These probes facilitate small optical fibers to transmit and receive light signals from crystal temperature sensors.[3] However, there is a major problem in their stability which renders them inferior to thermocouples, in addition to the very high prices that they are marketed for.[3]

1.3.2 THE THERMAL DOSE CONCEPT

The extended use of clinical hyperthermia for the treatment of human cancer has necessitated the development of a unique protocol that would be used for all hyperthermia applications and thus enable us to compare short and long term trials. It seems necessary to define a standard unit for measuring Thermal Dose, which to the present day has not been uniquely defined because of the fact that the biophysical dose response relationship is complicated and not well understood. Although there is not a formal definition of thermal dose one could consider the following explanation. There is an adequate level of temperature that must be delivered for an appropriate time period to the whole tumor tissue in order to obtain optimal therapeutic effects. The thermal dose time-temperature calculation should include considerations on the effect of the development of thermal tolerance as well as the changes induced in the tumor cellular environment. There have been several reports that attempt to express thermal dose units such as degree-minutes, or equivalent minutes at a

given temperature or even dimensionless units.[53,54,55] These attempts are constructive steps toward standardizing hyperthermia treatments and the measurement of their effects. Several models have been presented at times for the calculation of thermal dose and which are based on a thermodynamic or Arrhenius-type relationship that are empirically determined.[52,56,57] The thermal dose is considered as one of the most important factors that influence hyperthermia efficacy. Before any thermal dose calculation can be used clinically there are certain factors that should be considered, such as, better thermal mapping and understanding of thermal history and interaction of heat and radiation. It is also required to determine the physical and thermodynamic characteristics as well as the cell kinetics factors that control the response of tumor and normal tissue to heat alone or heat and radiation. It has been stated[25,27] as the goal of hyperthermia and any cancer therapy the maximum destruction of tumor tissue with minimal or acceptable normal tissue destruction and this is to be used as the base line when defining thermal dose and establishing hyperthermia protocols.

1.4 HYPERTHERMIA LABORATORY STUDIES-PURPOSE OF THIS PROJECT

Successful clinical hyperthermia requires exhaustive laboratory research with in vitro and/or in vivo experiments. Most of the in vitro experiments are performed with various cell lines originating from tumor or normal tissues from animals and humans, and the use of phantoms which are tissue simulating systems. In vivo studies are mostly performed using live animals.

There are two types of phantoms that are used for hyperthermia studies; the static (unperfused) and the dynamic (perfused) phantoms.

In this project experiments were performed using both types of phantoms. The work performed with the static phantom is included in Appendix A and it was based on the static phantom developed by Guy et. al.[85]

The major task of this project was to design, construct, test, and use experimentally, a dynamic phantom equivalent to human muscle. This dynamic phantom would have to simulate muscle in terms of its dielectric properties and in a relatively simple form its blood flow. A preliminary study of the literature was performed regarding the properties of muscle tissue in terms of dielectric and thermal behavior and of blood flow, and which is accounted for in chapter two. Next, the design of the dynamic phantom in terms of its theoretical modeling, practical design and specifications are detailed in chapter three. In chapter four the testing of the phantom is reported and analyzed. Following a study was performed using the dynamic phantom that dealt with the effects of blood flow on the temperature distributions and the probability of predicting the blood flow rate from the temperature decay with time after the steady state was reached. This work is presented in Chapter five. Finally, Chapter six concludes the work performed for this project and discusses the results achieved through this work.

2.1 MICROWAVE HYPERTHERMIA

2.1.1 INTRODUCTION TO MICROWAVE HYPERTHERMIA

Use of electromagnetic waves to induce non-invasive hyperthermia for cancer therapy has been of considerable interest for many decades. The idea of applying microwaves for therapeutic hyperthermia induction was initially presented in Germany in 1938 and 1939 by Holmann when he discussed the possibility of applying radio-waves of 25 cm wavelength and predicted that these waves could be focused to produce heating of the deep tissues without extensive heating of the skin. Similar ideas were also developed in the United States by Hemingway and Stenstrom, however, the lack of appropriate equipment at the time prevented their clinical application.[59] It was not until the 1950s and after when research on the use of microwaves for clinical hyperthermia expanded significantly and major findings were reported in literature.[59,50]

The definition of the microwave portion of the electromagnetic spectrum is usually arbitrary.[60] Several groups and scientific authorities choose to define microwaves as a particular region of the electromagnetic spectrum. The scientific committee 53 of the National Council on Radiation Protection and Measurements (NCRP, 1981) states the following on the account of microwaves: "For the purposes of this report, radio frequency radiation refers primarily to EM radiation in the frequency range of 300 KHZ to 300 GHZ. Such a range includes microwave radiation, i.e., the frequency range from approximately 300 MHZ to 300 GHZ." On the other hand the International Telecommunications Union (RCA, 1969) in 1959 designated the "radio" spectrum as extending from 3 KHZ to 3000 GHZ with no use made of the

term microwaves. For the purposes of this work the region of the EM spectrum between 10 MHZ and 10,000 MHZ is under consideration and the particular frequency that has been concentrated upon is that of 2450 MHZ and the frequencies in its immediate neighborhood.[60]

In North America,[63] the present form of microwave hyperthermia is operated at the authorized frequencies of 13.65 MHZ, 27.12 MHZ, 915 MHZ and 2450 MHZ. Microwave energy is currently generated by either a variety of microwave tubes or solid state devices, or by power oscillators or a low-power oscillator followed by a chain of amplifiers. The use of microwave hyperthermia is founded[58] on the fact that electromagnetic waves are transformed into heat when they are absorbed by a biological tissue. The patterns of microwave energy deposition in biological materials are much dependent on the size, the shape and the electrical characteristics of the tissue. Furthermore, this dependence extends to the frequency of the applied fields and the size and geometry of the electromagnetic wave applicator. For the above reasons, when microwave hyperthermia is employed for cancer therapy, the location, size and shape of the tumor are very important considerations in the selection of a proper source of EM radiation. Microwave radiation can be applied more conveniently than the other forms of clinical diathermy. Since the applicators are not in contact with the treated area there is no need of protective toweling. Also, by eliminating the use of pads or any kind of electrodes the danger of arc occurrence is nonexistent. An added benefit is the comfort provided to the patient, who by not being a part of the circuit is not attached to the equipment.[64]

2.1.2 THE INTERACTIONS OF MICROWAVES WITH BIOLOGICAL TISSUES: THEORY

Biological tissues are made of cells which contain various positively or negatively charged ions, polar protein molecules and polar water molecules. Electromagnetic waves consist of moving patterns of alternating electric and magnetic fields and they also exhibit general radiant characteristics which are more familiar in the description of optical or infrared radiation. When an electromagnetic field acts upon a biological material,[58,61,62] it exerts forces on its charged constituents and causes them to either be displaced or rearranged in order to modify the acting field. These interactions of the EM waves with biological tissue differ from those with free space or other solids because of the different dielectric and magnetic properties that each of the materials possesses. It should be noted that generally, in the interactions of microwaves with tissues, it is only the internal electric field which is of significance, since biological tissues are non-magnetic materials.

There are three basic types of effects that are involved in the interaction of EM waves with tissues:

a. The displacement or drift of the conduction charges, i.e. electrons and ions, in the tissue medium due to the force exerted by the electric field (E).
b. Polarization of atoms and molecules that results in the production of dipole moments.
c. The rotation of the existing dipole molecules in the direction of the applied electric field.

The displacement of the conduction charges in tissues results in

the development of conduction currents inside the material. Also, the result of the polarization effects will be in the form of an extra local polarization charge inside the tissue and polarization currents resulting from the displacement of the charges in a time varying field.

Due to the effects mentioned above conduction and dielectric losses arise, which result in energy removal from the microwave field that is eventually converted to kinetic energy for the tissue molecules causing the temperature of the biological material to increase.[61]

All the mechanisms discussed above in relation to the interaction of microwaves with biological tissues can be described by the following properties of the tissue:

1. The dielectric permittivity, i.e. $Re(\varepsilon) = \varepsilon'\varepsilon_o$; where ε' = dielectric constant, $\varepsilon_o = 8.854 \times 10^{-12}$ As/Vm
2. Electric conductivity, i.e. $\sigma = \varepsilon_o\varepsilon''\omega$; where ε'' = loss factor of biological medium; ω = angular frequency = $2\pi f$ (f = operational frequency)
3. Magnetic permeability, i.e. $\mu = \mu'\mu_o$; where $\mu' = 1$ for tissue, $\mu_o = 4 * \pi * 10^{-7}$ Vs/Am

The dielectric constant and electric conductivity values will be discussed further in the following sections.

The theoretical description of the EM wave interactions with tissues is presented by the appropriately modified Maxwell's equations, that is the polarization effects present in the biological tissue interacting with microwaves are accounted for along with the conduction effects. In the course of this work we will only consider

time harmonic radiation fields for which the wave equation is of the following form.

$$\bar{\nabla}^2\bar{E} + \gamma^2 \bar{E} = 0 \qquad (2.1)$$

where γ = propagation ct. of the wave in the tissue medium.

Furthermore, this work will concentrate on plane wave propagation in plane tissue layers. The propagation constant γ for energy transmission through biological materials can be expressed as follows:

$$\gamma = \gamma_o \, (\varepsilon^*/\varepsilon_o)^{1/2} = \beta - i\alpha = (2\pi/\lambda) - id^{-1} \qquad (2.2)$$

where γ_o = propagation constant of free space = $2\pi f/c_o$;

$c_o = 3 * 10^{+8}$ m/sec

$\varepsilon^*/\varepsilon_o$ = complex conjugate of permittivity of the tissue = $\varepsilon' - i\varepsilon''$

α = attenuation coefficient = [1/depth of penetration]=[1/d]

β = phase constant of the plane wave = $2\pi/\lambda$

The attenuation coefficient α, is a measure of the exponential decay of the field strength since it is equivalent to the inverse of the depth of penetration or skin depth d, which in turn is the distance at which the power density has decreased to $1/e^2$ of its value at the reference depth. The phase constant β is the equivalent of $2\pi/\lambda$, where λ is the wavelength and β is used to calculate λ as will be shown in a later section.

Besides the power transmission that occurs during the propagation of microwaves through plane layers of tissue, there is reflection of energy that takes place between the different tissue interfaces. The complex reflection coefficient R of a wave that is propagated from one tissue of intrinsic impedance $\bar{Z}_1$ to another tissue of intrinsic

impedance $\bar{Z}_2$ at right angles of incidence, can be expressed by the following formula:

$$R = \frac{\bar{Z}_2 - \bar{Z}_1}{\bar{Z}_2 + \bar{Z}_1} = \frac{\sqrt{\bar{\varepsilon}_1^*} - \sqrt{\bar{\varepsilon}_2^*}}{\sqrt{\bar{\varepsilon}_1^*} + \sqrt{\bar{\varepsilon}_2^*}} = re^{i\phi} \qquad (2.3)$$

where $\bar{Z}_n = Zo/\sqrt{\bar{\varepsilon}_n^*}$, r = magnitude of R, and ϕ = phase angle of R, ε_n = dielectric constant.

The reason for the reflection of the propagated wave is that, in each layer of tissue that it is transmitted through, it establishes different propagation characteristics regarding the wave impedance and the propagation constant. The magnitude of the reflected wave depends on the difference in the dielectric behavior between the various layers, the frequency of the wave, its polarization and the angle of incidence.

The calculation of the power absorbed in tissue from a propagating EM field can be performed at any point in the medium of propagation at which the field is known. The average power conveyed per square meter of area of wavefront in a conductive medium by an EM wave is given by the Poynting vector $\bar{N}$:

$$\bar{N} = \bar{E} \times \bar{H} \ (W/m^2) \qquad (2.4)$$

where $\bar{E}$ = electric field vector

$\bar{H}$ = magnetic field vector

The power absorbed by the tissue is derived by Maxwell's equations and Poynting vector as follows: $P = 1/2\sigma|\bar{E}|^2 \ (W/m^3)$ For plane wave propagation in plane layers of tissue the above expression for absorbed power is:

$$P = (1/2)\ \sigma E_0^2[e^{-2\alpha x} + r^2 e^{2\alpha x} + 2r\cos(2\beta x + \phi)] \qquad (2.6)$$

where E_o = the maximum value of the electric field strength (V/m).

r, ϕ = reflection coefficient's magnitude and phase constants.

α = attenuation coefficient (m^{-1}).

β = phase constant of the propagation (radians/m).

x = depth inside the conducting medium (m).

σ = electric conductivity (mho/m).

For dosimetry purposes the National Council of Radiation Protection and Measurements (NCRP, 67, 1981) recommends the use of the Specific Absorption Rate value (SAR) given in Watts/kg in order to quantify the rate of energy absorbed per unit mass in tissues exposed to EM fields:

$$SAR = \frac{d}{dt}\left(\frac{dE}{dm}\right) = \frac{10^{-3}}{\rho} P = c\frac{dT}{dt} \text{ (W/kg)}. \qquad (2.7)$$

where dE = increment of absorbed energy in the mass element dm during time dt.

ρ = density of the tissue (kg/m^3).

c = specific heat of tissue (J/kgk)

dT = increment of temperature in the heated tissue (°C).

2.1.3. THEORETICAL CALCULATIONS OF THE WAVE PARAMETERS; ABSORBED POWER; SAR

In the previous sections the interaction of microwaves with tissues was discussed and the wave parameters involved were presented in terms of the dielectric properties of tissues. Also, the expressions for absorbed power and SAR values resulting from a plane wave propagation were presented. The calculation of these values

requires the knowledge of the dielectric properties of tissues at the various microwave frequencies.

Several investigators have reported their measurements of the dielectric constant (ε'), the relative loss factor (ε'') and the electrical conductivity (σ) and these values have been collected and tabulated in this report in order to be used for the calculations mentioned above. The values were obtained from reports by Schwan et.al.,[64,50] Guy et.al.[61,63] and finally from the survey report by Stuchly and Stuchly[65] which is a summary of the dielectric properties of tissues accumulated through many years of research. More recent reports on the dielectric properties of tissues were also considered such as those by Smith and Foster (1985) and Shepps and Foster (1980).[66,67,68,69] The dielectric properties of human muscle and fatty tissue are plotted for the frequency range of 50 MHZ to 3000 MHZ as they were obtained from the literature (Figure 2.1). The wave parameters were calculated using the values from Figure 2.1 on a microcomputer (see Appendix B for the programs used), as well as the values of absorbed power and SAR.

Some of the values obtained for the wave parameters are shown on Figure 2.2 which shows the depth of penetration as a function of frequency for fatty and muscle tissue, and the range of the values at each frequency is indicated. The magnitude of the reflection coefficient was calculated and is also plotted as a function of frequency, in the following form: r^2 vs. f(MHZ) (Figure 2.3), where r^2 represents the fraction of the reflected power at the fat-muscle and air-muscle interface.[50,64] The calculation of the absorbed power was performed for E_0 = 10V/m and the SAR values for muscle and fat

Figure 2.1: The dielectric constant and electrical conductivity of muscle and fatty like tissues for the frequency range of (50-3000) MHz. The error bars signify the range of the value at the specific frequencies.

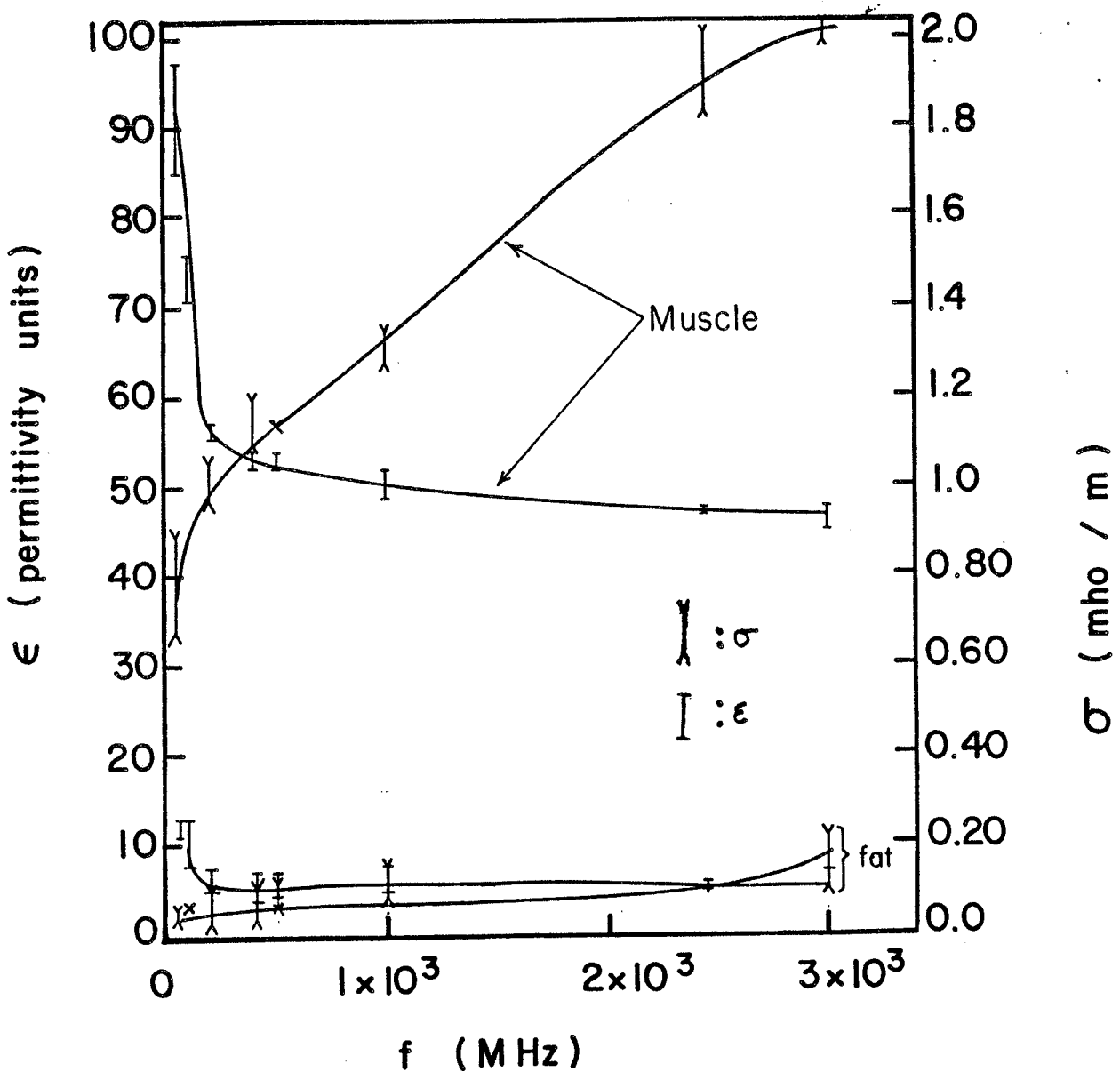
100
90
80
70
60
50
40
30
20
10
0
2.0
1.8
1.6
1.4
1.2
1.0
0.80
0.60
0.40
0.20
0.0
Muscle
: σ
: ε
fat
0
1×10³
2×10³
3×10³
f (MHz)
ε (permittivity units)
σ (mho / m)

Figure 2.2: The depth of penetration is plotted as a function of frequency. The error bars correspond to the range of the values at the specific frequencies.

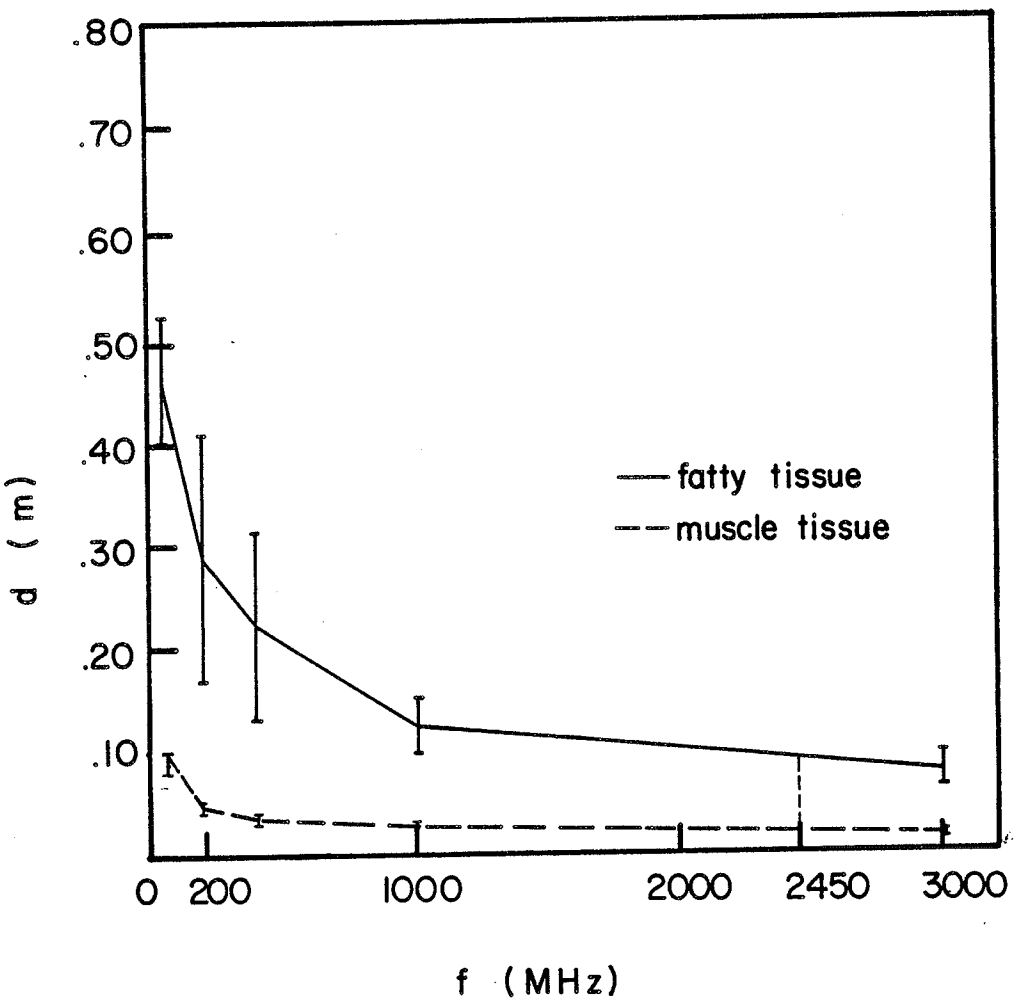
.80
.70
.60
.50
.40
.30
.20
.10
d (m)
fatty tissue
muscle tissue
0
200
1000
2000
2450
3000
f (MHz)

Figure 2.3: The percent reflected power at tissue interfaces as a function of frequency.

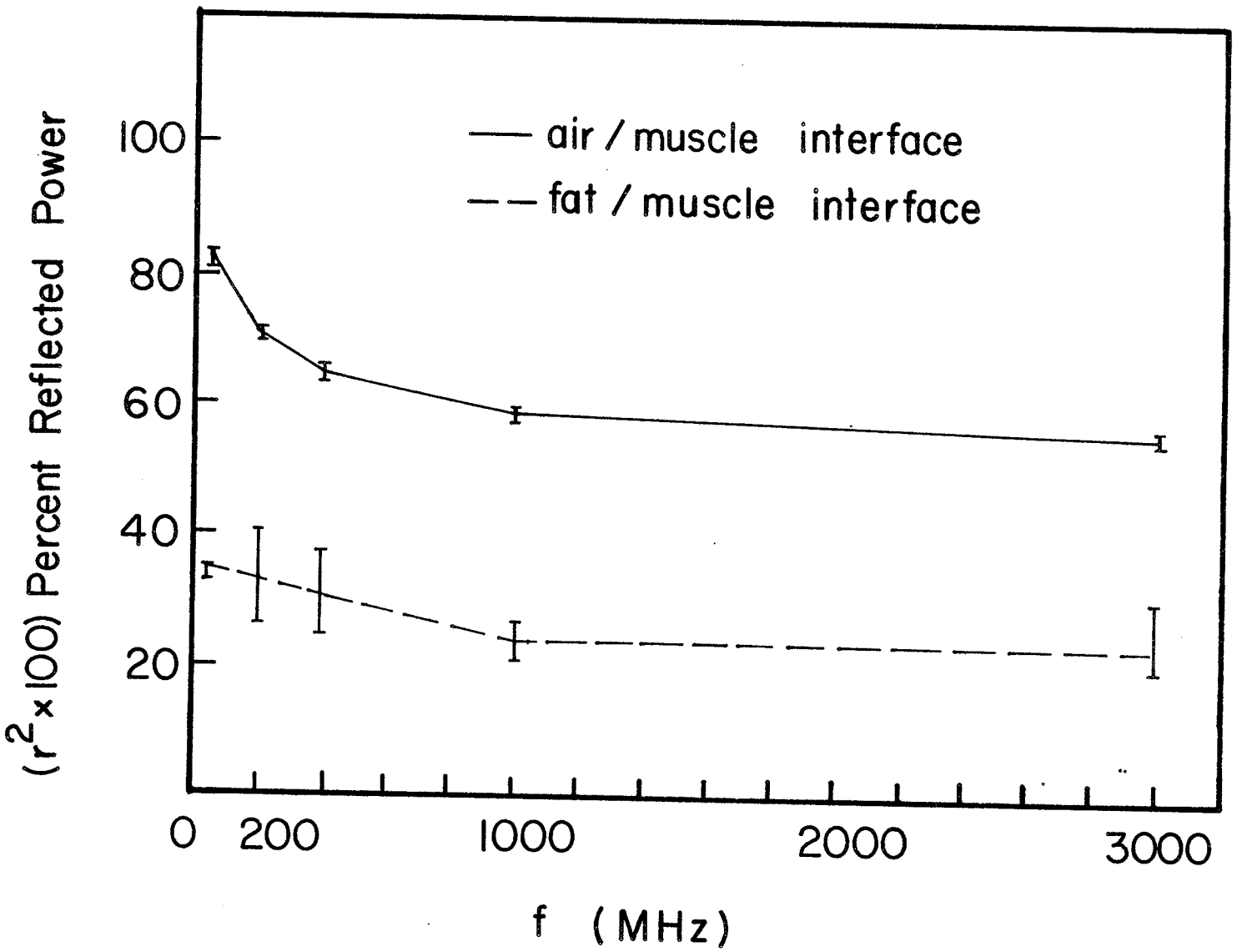
air / muscle interface
fat / muscle interface
100
80
60
40
20
$(r^2 \times 100)$ Percent Reflected Power
0
200
1000
2000
3000
f (MHz)

Figure 2.4: The specific absorption rate is plotted as a function of position inside tissues of defined thickness at a fat muscle interface, at different frequency values, (the left side of diagram refers to fat layer; the right side of the diagram refers to muscle).

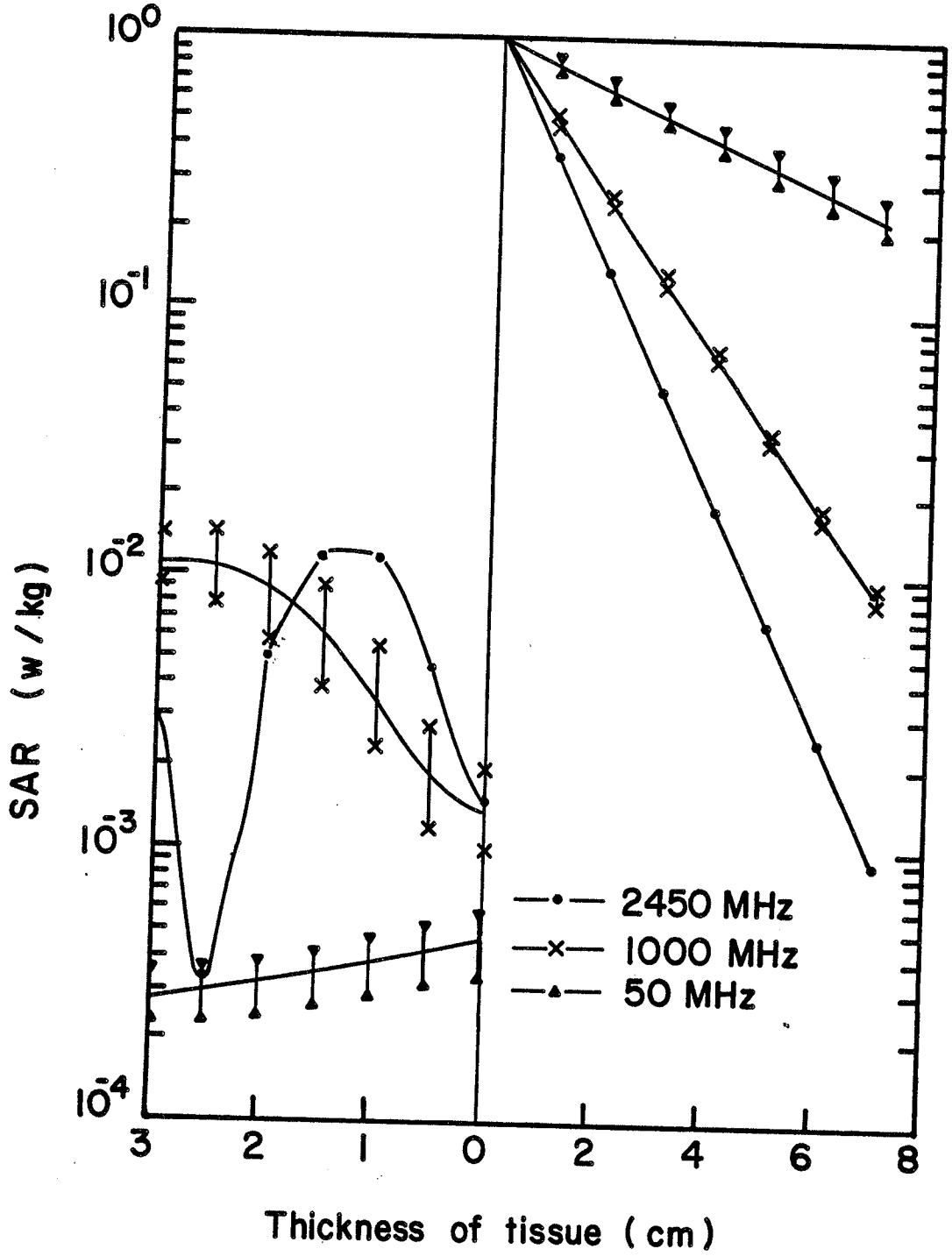
10^{0}
10^{-1}
10^{-2}
10^{-3}
10^{-4}
SAR (w / kg)
3
2
1
0
2
4
6
8
Thickness of tissue (cm)
2450 MHz
1000 MHz
50 MHz

were obtained using the following densities respectively d_m = 1.07 g/cm^3; d_f = .937 g/cm^3.[70] In Figure 2.4 the SAR values are plotted versus the thickness of fat and muscle tissue. The thickness of fat was assumed to be equal to 3 cm according to the values reported in literature on the thickness of fat in human (i.e. 1-3 cm).[61] The values of SAR in the muscle tissue were normalized to one and the medium thickness (muscle) was considered up to 7 cm. The error bars in the figures signify the variation range of the values of ε' and σ reported in literature for the specific frequencies. These variations in the reported ε' and σ values are a consequence of the different approaches used to obtain them experimentally. One method,[71] that was used to measure the dielectric properties of mammalian tissue between 1 and 18 GHZ, has the following experimental procedure:

The tissue sample is placed into a sample holder, from a precision 7 mm air-line, which is surrounded by a water jacket in order to thermostatically control the tissue temperature. The microwave signal is reflected from a short circuit that is placed immediately behind the sample, and the resulting standing wave profile is measured and recorded using a slotted line connected through a digital voltmeter to a microcomputer. The standing wave profile is then analyzed with a least squares curve fitting program in order to obtain the permittivity (ε') and the dielectric loss factor (ε'') of the tissue sample.

Another method[72] that is used for measuring the dielectric properties of materials at the lower frequency range is to measure the capacitance (C_o) of an empty cell condenser and the capacitance (C) and the resistance (R) or the conductance (G) of the cell condenser

when filled with the dielectric material. The complex capacitance is given by $C^* = C + G/j\omega = C + 1/j\omega R$ (2.8); where C in Farads, G in mho, R in ohm. The quantities C and R from equation (2.8) may be considered to be combined in parallel with each other, giving an impedance $(1/G + j\omega C)$ for the condenser filled with a specimen.

Thus we have the permittivity $\varepsilon' = C/Co$ and the conductivity

$$\sigma = \frac{\varepsilon_o}{C_o} G = \varepsilon o/C_o R \; ; \; \varepsilon_o = \text{absolute dielectric constant of free space.}$$

The two principal methods of measuring C and G or R are the alternating current bridge method and the resonance method.

2.2 DIELECTRIC BEHAVIOR OF TISSUES

2.2.1 DIELECTRIC CONSTANT AND ELECTRICAL CONDUCTIVITY

The relation between the response of biological tissues to microwaves and their dielectric properties was emphasized in the previous section, but a detailed discussion will be undertaken in this section.

As was mentioned before, the complex dielectric constant, $\varepsilon^*/\varepsilon_o = \varepsilon' - j\varepsilon''$, describes the dielectric behavior of tissues and other materials in general. The dielectric constant, ε', is equivalent to the capacitance of 1-cm cube of the material corrected by a constant factor which depends on the units of measurement of the capacitance. The conductivity of the tissue, $\sigma = \varepsilon_o \varepsilon'' \omega$ = 1/specific resistance (resistivity), is the inverse of the resistance of a 1-cm cube of material.[64]

There are three factors that determine the value of these dielectric parameters: 1. The frequency of the applied field; 2. The H_2O content of the material upon which the field acts; and 3. The ambient temperature in which the material is found during the application of the field. Throughout the frequency range of 10 and 10^4 MHZ the values of ε and σ go through three different stages of frequency dependent response and each of these differentiated responses is due to the cellular structure of tissue, its electrolyte and water content and finally its protein and other solid constituents content.[50,61,64,68,73]

In the low frequency range (10-300 MHZ) the response is due to the presence of the cell membranes which behave as thin layers of high capacity and resistance. At these frequencies the time constant of charging is sufficiently long to fully charge and discharge the cell membrane in a single cycle; this results in high values for the tissue capacitance and hence high dielectric constant. The reason for the low conductivity at this frequency range is that the cell membranes act as insulators, allowing the currents to flow only in the extracellular medium.

As the frequency increases, the membranes become short circuited and the cell interior gets involved in the conduction of the electrical current, thus causing the effective resistance of the tissue to decrease and its electrical conductivity is increased. Furthermore, the increased frequency will result in a decrease in the dielectric constant of the tissue due to the fact that the time constant is insufficiently long and prevents the cell membrane from becoming totally charged during a full cycle. In the frequency region

between 300-3000 MHZ a minimum frequency dependence is observed for both ε and σ. In this range the cell membranes are short circuited and stop influencing the dielectric parameters of the tissues. Also, the tissue water is not as strongly dependent on frequency in this region. Therefore, tissues studied at this frequency range in terms of their dielectric behavior, act as salt solutions which contain solid constituents such as proteins or other solid substances. These solid constituents are mostly of low conductance and dielectric constant and behave in a first approximation like dielectric holes in salt solution (Schwan and Piersol 1954).[64] Moreover, the existence of the low conductivity and dielectric constant solids causes the overall σ and ε of the tissue to be smaller than that of a salt solution of an ionic strength typical for tissue electrolytes. Finally, in the frequency range between 3000 and 10^4 MHZ the frequency dependence is mostly due to the H_2O content of tissues. The polar properties of the water molecules causes them to rotate with the field up to a critical frequency value (approximately at 22 GHZ). Beyond this critical frequency value a rapid drop is observed in both the ε and σ values in consequence of the Debye theory of polar molecules.

The above discussion on the dielectric behavior of tissues is mainly referred to tissues with high water content, such as muscle, brain, etc. Furthermore, the dielectric behavior of tissues with low water content, such as fat, bone, etc. is quantitatively alike with that of high water tissues but, the ε and σ values are an order of magnitude lower and not as well understood.[61]

The ambient temperature at which the phantom is found during the application of the various fields affects the dielectric response of

the tissue. The temperature effect is far less obvious on the dielectric constant than the conductance. This dependence is well understood and explained by various researchers such as Schwan and Piersol,[64] Schwan and Foster,[74] etc. and there are several measurements of the effect in the existing literature.[59,61,63,64,74] Muscle data have indicated that there are at least three types of relaxation mechanisms when its dielectric behavior is studied as a function of frequency; the α-dispersion, the β-dispersion and the γ-dispersion. The temperature dependence of the dielectric constant and conductivity can be explained in relation with these dispersions.[74,63,64] For each dispersion the temperature coefficient reflects the response of permittivity, conductivity and relaxation time. The fc (critical frequency) increases with temperature at a rate of about 2%/°C. The α-dispersion[74] may be a consequence of the frequency dependent access impedance of the inner membrane system of the cell. The access is ionic and therefore the temperature coefficient of ε' is equal to that of the conductivity of an electrolyte, i.e. about 2%/°C. The β- dispersion[74] range is caused by the Maxwell-Wagner polarization effects during which the cell membranes are charged through the electrolytes. Therefore, the time of membrane charging varies inversely with the conductivity of the electrolyte, which results at about -1/2%/°C temperature coefficient for ε'. In the γ-dispersion[74] the relaxation is close if not identical to that of free H_2O and therefore its temperature dependence is equal to that of water and which is again for ε' close to the 2%/°C value. In Table 2.1 the characteristic temperature coefficients of high and low H_2O content tissue and at microwave frequencies are

Table 2.1: The values of the temperature coefficients for ε and σ as obtained from the literature, for the frequency range studied in this project (i.e. 300-3000 MHz)

	$\Delta\varepsilon/\varepsilon$	$\Delta\sigma/\sigma$
High H_2O Content Tissues	-.5%/°C	2%/°C
Low H_2O Content Tissues	$\sim$1.1%/°C	$\sim$-4.2%/°C

shown, as obtained from the literature. For the electrical conductivity temperature dependence the same considerations can be applied with the only difference that the infinite frequency value of $\sigma(\sigma\infty)$ is much greater than that at zero frequency ($\sigma 0$), as opposed to the dielectric constant (where $\varepsilon_o >> \varepsilon\infty$). In this case, the temperature coefficient of conductivity is about 2%/°C at frequencies well above and below the characteristic frequency and about 1%/°C in the range of dispersion.

2.3 THERMAL BEHAVIOR OF TISSUES

2.3.1 THERMAL PROPERTIES OF TISSUES

Biological tissues are very complex non-homogeneous materials that are very difficult to describe analytically in terms of their thermal behavior. However, the basic mechanisms of heat transfer are very important in the applications of hyperthermia, whether it is applied clinically or experimentally. Hyperthermia research requires the knowledge of the thermal properties of tissues along with the electrical ones in order to be able to define theoretical and experimental models that will help study the phenomenon and improve its effectiveness clinically.

The thermal conduction of tissues is described by two constants; the thermal conductivity k (W/mK) that determines the temperature gradient for a given steady state heat flux, and the thermal diffusivity, $\alpha = k/\rho*c$ (ρ = density of tissue, c = specific heat) that defines the ability of a thermally perturbed medium to relax back to steady state conditions. The latter is generally less important in

hyperthermia than the former because of the long time interval the tissue is kept at a temperature relative to the thermal relaxation time. Another quantity that is important is the specific heat capacity (c) of tissues. It is defined as the amount of heat required to raise the temperature of unit mass of a tissue by one degree (c units J/kg K).

The values of thermal conductivity of various tissues have been reported in literature by several investigators. The early work of Grayson (1952) and Spells (1959) was followed by Chato (1969) and Balasubramaniam and Bowman (1975, 1977).[75] The thermal conductivity measurements vary from one report to the other by as much as 10%. Bowman et. al. (1977) reported a typical variation of (1-2)% in their k values and a 5% variation in their α values. In Table 2.2 the values of k and c are reported for various human tissues as obtained from literature.[70,76]

2.3.2 THE CONVECTIVE COMPONENT OF THE TISSUE THERMAL BEHAVIOR: BLOOD FLOW

In Chapter 1 the effects of blood flow in relation to the biological effects of hyperthermia were discussed. It is of interest in this report to review the values of blood flow in human tissue reported in the literature. What is clear is that not enough information is available for the blood flow and its reaction to hyperthermia in many regions of the body, especially for human tissues, normal or tumor tissues.

Several reports of the different blood flows in normal and tumor tissues have been stated in the literature which indicate that the

Table 2.2: The values of k, σ, and ρ are tabulated for human tissues as reported in literature. The values in the parentheses indicate the range for the k values.

Tissue	Thermal Conductivity $k(W/m°C) \pm \bar{\sigma}$	Specific Heat $c(10^3 J/kg - °C)$	Density ρ (g/cm^3)
Muscle	(.449 - .546) .508 ± .044	3.47	1.07
Fat	(.258 - .272) .222 ± .023	1.721	.937
Skin	(.200 - .246) .266 ± .007	-	-

blood flow in tumor tissues is much slower than that of normal tissue.[76,77,78,79,80,81] These different blood flows react differently to moderate hyperthermia temperatures.

As reported by Song et. al. the blood flow of normal tissues increased as much as seven times its initial value when the tissues were treated by 42°C to 43°C hyperthermia while the tumor blood flow either stayed the same or decreased. Furthermore, it was reported that at higher temperatures (above 43°C) tumor blood flow was stopped.[82] It was pointed out in all of the reports, however, that the reaction of the tumor blood flow to hyperthermia was dependent on the size of tumor. It is important in this study to know the blood flow values for human tissues and tumors in order to be able to apply them experimentally for obtaining the relationship between the temperature distribution patterns and the particular blood flows. In Table 2.3 the values of blood flow for various human tissues and tumors are recorded as obtained from the literature.[76,79,83,84]

Table 2.3: The blood flow values of human tissues, normal or cancerous, during resting or maximum activity periods as reported in the literature.

Tissue	Resting blood flow to max. activity values (ml/100 g - min)
Muscle	1.6 or 2.2 - 60
Fat	3.3 - 30
Skin	5.0 - 170
Human lymphoma	18.0 - 60.0
Anaplastic carcinoma	3.0 - 20.0

3.1 INTRODUCTION

3.1.1 INTRODUCTION TO PHYSICAL MODELING

Physical modeling (Phantoms) of tissues has been proved an effective means for the study of microwave hyperthermia in vitro. There are two types of phantom systems that are used experimentally to simulate biological tissue electrically and thermally. Firstly, there are the static or unperfused phantoms, which are electromagnetic tissue equivalent materials that simulate various biological tissues, eg. muscle, fat, bone, etc. but, do not involve the tissue circulation as a part of the simulation. The other class of phantoms involves the dynamic or perfused phantoms which simulate tissue perfusion along with its electrical and thermal properties.

In the present chapter, both types of phantoms will be discussed, but the major topic will be the theory and the practical design of the dynamic phantom developed.

The development and establishment of appropriate hyperthermia treatment techniques requires the knowledge and understanding of the microwave power deposition patterns as well as the overall effects of tissue heterogeneity and the various convective flow processes. Moreover, the effects of thermometry probes in the vicinity of the microwave fields have to be known and well documented in order to achieve a well planned hyperthermia treatment.

Simple static phantoms, such as those developed by Guy et. al.,[85] M G. Bini et. al.,[86] Lagendijk and Nilsson,[87] are used for the study of microwave power absorption patterns as a function of tissue heterogeneity and field perturbing temperature probe positioning.

Dynamic phantoms constitute a more sophisticated class of

phantoms in that they are designed to study specific cases of hyperthermia applications and they also help establish a better understanding of the process by including the circulation in the simulation. Simple dynamic phantoms, however, are not realistic, neither do they offer results that can be quantitatively applied in clinical situations.

Phantoms, in general, are a very appropriate means for testing mathematical models because they can be controlled according to specifications, while animal experiments are very difficult to control or reproduce.

Simple dynamic phantoms have been developed by various research teams, eg. Baish and Foster,[88] Sandhu,[89] Cetas and Connors,[70] D-J Lee et. al.,[90] which were designed and manufactured according to the requirements of their studies.

The dynamic phantom developed in our lab was expected to complement previous studies with a static phantom in terms of determining the power deposition pattern and temperature distributions when irradiated at 2450 MHZ. In addition, the effects of the simulated blood flow upon the temperature distributions were to be studied and any correlations to the clinical situation to be drawn.

The dynamic phantom which is to simulate human tissue of high H_2O content, i.e. human muscle tissue, is based on the following theoretical model and practical design.

3.2 THEORETICAL MODELING OF A DYNAMIC PHANTOM

3.2.1 DIELECTRIC THEORY APPLICABLE TO THE SIMULATION

It was mentioned previously (Chapter 2) that at microwave frequencies the cell membranes cannot affect the electrical properties of cellular solutions and tissues because the membrane reactance becomes small compared with the internal impedance and furthermore at the higher end of the range the polar properties of water become important and cause γ-dispersion; ie. that relaxation frequency is close if not identical to that of free H_2O.[61,88] Therefore at these frequencies biological tissues of high H_2O content act simply as suspensions of protein molecules in a salt solution. The dielectric properties of such tissues as well as those of blood are quite similar with each other in the microwave frequency range.

The biological suspensions of this type are considered as non ideal dielectric mixtures with surface charges appearing at the boundaries between components, which are composed of both bound and free charges. When at the steady state condition these surface charges will distribute so as to counterbalance the effect of the external electric field, and there will be no net field or conduction within the conducting regions. To explain the concept of dielectric conductivity[91] one could consider the case of a capacitor filled with dielectric, which has a capacitance C and a resistance R. The total current developed across the capacitor when an ac voltage $V = e^{j\omega t}$ is applied to the plates is given by the following expression.

$$I = I_C + I_D = V/R + C\frac{dV}{dt} = V\frac{A}{d}(\sigma + j\omega\varepsilon_o\varepsilon) \qquad (3.1)$$

where I_C is the resistive current in phase with the ac voltage, I_D is the charging or displacement current that leads the voltage in phase by 90°, ε and σ are the macroscopic values of the electrical permittivity and conductivity, A is the area of the capacitor plate and d is the distance between the plates.

The current density is defined as $\bar{J} = (\sigma + j\omega\varepsilon_o\varepsilon)\,\bar{E}$ (3.2) so that from Ohm's law we define the complex conductivity as $\sigma^* = \sigma + j\omega\varepsilon_o\varepsilon$ (3.3), and equation (3.1) becomes

$$I = \frac{j\omega\varepsilon_o A}{d}\left(\varepsilon - \frac{j\sigma}{\omega\varepsilon_o}\right) V \qquad (3.4)$$

The relation between the current I that is seen experimentally, and the applied ac voltage V in a capacitor, defines the permittivity of the dielectric medium. By taking into account only the intrinsic quantities that are controlled by the dielectric medium one can define the complex permittivity as follows:

$$\varepsilon^* = \varepsilon' - j\varepsilon'' = \varepsilon - \frac{j\,\sigma}{\omega\varepsilon_o} \qquad (3.5)$$

From the above expressions we can observe that for high frequencies the dielectric properties of the materials are important while for low frequencies the conduction phenomena are important. This seems to be the sole justification for introducing both expressions (3.3) and (3.5), which can otherwise be expressed as:

$$\sigma^* = j\omega\varepsilon_o\,\varepsilon^* \qquad (3.6)$$

Hanai has developed a theory for the dielectric properties of heterogeneous systems, that is concentrated dispersions of the oil in water type (o/w) for which Wagner's theory does not apply since it was developed for dilute dispersions.[92] A concentrated disperse system is

obtained, according to the model, by successively adding infinitesimally small quantities of disperse into a dispersion medium. After a succession of additional quantities of disperse the system will reach its final concentration Φ and the complex dielectric constant ε^* is given by the following equation:

$$\int_{\varepsilon_m^*(C)}^{\varepsilon^*} \frac{2\varepsilon^* + \varepsilon_p^*}{3\varepsilon^*(\varepsilon^* - \varepsilon_p^*)} \, d\varepsilon^* = \int_0^{\Phi} \frac{-d\Phi'}{1 - \Phi'} = \log (1 - \Phi) \qquad (3.7)$$

where ε_m^* is the complex dielectric constant of the dispersion medium, ε_p^* is the complex dielectric constant of the disperse. The left part of the integral is integrated along a certain contour C from ε_m^* to ε^*, which is successively determined by the correlation of ε' and ε'' (i.e. $\varepsilon^* (\varepsilon', \varepsilon'')$) at each stage of a series of successive additions.

The solution of equation (3.7) for ε^* results in the following equation:

$$\varepsilon^* = (\varepsilon'^2 + \varepsilon''^2)^{1/2} * \exp \left(-j \tan^{-1} \frac{\varepsilon''}{\varepsilon'}\right) \qquad (3.8)$$

Following this, Hanai applied his theory to biological systems and presents the complex analogue of Maxwell's equation for the complex dielectric constant which is:[91]

$$\varepsilon^* = \varepsilon_{mh} + \frac{\varepsilon_{ml} - \varepsilon_{mh}}{1 + j_\omega t} + \frac{\sigma_{ml}}{j_{\omega\varepsilon o}} \qquad (3.9)$$

and complex electrical conductivity

$$\sigma^* = \sigma_{ml} + \left[\frac{j\omega\tau \, (\sigma_{mh} - \sigma_{ml})}{1 + j\omega\tau} \right] + j \, \omega\varepsilon_o\varepsilon_{mh} \qquad (3.10)$$

where the subscripts "ml" and "mh" correspond to the low and high

frequency values of the dielectric parameters of the mixture; τ = relaxation time and $\omega = 2\pi f$ = angular frequency. In this simulation the target frequency is at 2450 MHZ and therefore the expressions that will be used for the calculations are those designated by Hanai, for high frequencies and more concentrated mixtures, as follows:

$$\frac{\varepsilon_{mh} - \varepsilon_2}{\varepsilon_1 - \varepsilon_2} \cdot \left(\frac{\varepsilon_1}{\varepsilon_{mh}}\right)^{1/3} = 1 - \Phi \qquad (3.11)$$

$$\sigma_{mh} = \frac{3\left[\dfrac{\sigma 1 - \sigma 2}{\varepsilon_1 - \varepsilon_2} + \dfrac{\sigma 2}{\varepsilon_{mh} - \varepsilon_2}\right] - \dfrac{\sigma 1}{\varepsilon_1}}{\dfrac{3}{\varepsilon_{mh} - \varepsilon_2} - \dfrac{1}{\varepsilon_{mh}}} \qquad (3.12)$$

where σ_1, ε_1 = dielectric constant and conductivity of the dispersion medium

σ_2, ε_2 = dielectric constant and conductivity of the disperse.

$\sigma_{mh}, \varepsilon_{mh}$ = dielectric constant and conductivity of the mixture.

Φ is the volume fraction of the disperse and in the case of our simulation it is going to be considered as the weight fraction of the disperse since the density of human muscle is equivalent to $1 gm/cm^3$.[59]

3.2.2 CALCULATIONS FOR THE VERIFICATION AND COMPOSITION OF THE MODEL

The theoretical model discussed above was used to calculate the composition of the dynamic phantom in order to dielectrically simulate human muscle. However, before that and in order to verify its validity, the theory was applied to an already accepted muscle

phantom, namely the phantom developed by Guy et. al.[85] The procedure for the calculations for the verification was as follows. Biological tissues are made of two major constituents that can be categorized into liquid and dry constituents. In the case of applying the theory discussed previously to biological tissues, the liquid part of the tissue will correspond to the dispersion medium and the dry part to the disperse. This is because proteins (dry constituents) behave dielectrically as insulators with low dielectric parameters in the same manner as oils, glasses, etc. while the liquid part of tissue acts as a salt solution and in a more simplified respect as plain water.

The static phantom developed by Guy et. al.,[85] consists of water, powdered polyethylene (a plastic), salt (NaCl) and a jelling agent to hold the phantom together. In Table 3.1 the values of the dielectric parameters of the phantom as calculated using equations (3.11) and (3.12) are given as well as the resulting composition, along with the values published by Guy et. al. The calculations were performed by considering the dielectric values at 37° C and at 2450 MHZ frequency range. The dielectric constant of the water is adjusted for the salt content of 12 g/l as indicated by the recipe instructions. Using equation (3.11) the composition of the phantom was calculated to within a small percentage error as indicated in table 3.1. Furthermore, using the values for the dielectric parameters at the indicated salt concentration the value of the electrical conductivity was also calculated and compared to σ reported by Guy. To perform these calculations the dielectric parameters of powdered polyethylene[85] and H_2O[93,58] were used ($\varepsilon_2 = 2.25$, $\sigma_2 = 10^{-8}$ mho/m)

Table 3.1: Composition and the dielectric parameters of the static phantom as per Guy recipe and theory calculations

A.	% weight composition	
	dry constituents	liquid constituents
Recipe	23.6%	75.50%
Theory	23.0%	76.99%
Variation with respect to recipe values	2.5%	.64%

B.	Dielectric Parameters at 2450 MHZ	
	Dielectric Constant (E)	E. Conductivity (mho/m)
Reported by Guy	50	2.72 mho/m
Theory	--	2.63 mho/m
Variation	--	3%

(ε_1 = 72.573 , σ_1 = .039 mho/cm) in addition to the values for the static phantom as per Guy[85] (ε' = 50, σ = 2.72 at 2450 MHZ).

It can be observed from the above calculations that the theoretical model by Hanai is a valid one for applications to the simulation of biological tissues. The small percentage variation in the phantom's composition can be attributed to the frequency values used because as has been shown from other studies[94], the composition of this phantom needs to be readjusted from the general recipe given by Guy for the various frequency ranges.

The dynamic phantom will dielectrically simulate the properties of human muscle (37° C), at the working temperature of 25° C. It will be expected therefore from the phantom to behave at 25° C as muscle tissue at 37° C.

Using equations (3.11) and (3.12) we will calculate the weight composition of the constituents and the amount of NaCl content required for such a simulation to attain the correct electrical conductivity, and dielectric constant.

The materials used for this simulation were chosen on the basis of their dielectric behavior and some other factors in relation to the choice of the dry constituent such as flexibility (i.e. easily bent penetrated, perfused, but not permitting natural convection) as well as availability and cost. The liquid constituent would be a saline solution with the appropriate NaCl concentration that would result in the desired dielectric conductivity when incorporated in equation (3.12). The dry constituent was chosen to be fiberglass sheets, the properties of which complied with the set requirements. Dielectrically, fiberglass behaves in a similar manner to proteins and

in general as the dry constituents of human muscle. Its dielectric constant $\varepsilon_2 = 4$ and dielectric conductivity σ_2 is in the range of 10^{-12} mho/cm at the 2450 MHZ frequency range which compare favorably with the protein dielectric properties (i.e., $\varepsilon \simeq 2.7$ and $\sigma \simeq 10^{-12}$ mho/cm).[91] The dielectric properties of human muscle that was to be simulated were, $\varepsilon_{mh} = 47.5$ and $\sigma_{mh} = 1.84$ mho/m at 2450 MHZ, as they were reported by the collective review paper on the dielectric properties of biological materials by Stuchly and Stuchly.[65]

To obtain the dielectric constant and conductivity mentioned above experimentally in the dynamic phantoms, it was necessary to use specific volume fractions of each constituent. The volume fractions of H_2O and fiberglass required for the simulation were calculated through equation (3.11), where ε_{mh} is the muscle phantom dielectric constant to be achieved, ε_1 is the dielectric constant of the saline solution of concentration c (i.e. $\varepsilon_1 = 78 + (-\delta/2)*2*c$); δ = dielectric decrement for NaCl = 11, c = (gms of NaCl in solution)/ molecular weight of NaCl = 58.5 gms), ε_2 is the dielectric constant of fiberglass, and finally Φ is the volume fraction of the dry constituent.

Before these calculations could be performed, however, the NaCl concentration had to be determined in order to determine the exact value for the dielectric constant ε_1 before equation (3.11) could be solved for Φ. In equation (3.12) the following parameters are involved: σ_{mh} is the electrical conductivity of human muscle that is to be simulated, σ_1 is the conductivity of the NaCl solution, σ_2 is the conductivity of fiberglass.

To calculate the exact value of c required for obtaining σ_{mh}

experimentally eqn. (3.12) was solved for the various values of σ_1 in the concentration range of ($.1^{mole}/l$ - $.2^{mole}/l$).

In Table 3.2 the values obtained from the calculations are shown, corresponding to the various concentrations of NaCl. The concentration required for simulating the $\sigma_{mh} = 1.84$ was found by plotting the c values against the calculated values of σ_{mh} (see Figure 3.1) In this figure not all the values fall on the straight line due to possible small errors in the σ_1 values which were read off another graph.[58] However, to within small error the concentration c corresponding to the σ_{mh} of 1.84 mho/cm of the human muscle was found to be c = .114 moles/l . This is the concentration that was applied for the calculations involving equation (3.11) for determining the percent weight composition of the phantom. In Table 3.3 the volume fractions of the constituents are presented along with the dielectric parameter values that were used to calculate the percent composition from equation (3.11).

It was mentioned earlier that for muscle tissue the volume fractions are the same as the weight fractions because its density is equivalent to 1 gm/cm^3. In the case of the phantom it was necessary to find out the densities of the fiberglass (in the form incorporated in the simulation) and the phantom as a whole (at the composition described above).

The determination of the fiberglass density was made according to

$$V_{mixture} = V_{H_2O} + V_{fiberglass} = mH_2O/dH_2O + m_f/d_f \quad (3.13)$$

Where V_m = volume of the mixture of known value

V_{H_2O} = volumes of H_2O and fiberglass

m_{H_2O}, m_f = mass of H_2O and fiberglass of known values

Table 3.2: The calculation of the electric conductivity σ_{mh} of the phantom as a function of NaCl concentration at 25° C.

c (mole/l)	$E_1 = 78 + (-11/2)*2*C$	σ_1 (mho/cm)	σ_{mh}(mho/cm)
.1	76.9	.030	1.74
.125	76.625	.033	1.94
.150	76	.035	2.08
.175	76.1	.038	2.26
.200	76	.040	2.39

Figure 3.1: The conductivity of the mixture (saline solution-fiber-glass) is plotted as a function of salt concentration at 2450 MHZ and 25° C temperature.

Table 3.3: The percentage volume composition of the dynamic phantom and calculation parameters

Dielectric Constants involved in equation 3.11	c = .114 moles/l	
	%(1 − Φ) liquid	%Φ dry
E_1 = 76.75	70.20	29.80
E_2 = 4		
E_{mh} = 47.5		

Table 3.4: Experimentally determined values for the densities of fiberglass and the muscle phantom (Average values of four trials)

Material	Average Density ± Average Deviation
Fiberglass	(1.25 ± .18) gm/cm^3
Muscle Phantom	(1.07 ± .05) gm/cm^3

dH_2O = density of H_2O = 1 gm/cm^3

d_f = density of fiberglass in gms/cm^3

By solving equation (3.13) the density of fiberglass was calculated in four different trials. The density of fiberglass and the volume fractions were calculated before they were applied to the following equation

$$d_{mp}^{*} \Sigma(VF) = (VF)_f * d_f + (VF)H_2O * dH_2O \qquad (3.14)$$

in order to calculate the density of the muscle phantom.

d_{mp} = density of the muscle phantom (gm/cm^3).

$(VF)_i$ = the volume fraction of the constituents where i = H_2O or f.

The average value of the muscle density calculated over the four trials is tabulated in Table 3.4 along with the fiberglass density.

The experimentally calculated density of the muscle phantom compares favorably to the density values reported for human muscle in the literature which are in the range of 1 - 1.07 gm/cm^3.[59]

This means that the simulation is quite successful in terms of composition and structure relative to human muscle. For the solution of equation (3.14) the value of the density of the water plus NaCl solution was assumed to be equal to that of pure water since the amount of added NaCl was very small (i.e. c = .114 moles/l).

3.3 THERMAL PROPERTIES OF THE DYNAMIC MUSCLE PHANTOM

3.3.1 CALCULATION OF THE THERMAL PARAMETERS

The dynamic muscle phantom was predominantly designed to simulate the dielectric behavior of human muscle, but the thermal response of

the phantom is also of interest in the simulation with respect to that of real muscle. The thermal behavior of human muscle tissue was discussed in Chapter 2. In this section the dynamic phantom's thermal properties will be calculated on the basis of the thermal properties of the constituents, i.e. H_2O and fiberglass. Calculations of the thermal properties of tissues have been reported in the literature[94] for various types of phantom materials for muscle or fat simulation. The expression for these calculations is that derived by Hanai, applied to the thermal response of tissue, that is:

$$\frac{k - k_2}{k_1 - k_2} \cdot \left(\frac{k_1}{k}\right)^{1/3} = 1 - \Phi \qquad (3.15)$$

where k = thermal conductivity (in W/mk) for the phantom muscle to be calculated

k_1 = thermal conductivity of H_2O = .603 W/mk[94]

k_2 = thermal conductivity of fiberglass = .40W/mk[95]

$1-\Phi$ = .702

Solving equation (3.15) for k[97] we found the thermal conductivity for the muscle phantom equal to .528 W/mk which is very close to that of real human muscle (See Chapter 2 Table 2.2). The thermal conductivity value is therefore comparable to that of human muscle but it is only a calculated value which has not been measured experimentally.

Similarly the calculation of the specific heat value for the phantom was undertaken using the method of mixtures, that is

$$c_{mp} * \Sigma(VF) = (VF)_{H_2O} * c_{H_2O} + (VF)_f * c_f \qquad (3.16)$$

where c_{mp} = specific heat of muscle phantom (Joules/kg°C)

c_{H_2O} = specific heat of H_2O = $4.2256 * 10^3$ J/kg°C at 25°C

c_f = specific heat of fiberglass = .833 * 10^3 J/kg°C at (20-100)°C[95]

The value of the specific heat of the phantom was found equal to c_{mp} = .77 * 10^3 Joules/kg°C; that is a 7% variation from the specific heat value for human muscle tissue reported in the literature.[59] Whether these calculated values are a correct prediction of the true thermal properties of the phantom was not justified with individually performed experimental measurements, but the overall response of the phantom during the testing and the blood flow prediction measurements (See Chapters 4 and 5) would be an indication of the success of the simulation dielectrically and thermally.

3.4 BLOOD FLOW SIMULATION

3.4.1 ELECTRICAL PROPERTIES AND PHYSIOLOGICAL CONSIDERATIONS

Dynamic phantoms are characterized by their ability to simulate blood flow. In the design of the dynamic muscle phantom there were several facts to be considered regarding the blood flow due to its complicated nature and the difficulty of interpreting this phenomenon experimentally.

Tissue blood flow is an omnidirectional flow at the cellular level while it is usually two-directional with respect to the artery-vein complex and its subdivisions. To date the simulation of blood flow in either of the above cases has not been successfully achieved due to the complication of such experimental set up or a theoretical model.

However, there have been several simple approaches that help a

better understanding of the heating process in the tissue by providing quantitative information of the response process. Furthermore, there is another property of blood flow that is difficult to duplicate experimentally, which is the increase in its flow-rate due to the effects of the increased temperature upon the tissue that causes vasodilation of the vasculature system and thus the increase of blood flow.

The dynamic muscle phantom was designed under the following specifications. It was firstly, assumed that the flow would be unidirectional at the cellular level with no incorporation of the blood carrying vessels, which can be a study all by itself. This is because, depending on the size of the vessel, its function under heating conditions can be classified as cold (large vessels) or hot (small vessels) tubes through a heated region. The unidirectionality of the flow in the dynamic phantom has automatically reduced the model to a simple, relatively realistic simulation which results in the fact that any measurements obtained in the phantom cannot be quantitatively applied in clinical situations. However, the information obtained from such a phantom is superior to that from a static phantom since its time-temperature measurements are a function of flow and flow rates. Furthermore, the equipment associated with such a flow simulation are readily uncomplicated and less expensive and thus they do not require an extensive experimental set-up. Another advantage of the unidirectional flow is that, it can ensure the best uniformity in the flow as well as the reproducibility of the flow-pattern, since it is created in relatively simple and easily reproduced steps.

From the physical and electrical point of view the blood flow

simulation was considered at a working temperature of (23.5 ± 1°C). It was generally assumed equivalent to the saline solution used (i.e. c = .114 moles/l) with respect to its dielectric and thermal behavior. The dielectric properties of the saline solution (ε_1 = 76.75, $\sigma_1 \simeq$ .031) are somewhat different than those of human blood (ε = 65, $\sigma \simeq$ .015). It is however essential that this assumption is made in order to incorporate the blood flow at the cellular level in the simulation and because it is of major importance to correctly simulate the dielectric behavior of the muscle tissue. The flow rates to be simulated are the same as in human muscle under different conditions.

3.5 PRACTICAL DESIGN OF THE PHANTOM

3.5.1 SUPPORTING SYSTEM'S DESIGN AND CONSTRUCTION

The need of a supporting system for the dynamic muscle phantom was the idea behind the practical considerations. The ideal supporting system was designed to be as simple as possible and to be formed in such a manner as to achieve the more realistic perfusion in terms of direction and uniformity. It was also designed as to provide flexibility in the experimental set up.

The support system of the phantom consisted of the following parts: 1. a plexiglass box that would contain the muscle phantom, with compartments for the saline solution intended to simulate the blood flow. 2. A liquid flow pump that would circulate saline through the phantom at the various rates. 3. Plastic tubing that was used to connect the "in" and "out" pump outlets to the respective

parts of the box.

The material chosen for the box construction, ie. plexiglass, was adequate for avoiding microwave field perturbations and offered the advantage of transparency from all four sides of the box. The volume of the box occupied by the muscle phantom was (25 x 25 x 7) cm^3. These dimensions were chosen in relation to the size of the microwave applicator in order to avoid any reflections from the sides of the bottom of the box (the size of the circular applicator is 13 cm in diameter and the depth of penetration 2 cm). The actual height of the box was at 9 cm to allow any additional layers of phantom, i.e. fat, and at the same time to prevent overflow of the saline solution if there was such a case. At two opposite sides of the box the circulating saline solution compartments were attached for collecting the "in" and "out" flowing saline, with the following dimension for each of the reservoirs (25 x 3 x 9)cm^3. Inside each of the saline reservoirs and at about 2 cm from the inlet/outlet a baffle plate was installed in order to diffuse the inflowing jet of water and contribute to the uniform distribution of the flow inside the phantom. At the same opposite sides of the phantom box the solid walls after the saline compartments were replaced by movable plates with holes symmetrically distributed on them. This was a further measure for ensuring the uniform distribution of the flow inside the phantom. To avoid any flow from the sides around the hole bearing plate a tight fitting was required. In Figures 3.2 and 3.3 the plans of the supporting box are shown as designed, and accordingly constructed by the machine shop of the Manitoba Cancer Foundation. The pump which was used to circulate the saline solution had adjustable flow rate

Figure 3.2: The mechanical drawing of the phantom's supporting box. a. The top view of the box. b. The cross section of the box.

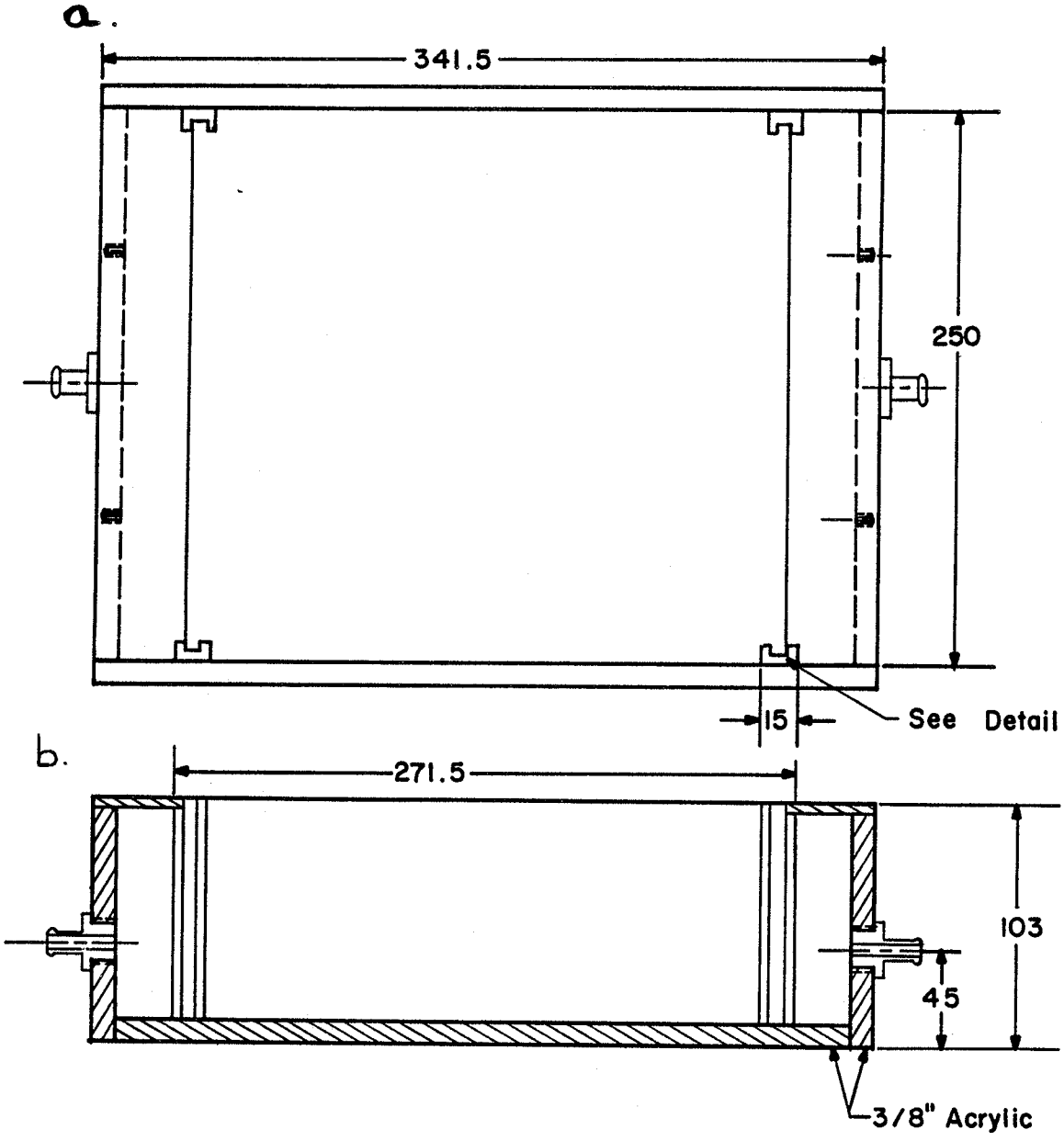
a.
341.5
250
15
See Detail
b.
271.5
103
45
3/8" Acrylic

Figure 3.3: Another part of the mechanical design of the phantom's supporting box. a. The hole bearing plate that helps diffuse the flow uniformly throughout the phantom. b. A cross section of the box that indicates the site of plate insertion.

a.

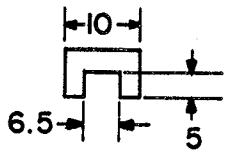

Material: 3/4" Acrylic
4 Req.'d

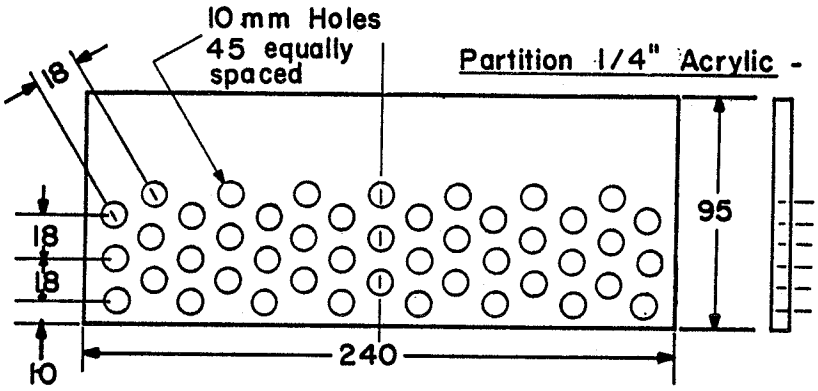

Partition 1/4" Acrylic - 2 Req.'d.

b.

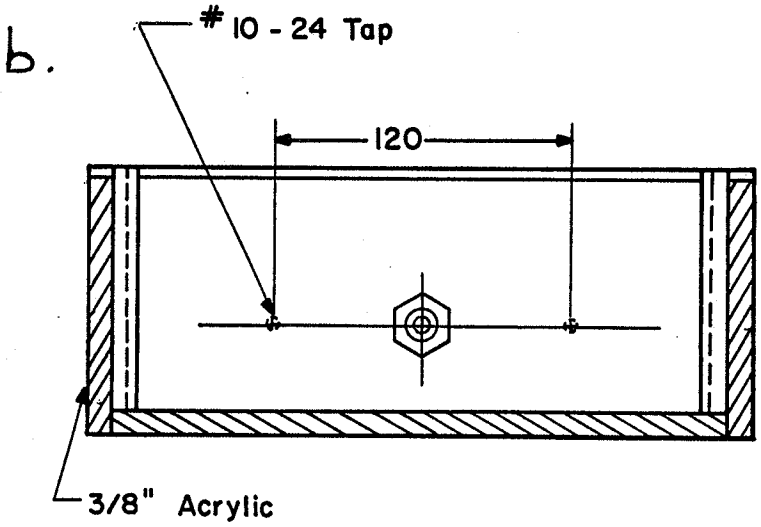

controls thus enabling its operation at different flow rates, and it was resistant to corrosion by the saline solution. The plastic tubing that connected the pump to the supporting box was of 1 cm inner diameter.

3.5.2 CALCULATION OF THE FINAL VALUES OF THE PHANTOM CONSTITUENTS

The construction of the supporting system along with the theoretical and practical considerations provide adequate information for the calculation of the size of the phantom and the weights of its constituents.

The total volume of the muscle phantom was determined equal to (25 x 25 x 7) cm^3 = 4375 cm^3 = V_m and the mass corresponding to this volume is $m_m = V_m * d_{mp}$ = 4681.25 gms ± 218.75 gms = 4.681 kg ± .219 kg. In the previous section 3.2.2 the volume fractions of the constituents were calculated with $(VF)_f$ = .298 and $(VF)_{H_2O}$ = .702. These volume fractions and the densities of the materials[2] involved are going to be used for the calculation of the weight composition of the muscle phantom. The mass of fiberglass was calculated equal to $m_f = (VF)_f * V_m * d_f$ = 1629.69 gms ± 234.68 gms; and the mass of the water in the phantom was calculated equal to $m_{H_2O} * V_m * d_{H_2O}$ = 3071.25 gms ~ 3071.25 ml. The error values associated with the calculated values are due to the experimental error in the density values. Comparison of the sum of the mixture calculated shows that they are both resulting in the same mass value for the muscle phantom of 4700 gms.

Table 3.5: The amount of water required for the dynamic muscle phantom simulation

Site of Measurement	Amount of H_2O in ml
1. Muscle phantom	3071.25
2. Saline Solution Reservoir [2 * (25 * 3 * 7)]	1050.00
3. Plastic tubings and inside pump	245.00
(ml of H_2O)	4366.25

To calculate the total amount of salt required for a solution of c = .114 moles/l it was first necessary to measure the total amount of water in the system. In Table 3.5 the different amounts of H_2O measured are shown as well as the value of the sum. The amount of salt in (gm/l), that corresponds to c = .114 mole/l is 6.67 gms/l which means that the total amount of salt required for 4.36625 l of H_2O is = (6.67 gms/l * 4.36625 l) = 29.123 gm.

Therefore, for setting up the experiment, 1629.69 gms of fiberglass sheets were weighed and arranged inside the box, which were followed by 4366.25 ml of saline solution (c = .114 mole/l). By turning the pump on the saline solution was distributed in its respective positions and the fiberglass sheets were allowed to mix evenly with the saline solution.

3.5.3 CONSTRUCTION, CALIBRATION AND TESTING OF THERMOCOUPLE PROBES

The testing and assessment of the suitability of the dynamic phantom required an appropriate thermometry system that would record temperatures at predetermined points inside the phantom. There are various thermometry systems available for this purpose such as fiberoptic probes that can provide very accurate readings without interfering with the irradiating fields, which, however, are very expensive and have limited number of sensors available. Thermocouple arrays, on the other hand, are of equivalent sensitivity and provide the advantage of multiple temperature recording junctions per sensor probe and relatively cheap and easy manufacture. They are however, susceptible to interfering with the irradiating field and there is

Figure 3.4: Thermocouple array; A partial schematic representation of the copper-constantan (a-b) thermocouple wires and the protective plastic tubing.

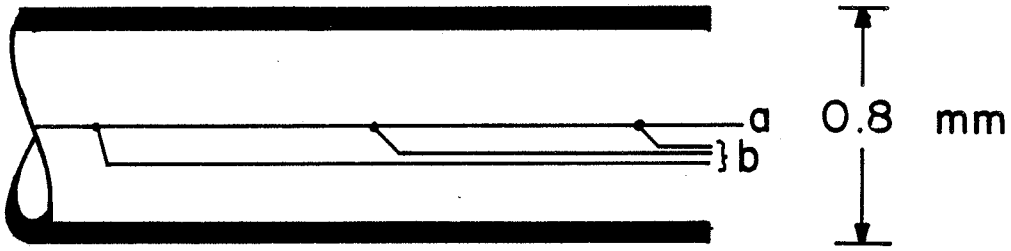
a
b
0.8 mm

induction of self heating on their metallic leads.

The thermometry system selected for the phantom testing consisted of two thermocouple arrays with four junctions in each of them. The four junctions were spaced at (10 ± 1) mm apart thus covering a depth of 3 cm inside the phantom and therefore providing an adequate number of readings for evaluating the phantom. (Figure 3.4)

The construction of each array involved a copper bus wire (diameter: 50 μm) and four constantan wires (diameter: 50 μm each) soldered on it according to the spacing mentioned above. The fragile array is protected inside plastic tubing of outside diameter equal to 0.8 mm and is connected to an AD 574, 12 bit analog to digital converter, with a circuitry that presents a (± .06 °C) fluctuation range in the data readings of temperature.

The thermocouple arrays were calibrated to a temperature range of about 10° C, i.e. covering the range of (20 - 29.5)°C using one of the clinical programs available for calibration of the temperature sensors (Appendix B).

It was mentioned earlier, that one of the disadvantages associated with the use of thermocouples is the resulting disturbance of the microwave field due to their metallic nature. However, appropriate positioning of the array relative to the applicator and monitoring of the power output of the applicator in such a manner as to minimize the negative effects in the thermocouple performance, and thus make its presence possible inside the phantom while the field is turned on. The testing of the field interference in the thermocouple performance was conducted as follows: the array was positioned inside the phantom with no flow present, perpendicularly to the irradiating

Figure 3.5: The interference and self-heating effects on the performance of a normal thermocouple junction due to exposure to EM fields of 15 Watts and 25 Watts.

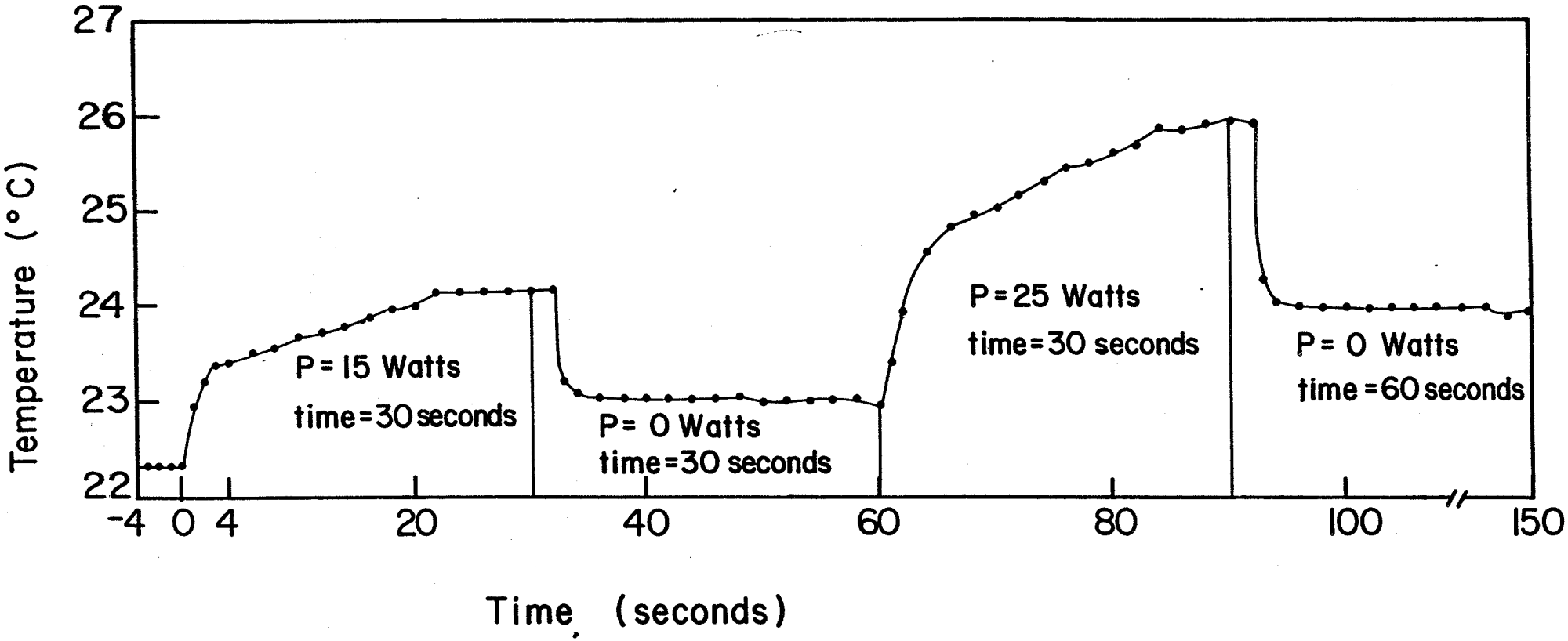
27
26
25
24
23
22
Temperature (°C)
P = 15 Watts
time = 30 seconds
P = 0 Watts
time = 30 seconds
P = 25 Watts
time = 30 seconds
P = 0 Watts
time = 60 seconds
-4
0
4
20
40
60
80
100
150
Time (seconds)

field, in order to minimize any interference effects. While the field was turned on, readings were recorded for 30 sec intervals of heating at 15 and 25 Watts respectively and for 30 sec and 60 sec intervals of cooling, i.e. while the field was turned off. In Figure 3.5 the respective readings are plotted versus time and the following was concluded. It can be seen from the plot that there are no significant interference effects (i.e. not abrupt changes in temperature pattern but gradual decrease indicating the self heating of the probe) at these power outputs there is an obvious self-heating of the thermocouple wires that lasts for a time interval measured in time constants of the probe after the field is turned off.[98] This self heating of the probe can result in overestimation of the temperature if the temperature recording starts immediately after the field is turned off. However, if measurements are recorded after the time interval of decay of the self heating is over, it will not affect the results.

The determination of the time constant of the probe was required in order to calculate its response time. Time constant values were determined for four different thermocouple configurations. These were the following:

1. a bare thermocouple (i.e. without any protective coating, just the two wires
2. a normal thermocouple (i.e. encapsulated in plastic tubing)
3. a normal thermocouple inside an air filled plastic tube of larger diameter
4. a normal thermocouple inside a water filled plastic tube of larger diameter

The procedure involved a constant temperature circulating bath (step rise from room temperature $\simeq$ 6°C) and the thermocouple-computer arrangement. The thermocouple temperatures were recorded every .5 seconds using the program "COOL" (Appendix B). The array was instantly immersed in the bath at a predetermined position and held there until the true bath temperature was registered on the recording device and for a few seconds afterwards to ensure that the bath temperature is steadily recorded. The time constant k_p is to be represented according to the following theoretical expression, and is a measure of the time required in seconds for the temperature of the probe to increase in such a manner as ΔT is decreased to $(\Delta T_o)e^{-1}$. [99,7]

$$\Delta T = \Delta T_o e^{-t/k_p} \qquad (3.17)$$

where ΔT = the difference between the indicated temperature and the final temperature.

ΔT_o = the step rise in temperature

t = time

In Figure 3.6 the plot of the temperature (T°C) as a function of time is shown as obtained from the experimental measurements for the four different configurations of the thermocouple array. By applying equation (3.17) to each of these curves the determination of the specific k_p can be accomplished.

In Table 3.6 the values of k_p are shown as they were determined from the experimental measurements. It can be seen that the longest k_p (sec) is that corresponding to the normal thermocouple inside an air filled tube. It has been reported from previous experiments in

Figure 3.6: The experimental measurements of the rise in temperature for the four different thermocouple configurations are plotted as a function of time in order to determine their respective time constants according to equation (3.17).

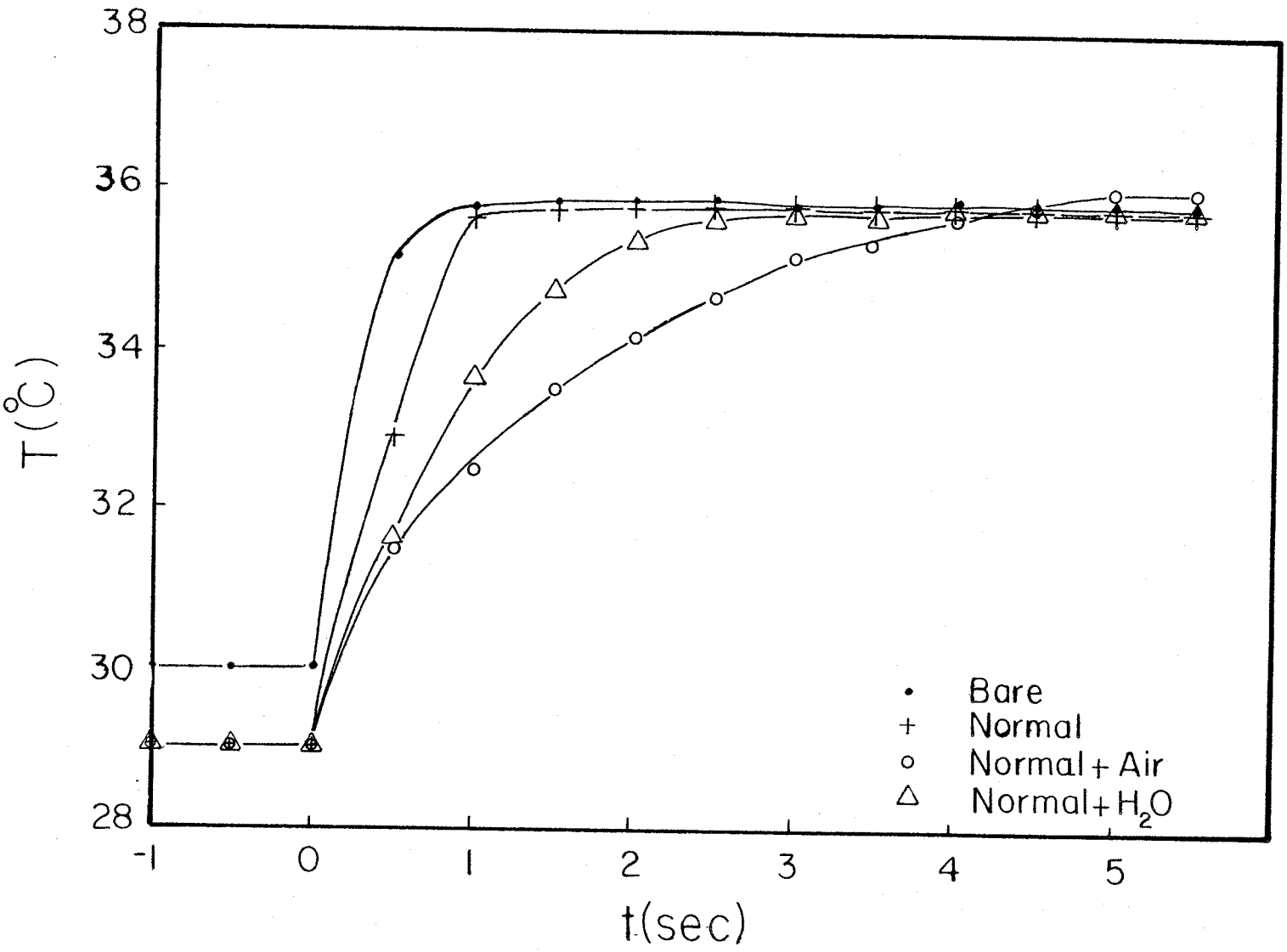
38
36
34
32
30
28
T(°C)
-1
0
1
2
3
4
5
t(sec)
Bare
Normal
Normal + Air
Normal + H2O

Table 3.6: The time constant, k_p values are determined for four different thermocouple configurations from experimental measurements in a constant temperature bath.

Type of Configuration of Array	k_p (sec)
1. Bare	0.268
2. Normal	0.580
3. Normal + Air	1.830
4. Normal + H_2O	0.984

our lab[7] that the time constant of the probe decreases if the medium between the normal thermocouple is water and it decreases even further if that medium is an oil based liquid. The measurements with air and water performed in this experiment reconfirm the former observations. A reexamination of Figure 3.5 in terms of the decay of the self heating of the normal thermocouple exposed to microwave heating shows the decay time to be equivalent to 3.5 time constants for both cases of 15 W and 25 W power input. This means that due to self heating of the thermocouple the temperatures recorded for 3.5 time constants after the field is shut off are incorrect because they provide overestimated readings of the temperature and they should not be considered as experimental results.

4.1 PHYSICAL AND THERMAL ASSESSMENT OF THE DYNAMIC PHANTOM

4.1.1 DENSITY STABILITY OF THE PHANTOM VOLUME

The dynamic phantom was assembled by placing the predetermined amounts of water and fiberglass (Ch. 3: Simulation and Design) into the supporting box constructed to house the phantom. The required amount of NaCl was not included in this first stage of assessment, because its presence would not have affected the outcome of the density stability tests or the flow rate measurements that followed. It should also be acknowledged that the extra amount of water found in the side reservoirs, the tubing and the pump, that has been accounted for elsewhere in this report, was included for these measurements.

After the phantom was assembled and for the following seven day interval, measurements were taken daily regarding the level of the mixture inside the box. The height of the phantom was designed to approximate three depths of penetration (theoretically d = 2 cm for f = 2450 MHz), that is a value of 7 cm was considered when estimating the masses of the constituents involved in the physical model. The measurements were recorded at the beginning of each day and the following observations were made. In the course of the seven days, the overall sinking of the fiberglass layers along the central region of the phantom changed the level of the phantom by (-2 to -3) mm in this region and along the sides the change was very small, namely -1 mm.

A way of correcting for this change is to rearrange the fiberglass layers to their correct position, whenever the measurements indicate that it is needed. The fact that the fiberglass has been

packed in the form of plane sheets made of thin fibers ensures the reproducibility of the arrangement. However, the problem was not considered solved in this way and it was considered incomplete until the NaCl was added to the phantom. After the NaCl addition the phantom was tested by heating it, at the 7 cm level and after the sinking had occurred, to finally find that the dielectric behavior of the phantom along the central region stayed the same regardless of the small changes in its density due to sinking, i.e., the depth of penetration measured experimentally did not change.

4.1.2 TESTS FOR NATURAL CONVECTION

Natural convection is defined as the process in which the motion of a fluid is due solely to the presence of a hot body in it, giving rise to temperature and hence, density gradients, the fluid thus moving under the influence of gravity. The generation of natural convection currents in the phantom when it is heated would result in the overestimation of its thermal conductivity. Natural convection and its effects on the thermal behavior of dynamic phantoms are very important and mostly observable in dynamic phantoms operated at very low flow rates. The dynamic phantom designed for this project is tested for natural convection generation at the "no flow" state in order to find out the extent to which the phenomenon takes place and determine the effects of natural convection, if any, at low flow rates. The experimental set up for the natural convection testing included: A power supply; a resistor of the smallest size possible (i.e. 10 mm in length and 3 mm in diameter) for avoiding the

disturbance of the tissue like phantom material, which was implanted 5 cm deep into the side of the phantom; a thermistor probe that was used to register the temperature changes in the immediate neighborhood of the phantom-resistor assembly; a timer and a water soluble dye (1 cc) that was intended to provide a means of detecting any subsequently generated natural convection currents.

A temperature rise of 1° C/min in tissues requires a power input of about 100 watts per kg of tissue. The heating scheme of the test was modeled after the above statement with the resistor replacing the high water content tissue and solving for these conditions we found that a power input of 7.1 mW was the corresponding value for the resistor assembly in order to achieve this rate of temperature rise. However, a steeper gradient in temperature was required to study the natural convection in relation to experimental temperature gradients obtained during hyperthermia studies. The temperature step rise used was that of 5° C/min which corresponds to 35.5 mWatts of power input. The particular reason for choosing the side of the phantom to perform the test was that it offers the best visual advantage for detecting and measuring any natural convection currents that could result. The heating was administered for one minute intervals for three different trials and there was no significant change in the length and width of the dye distribution around the resistor-phantom assembly, which were measured to within $\pm$ 1 mm. It was, therefore, concluded from these tests that there are no natural convection currents generated in the phantom material during no flow heating, and consequently there will not be a resulting overestimation in the thermal conductivity of the phantom material.

4.1.3 FLOW STUDIES: STABILITY, UNIFORMITY AND REPRODUCIBILITY OF FLOW

The stability of the flow of saline through the phantom was studied and there was first discovered that the flow rate was dependent on the respective positions that the phantom-pump system had relative to each other. The changes in the flow rate were caused by the back pressure developed inside the pump when its position was changed relative to the phantom's surface. To study the back pressure effect on the flow rate, the pump was disconnected from the phantom and its inlet and outlet hoses were placed inside two beakers. The beakers were positioned at different heights relative to the pump and the flow rate was measured at the outlet beaker (mls of water accumulated in the outlet beaker over 1 minute). The variation of the flow rate at the different heights ranged from 590 ml/min to 750 ml/min. The above trials indicated a substantial effect from the developing back pressure in the pump and thus necessitated the positioning of the pump-phantom system on a permanent set up relative to each other throughout the experiments in order to avoid fluctuations in the flow stability. In addition to these position dependent trials the flow stability was studied in terms of linear velocity, over operation intervals equivalent to the time required for the experimental measurements (i.e. up to a maximum of 30 min). During each 30 min interval there were three linear velocity measurements accomplished over the central axis (distance traveled = 12.5 cm; and the time of travel over the 12.5 cm). These short term stability trials showed an average variation on the linear velocity of

about 1%. The long term stability was determined by compiling the averages of the four 30 minute interval tests resulting in a variation of about .5% in the linear velocity. The effect of the flow variation during the experiments is considered to be very small, practically non-existent, regarding the effects of other experimental factors that are going to be discussed in the following sections.

The flow distribution of the dynamic phantom was designed to be uniform and unidirectional throughout the phantom's volume. Although all the practical design considerations were planned as to accommodate these requirements, the flow had to be tested in order to verify its uniformity and direction.

The uniformity tests were performed over a (15 x 20) cm area centered at the center of the phantom's surface and at three different depths of 1, 2 and 3 cm inside the phantom. There were five axes of measurement along the 20 cm side with 4 points of measurement on each of the axes. The distance between each two axes and each two individual points is 5 cm respectively. In figure 4.1 the working surface described here is shown, with all the 20 points for measurements noted. The measurement of flow rate inside the phantom was obtained as follows: A standard quantity of water soluble dye (i.e. 1cc) was injected into the phantom at the prearranged points, one at a time, and the time required for the dye to appear on the other side from that it was injected at, was recorded along with the distance of travel (i.e. the distance between the injection point and the edge of the diametrically opposite side).

By recording the time and the distance of travel, the linear velocity of the saline through the phantom is calculated at the three

Figure 4.1: The plan of the phantom's surface used for the flow uniformity tests (the shaded area is the working area; 15 x 20 cm^2).

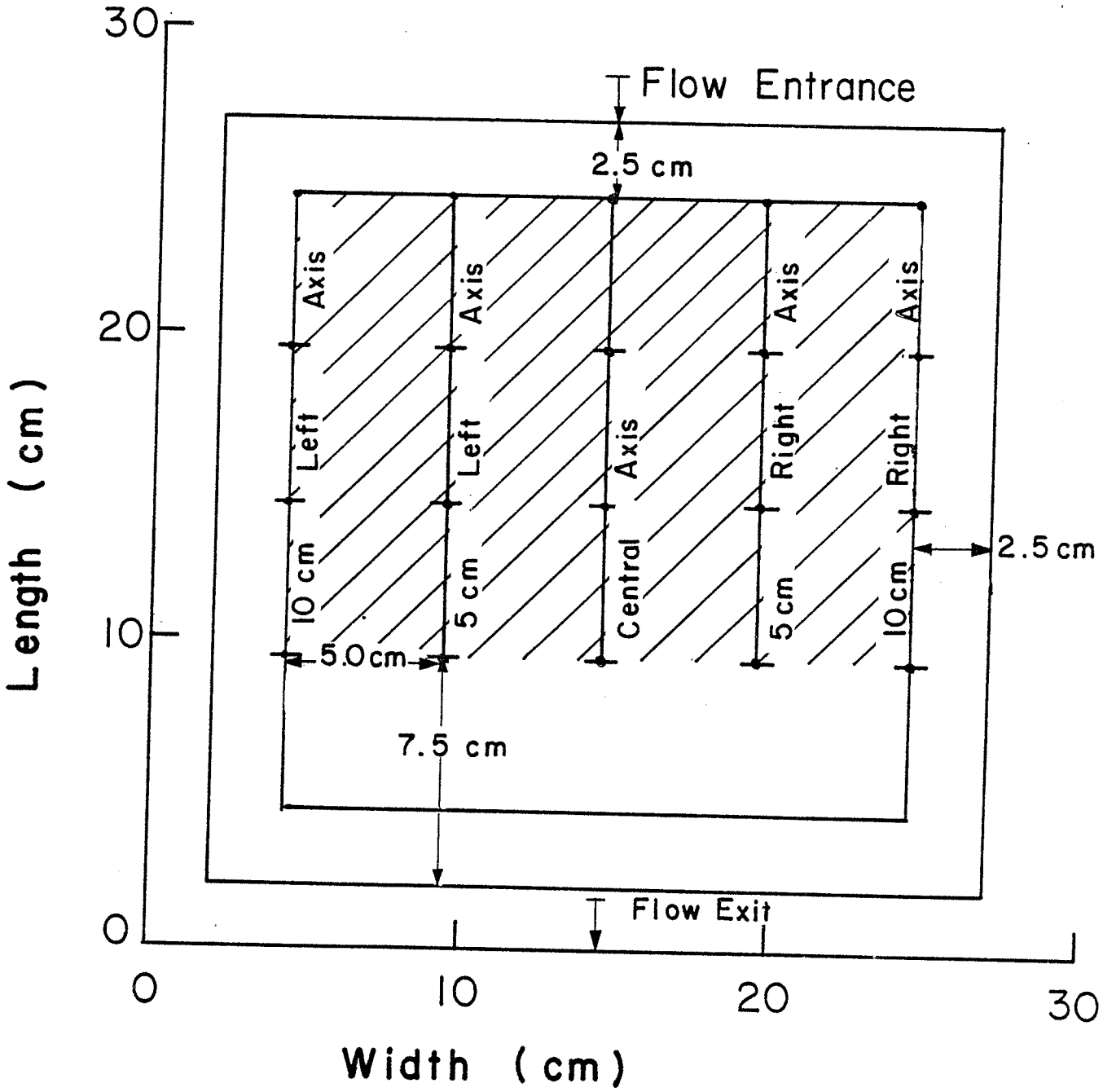
Flow Entrance
2.5 cm
Axis
Axis
Axis
Axis
Left
Left
Axis
Right
Right
10 cm
5 cm
Central
5 cm
10 cm
5.0 cm
2.5 cm
7.5 cm
Flow Exit
30
20
10
0
0
10
20
30
Length (cm)
Width (cm)

different depths inside the phantom. The time measurements were all performed under the same conditions; that is, the same flow rate, the same amount of dye was used (1cc) at the same points of injection while the phantom density distribution was undisturbed and subject to the random sinking of the fiberglass layers which as discussed previously (Section 4.1.1) is of minor importance. In Figures 4.2, 4.3 and 4.4 the linear velocity is plotted against the distance of travel for the three respective depths indicated. A study of the graphs indicates that the flow is relatively uniform across the areas studied, the uniformity improving with depth. The reason for this happening, is that in the upper parts of the phantom the pressure of the overlaying fiberglass layers is less than that in the lower parts of the phantom, thus allowing the flowing saline to achieve a faster and less uniform linear velocity. Furthermore, the slight sinking of the fiberglass layers at the center of the phantom may be the cause for the slower flow rate along the central axis and the faster on the side axes due to the increased resistance to flow in the center (i.e. increased density of the fiberglass-saline mixture) which causes the side flow resistance to decrease along the 5 cm to the left and right axes (i.e. decreased density of the fiberglass-saline mixture).

Another observation resulting from the study of the linear velocity graphs, is that the linear velocity decreases with depth. This again can be attributed to the increased pressure exerted by the overlaying layers of fiberglass which weight causes the overall flow to slow down at the deeper levels of the phantom.

In addition, during the flow rate trials it was observed that, when the circulation system was operated at a lower flow rate, i.e.

Figure 4.2: The flow uniformity at 1 cm below the surface of the phantom. The linear velocity is plotted as a function of distance of travel.

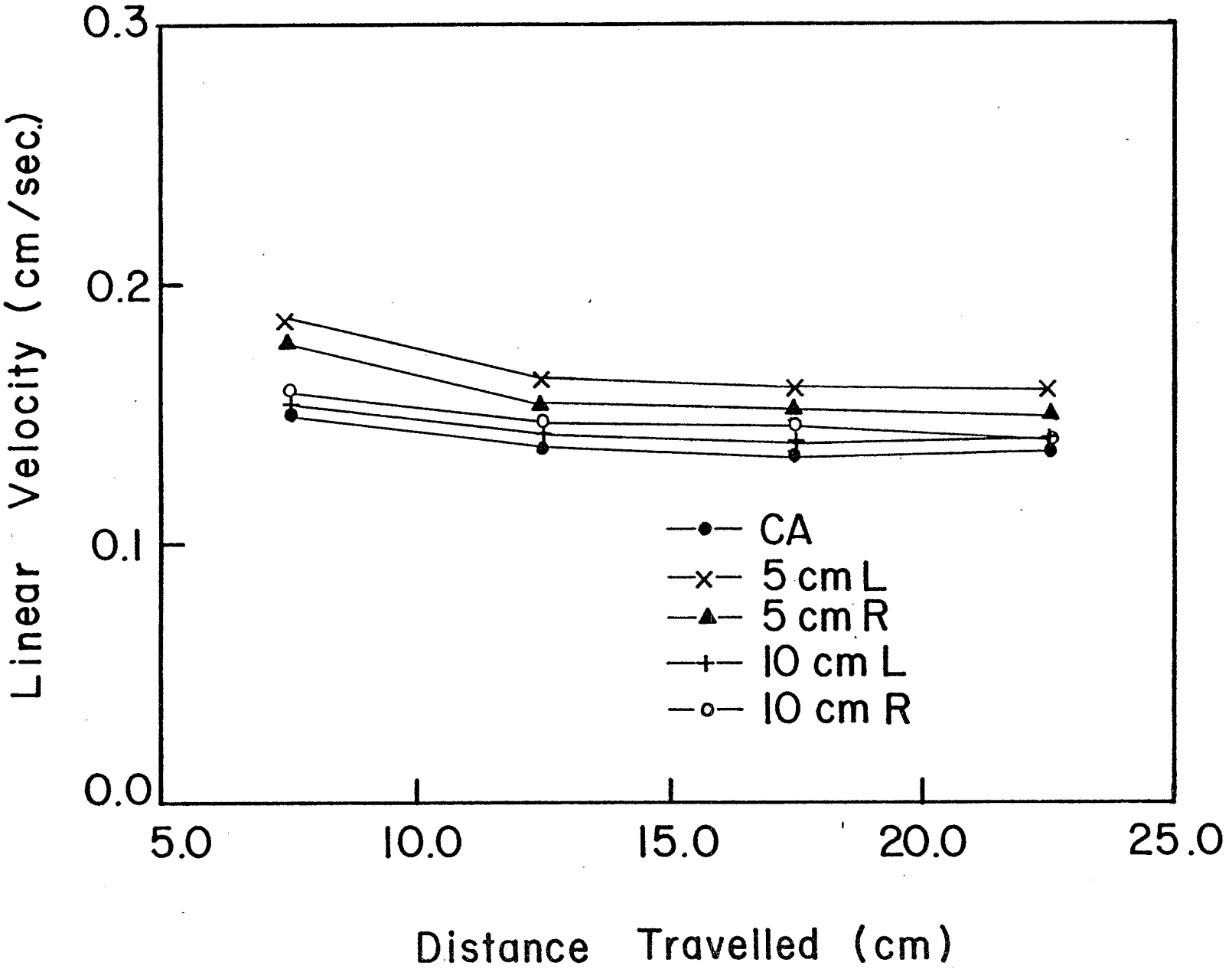
0.3
0.2
0.1
0.0
Linear Velocity (cm/sec.)
5.0
10.0
15.0
20.0
25.0
Distance Travelled (cm)
CA
5 cm L
5 cm R
10 cm L
10 cm R

Figure 4.3: The flow uniformity at 2 cm below the surface of the phantom. The linear velocity is plotted as a funciton of distance of travel.

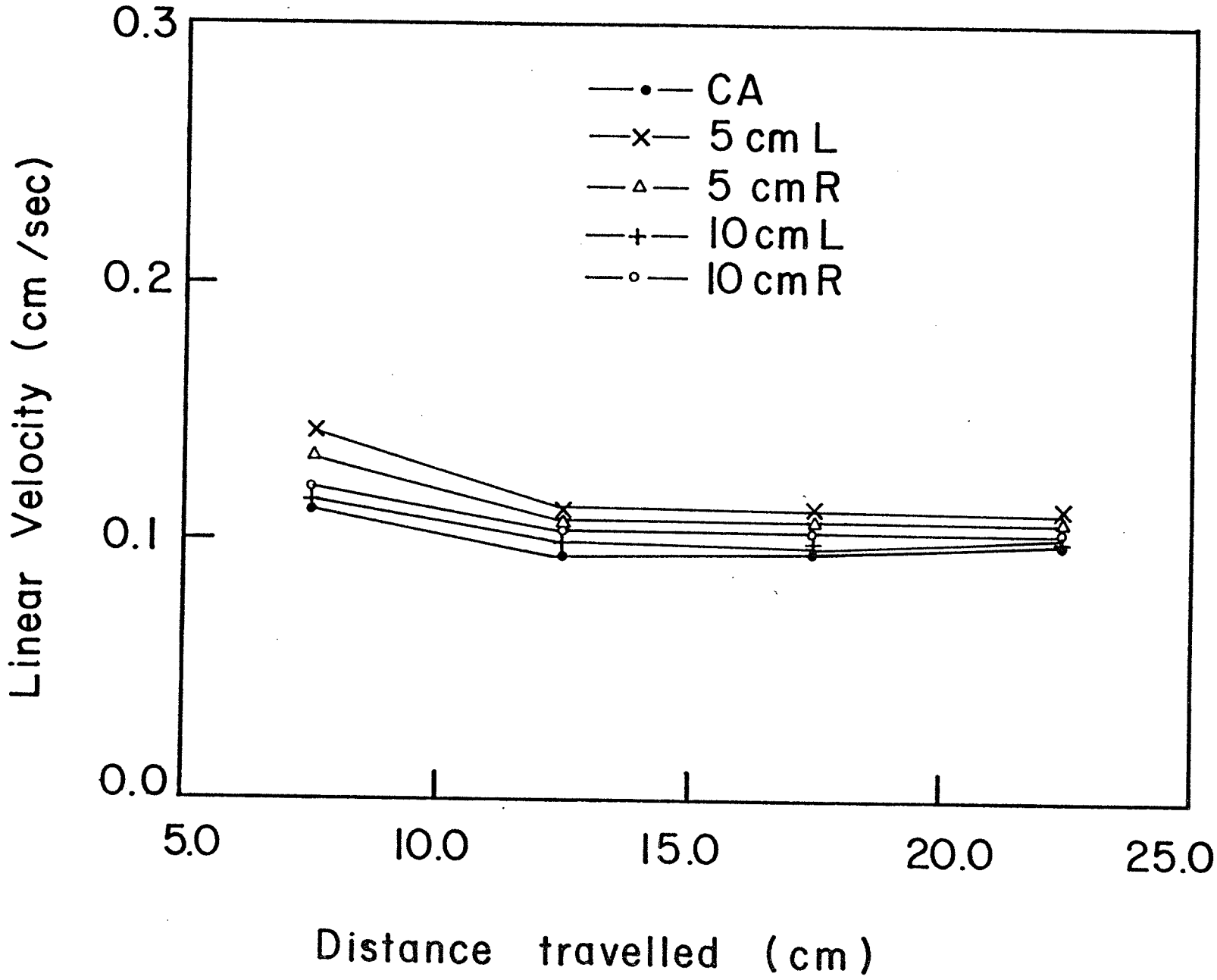
0.3
0.2
0.1
0.0
Linear Velocity (cm /sec)
CA
5 cm L
5 cm R
10 cm L
10 cm R
5.0
10.0
15.0
20.0
25.0
Distance travelled (cm)

Figure 4.4: The flow uniformity at 3 cm below the surface of the phantom. The linear velocity is plotted as a funciton of distance of travel.

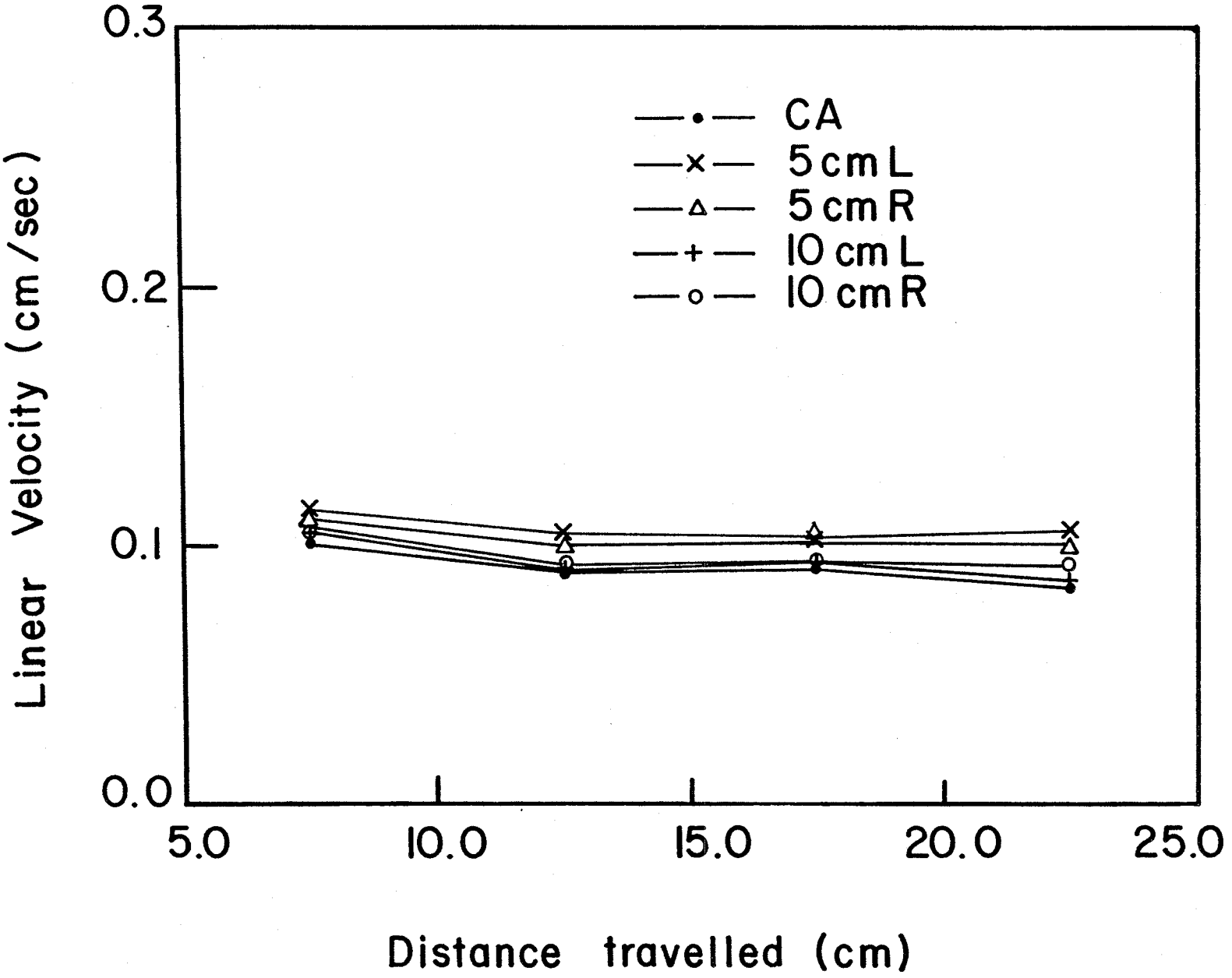
0.3
0.2
0.1
0.0
Linear Velocity (cm/sec)
CA
5 cm L
5 cm R
10 cm L
10 cm R
5.0
10.0
15.0
20.0
25.0
Distance travelled (cm)

linear velocity of .055 cm/sec. instead of the .15 cm/sec., the flow was more uniform throughout the test area. In Figure 4.5, the linear velocity is plotted versus the distance of travel at 1 cm depth, with the circulating system operating at approximately .055 cm/sec. It can be seen that the flow uniformity at the 1 cm depth level has increased greatly. Therefore, if a more uniform flow rate was desired than that obtained at the .15 cm/sec. rate, the flow rate could always be turned down to achieve it. However, this was not required since the measurements were performed at the central axis and the uniformity achieved at the higher flow rate was satisfactory for the experiments to be performed.

A requirement of the experiments that were to be performed, was that the flow should be reproducible in the short and the long term studies. For the short term variation study of the flow rate, four trials were repeated in the course of a day with the system operated in identical conditions for all four times (flow measurements were performed along the central axis, at a travel distance of 12.5 cm and at the 1 cm depth below the surface). The study for the long term reproducibility was carried out over the interval of four consecutive days by repeating the short term reproducibility procedure and averaging the values of the four daily trials. In Table 4.1 the short and long term variations of the flow rate are given in terms of the average linear velocity and the mean variation. In the short term the variation in flow reproducibility ranges between (3.7 - 9)% and in the long term the flow rate reproducibility variation is about 3.8%. This percent variation in the flow reproducibility is relatively low regarding the limited means of controlling the fluid circulating

Figure 4.5: The flow uniformity at 1 cm below the surface of the phantom at a lower flow rate (i.e. .055 cm/sec). The linear velocity is plotted as a function of distance of travel.

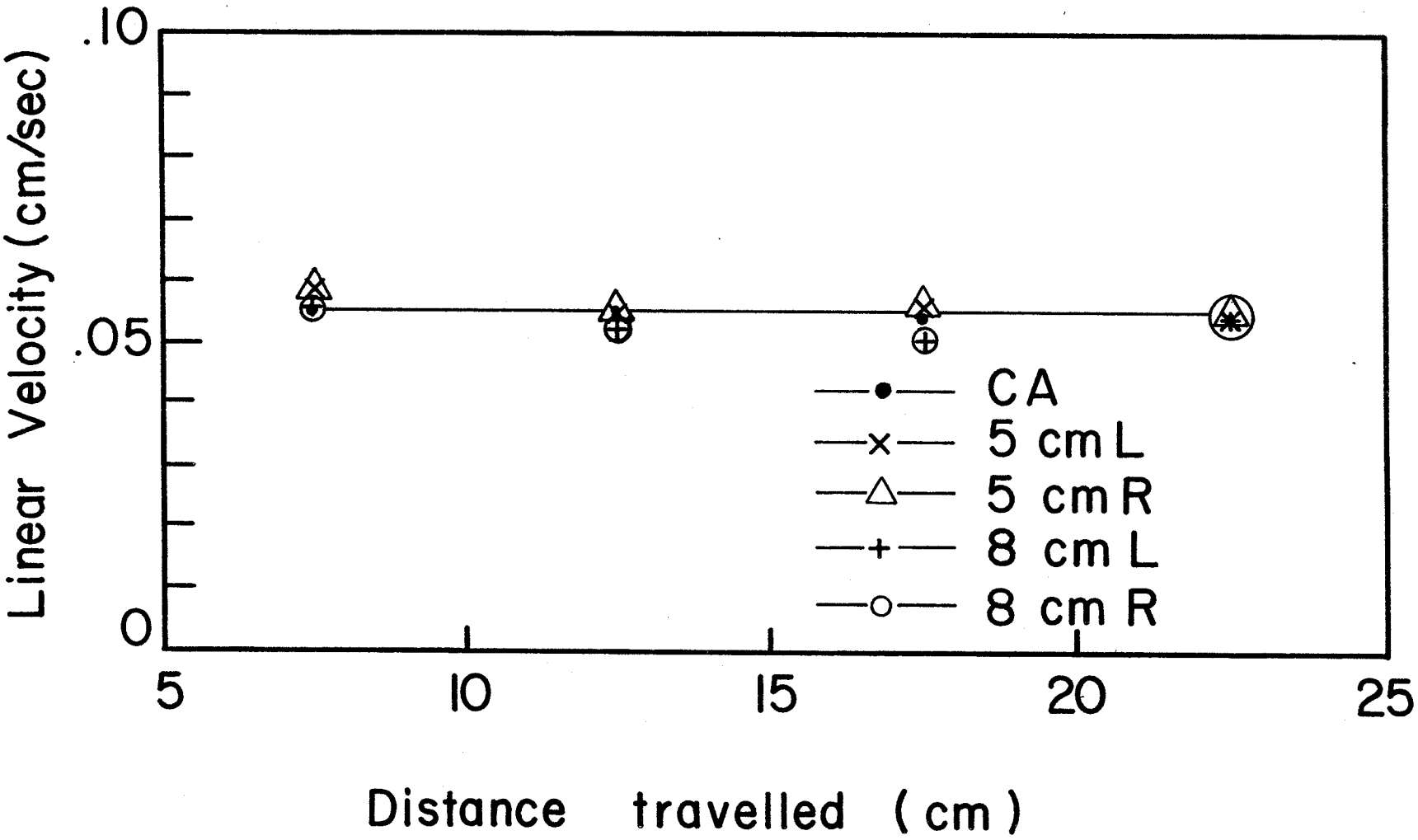
.10
.05
0
Linear Velocity (cm/sec)
5
10
15
20
25
Distance travelled (cm)
CA
5 cm L
5 cm R
8 cm L
8 cm R

Table 4.1: The short and long term variation in the reproducibility of the dynamic phantom's operational flow rate in terms of linear velocity (at 1 cm depth along the central axis; travel distance = 12.5 cm).

Trial Number	Linear Velocity (in cm/sec)			
	Day 1	Day 2	Day 3	Day 4
1	.140	.150	.160	.157
2	.150	.171	.160	.169
3	.160	.142	.160	.169
4	.150	.150	.170	.157
Short term Reproducibility (Ave. Linear Velocity $\pm$ σ) [% variation]	(.150$\pm$.007) [4.7%]	(.153$\pm$.014) [9%]	(.162$\pm$.013) [8.3%]	(.163$\pm$.006) [3.7%]
Long term Reproducibility (Ave. Linear Velocity $\pm$ σ) [% variation]		(.157 $\pm$ .006) [3.8%]		

(Note: σ is the standard deviation)

system and the other factors involved in the experimental set up (i.e. positioning of the applicator, thermocouples etc).

4.2 DIELECTRIC BEHAVIOR ASSESSMENT OF THE PHANTOM

4.2.1 ACCURACY OF THE SIMULATION

The testing of the phantom in terms of its dielectric behavior was undertaken after the addition of the required amount of NaCl and in Figure 4.6 the phantom and the equipment used for these studies are shown. It was, firstly, necessary to decide on the experimental set up to be used for irradiating the phantom, in terms of the thermocouple positioning inside the phantom and relative to the applicator, and the applicator positioning above the phantom. It was found from previous experiments with a static phantom that the shape of the EM-field produced by the microwave applicator available in our lab (TAG-MED; 2450 MHZ)[7] is of an elliptic form and that the 50 percent region of the field is 3.5 cm off the central axis, as per relative SAR measurements of the static phantom. It was therefore decided to implant the two thermocouple arrays at the center of the phantom and at 3.5 cm off the central axis at one of the x or y axes. The positioning of the thermocouple arrays was reproducible to within $\pm$ 1 mm. It was also secured that the thermocouples were positioned perpendicularly with respect to the applicators to avoid perturbation of the EM field, as it has been explained earlier. Previous tests with the static phantom have also indicated that the optimum placement of the applicator relative to the phantom surface, which results in the minimum reflected power, is at 1 cm above the surface.

Figure 1

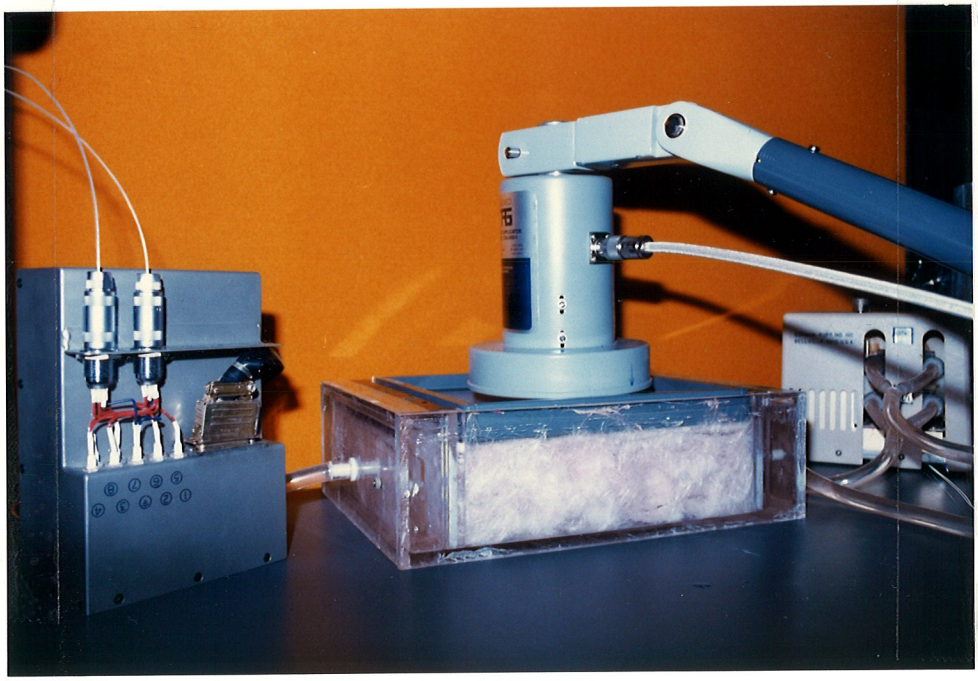

Figure 2

Figure 4.6: The dynamic phantom and equipment assembly used for the experiments of this work. (Figure 1; From left to right: Microcomputer used, dynamic phantom, flow pump, generator and applicator assembly. Figure 2; From left to right: Thermocouple assembly and their fitting box, dynamic phantom with the applicator, flow pump).

Furthermore, the shape of the field pattern requires the applicator orientation to be the same for all heating sessions if they are to be comparable. It was, therefore, very important to devise a set up that would be easily reproducible. To accomplish this task, the applicator opening was traced on graph paper and its center and 3.5 cm off the central axis points were recorded on the same paper. The whole figure was subsequently reproduced on the thin plastic layer that is used to prevent extensive evaporation of the water in the phantom. The stability of this arrangement was secured by the plastic tubing, which is used to protect the thermocouples from bending when they are being inserted into the phantom, and which were kept in place when there was not any heating administered to the phantom and the thermocouples were removed.

To test the accuracy of the simulation the dielectric behavior of the phantom has to be assessed, that is to measure the depth of penetration in the phantom and compare it to that theoretically predicted. The flow is shut off during this measurement because it does not alter or contribute anything to the dielectric behavior of the phantom. However, the flow was turned on before these measurements, to ensure uniform distribution of the NaCl throughout the phantom volume and it was turned off before the irradiation allowing enough time for the system to achieve the no flow state.

The theoretical depth of penetration corresponds to the distance inside the phantom at which the power falls off to e^{-2} of its initial value, ie 13.5% its initial value, and its value was calculated to be 2 cm at 2450 MHZ (as per Ch. 2)

The experimental depth of penetration was obtained by the

following method: The phantom was irradiated at 15 Watts for a period of time (~ 2 min) required to obtain a temperature rise of about 4°C registered on the monitoring thermometer, i.e. the thermocouple junction of the array that corresponds to the surface reading on the central axis. Temperatures were recorded using one of the hyperthermia programs available and they were subsequently printed out for the calculation of the relative specific absorption rate values (SAR).

The relative SAR values were calculated for the three depths inside the phantom (1.1, 2 and 3.1 cm), on the central axis and the 50 percent region (as per equation 2.7). The surface readings of the thermocouples were not involved in the calculations in order to avoid incorporation of the errors due to cooling generated at the surface from the existing temperature gradients between the heated surface and the ambient temperature.

The calculated values of the relative SAR were normalized to 1 at the value calculated at the 1.1 cm depth and plotted versus the exact depth inside the phantom. (Figure 4.7). The graph includes the theoretical relative SAR values to which the experimental values are compared. The depth of penetration is read off this graph and it is found to range between (2.01 - 2.1) cm.

Comparison between theory and experiment indicates satisfactory agreement to within (1 to 5)%.

It can be, therefore, concluded that a successful simulation was obtained experimentally, regarding the dielectric behavior of the phantom. However, these results are representative of the specific region of the phantom that was tested. The confirmation of these

Figure 4.7: Testing for the accuracy of simulation. The relative Specific Absorption Rates are plotted as a function of depth inside the phantom as they were recorded from theoretical calculations, and from measurements at the central axis and the 50% region. (depth of penetration: Theory; d = 2 cm, CA; d = 2.01 cm, 50%; d = 2.02 cm).

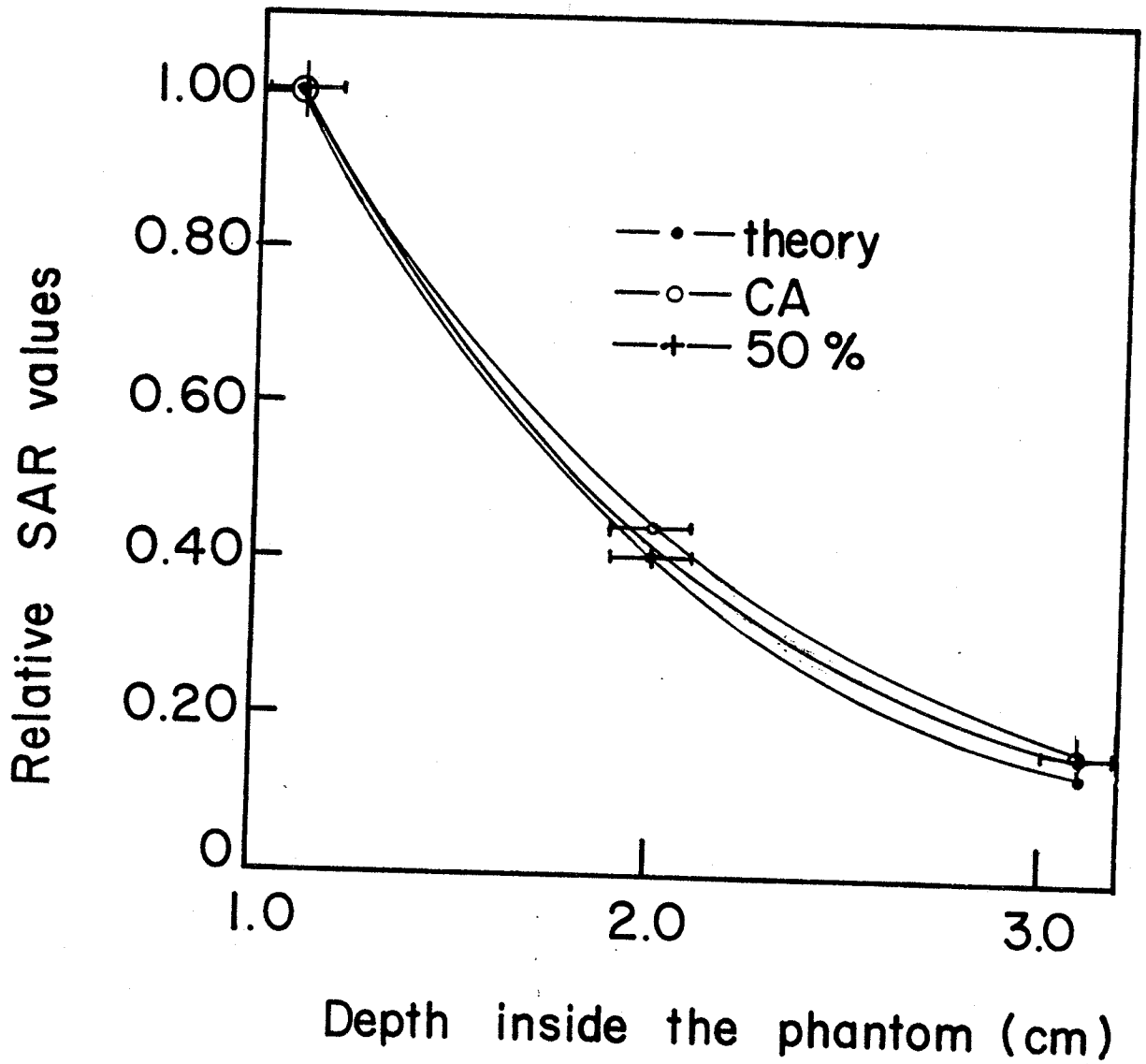
1.00
0.80
0.60
0.40
0.20
0
Relative SAR values
theory
CA
50 %
1.0
2.0
3.0
Depth inside the phantom (cm)

findings was obtained by performing a dielectric behavior homogeneity test at different sites of the phantom surface and the results are shown in Figure 4.8. The testing sites were at distances of about 5 cm from the center of the phantom and the measurements were performed in the same manner as described above. The values of the depth of penetration at the different sites on the phantom fluctuated between 2.1 cm and 2.16 cm, which corresponds to a 3 to 5% error when compared to the theoretically calculated value.

4.2.2 SHORT AND LONG TERM STABILITY OF THE DIELECTRIC BEHAVIOR

The dielectric behavior of the phantom is highly dependent on its respective water and NaCl content at microwave frequencies in the neighborhood of 2450 MHZ, which is the frequency of the generator available for these studies. It was observed since the phantom was assembled that water evaporation was occurring. However, this was an easily solved problem. By measuring the level of H_2O in the phantom volume and the side reservoirs the amount of lost water was found and replaced whenever the levels were below their predetermined values, i.e. 7 cm. After the addition of NaCl, however, it was observed that along with the water evaporation, NaCl was crystallized outside the phantom volume and thus, lost from the phantom resulting in changes of its dielectric behavior (i.e. depth of penetration etc.) that altered its response to microwaves. To measure the amount of salt lost in this manner the following method was used: the static electrical conductivity of solutions with different NaCl concentrations was measured and plotted; i.e. σ_0 versus concentration (c);(see Figure

Figure 4.8: Dielectric Behavior Homogeneity. The relative Specific Absorption Rates are plotted as a function of depth inside the phantom as they were recorded from theoretical calculations, and from measurements at the central axis and at three different sites over the surface of the phantom. (depth of penetration: Theory; d = 2 cm, CA and site measurements; d = (2.1 - 2.16 cm).

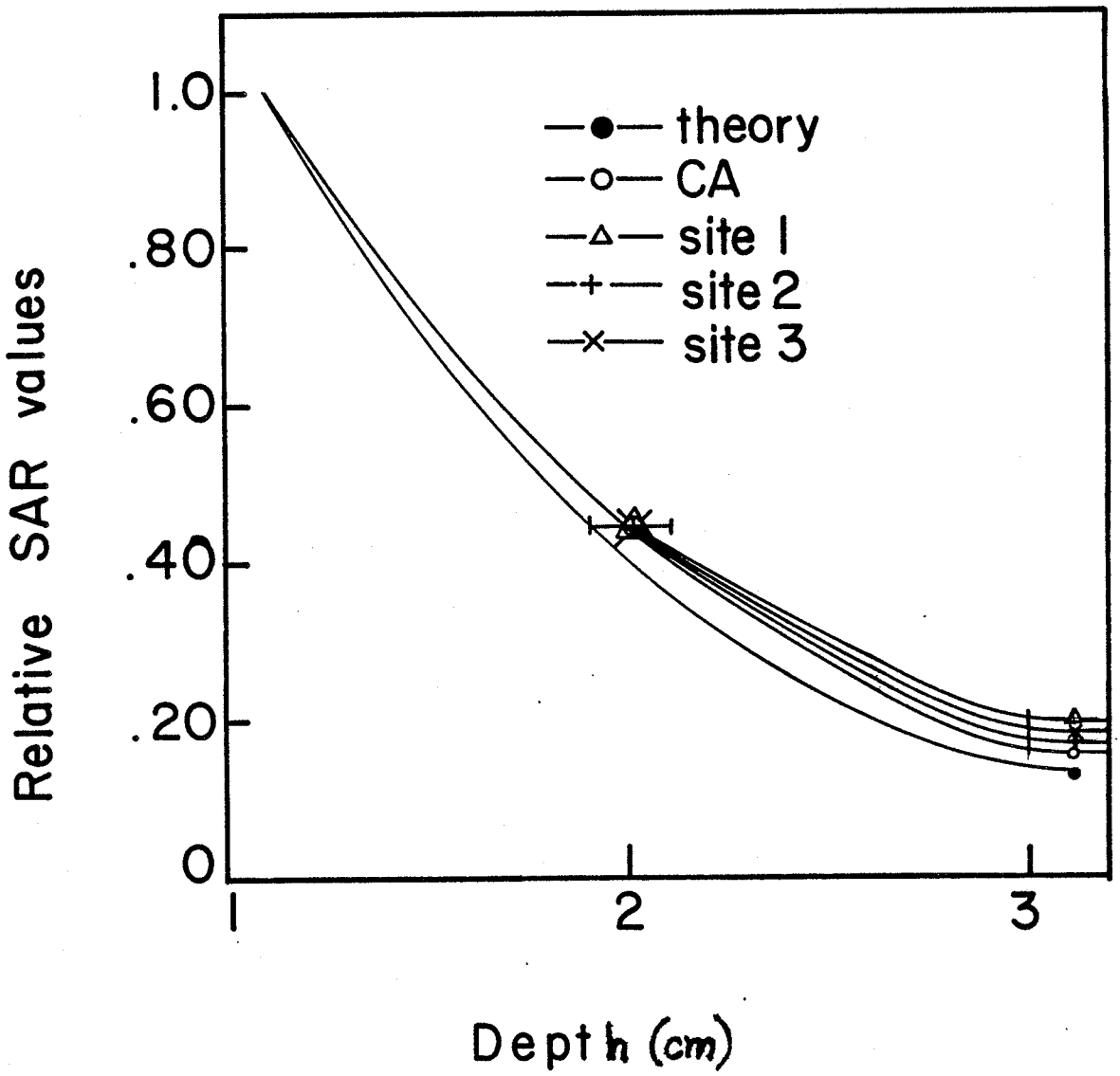
Relative SAR values
1.0
.80
.60
.40
.20
0
1
2
3
Depth (cm)
theory
CA
site 1
site 2
site 3

Figure 4.9: The static dielectric conductivity (σ_o) of the muscle phantom is plotted as a function of NaCl concentration (c) at 23.5° C temperature.

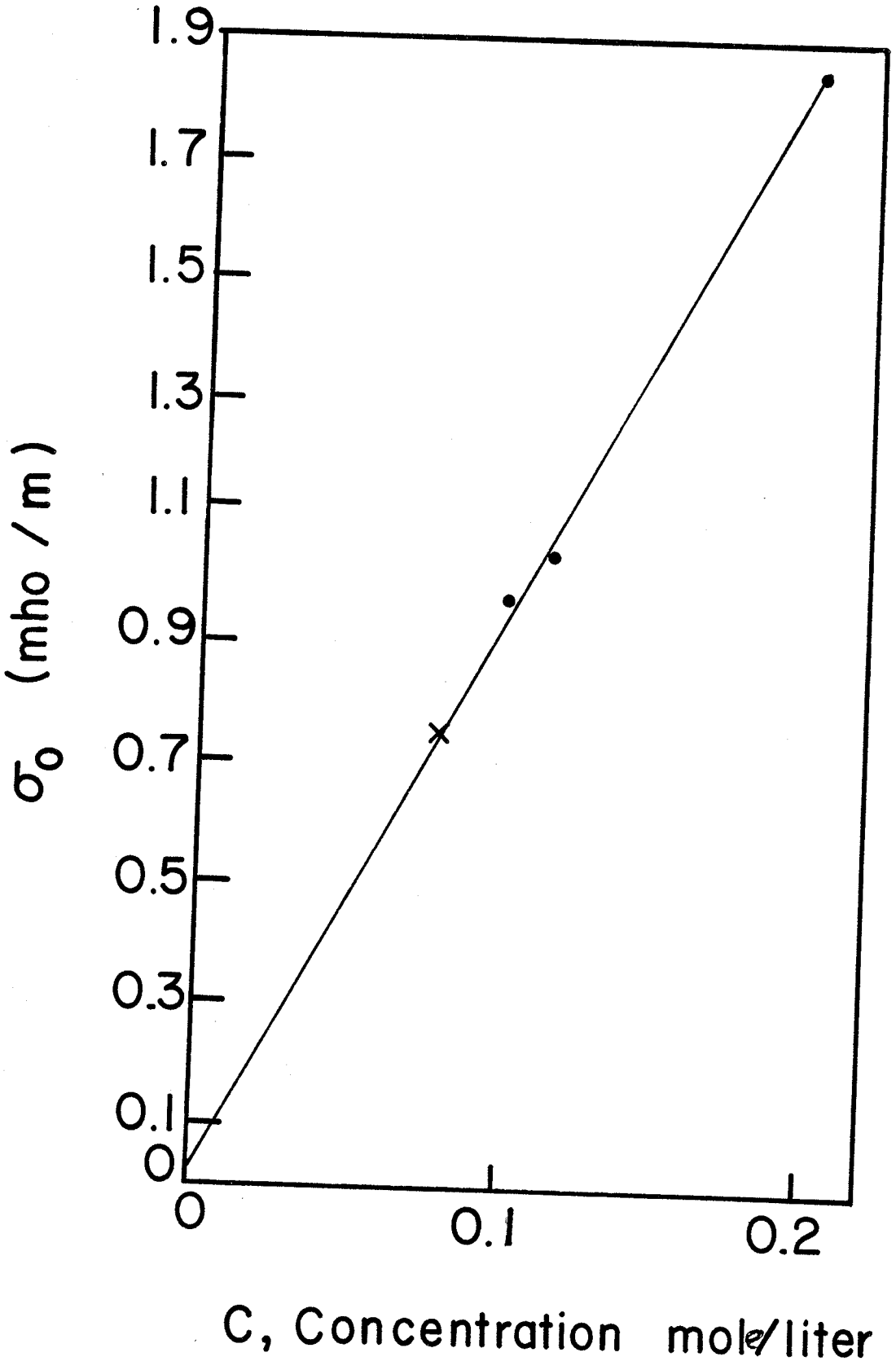
1.9
1.7
1.5
1.3
1.1
0.9
0.7
0.5
0.3
0.1
0
σ_o (mho / m)
0
0.1
0.2
C, Concentration mole/liter

4.9). The solutions were measured for a range from zero NaCl concentrations to .2 moles/liter, using a static conductivity determination probe which was calibrated using plain water i.e. c = 0 mole/l. These measurements covered the range within which the phantom's NaCl content is included (i.e. phantom NaCl content C = .114 moles/liter). The fact that σ_0 is temperature dependent required that all measurements be taken at the same temperature which was chosen to be the ambient temperature of the phantom (T = 23.5° C ± 1° C.)

The measurements were recorded at about two weeks time after the NaCl was added to the phantom. The value for NaCl concentration of the phantom that corresponded to its σ_0 measured was .078 moles/liter instead of the .114 moles/liter concentration originally existing in the phantom. In order to examine the effect of this change on the dielectric behavior of the phantom the value of the dielectric conductivity for the NaCl solution sample at 2450 MHZ was considered and the following values were calculated for the phantom: Its dielectric constant (ε = 47.72), electrical conductivity (σ = 1.59 mho/m) and its theoretical depth of penetration (d = 2.3 cm). It can be seen from these values that the loss of NaCl causes the conductive losses to decrease and thus results in the observed increase in the depth of penetration. The theoretical value of the depth of penetration (d = 2.3 cm) was subsequently compared to the experimental value measured for the NaCl concentration of .078 moles/l. The experimental value was found to be equal to 2.6 cm, that is 13% different (Figure 4.10) than the theoretically calculated value. After the lost amount of NaCl was replenished the measurement of d was

Figure 4.10: The effect of the change in the NaCl concentration on the dielectric behavior of the phantom. The relative Specific Absorption Rates are plotted as a function of depth inside the phantom [c = .114 moles/l: d_{theory} = 2 cm; d_{exptal} = 2.1 cm, c = .078 moles/l : d_{theory} = 2.3 cm; d_{exptal} = 2.6 cm]

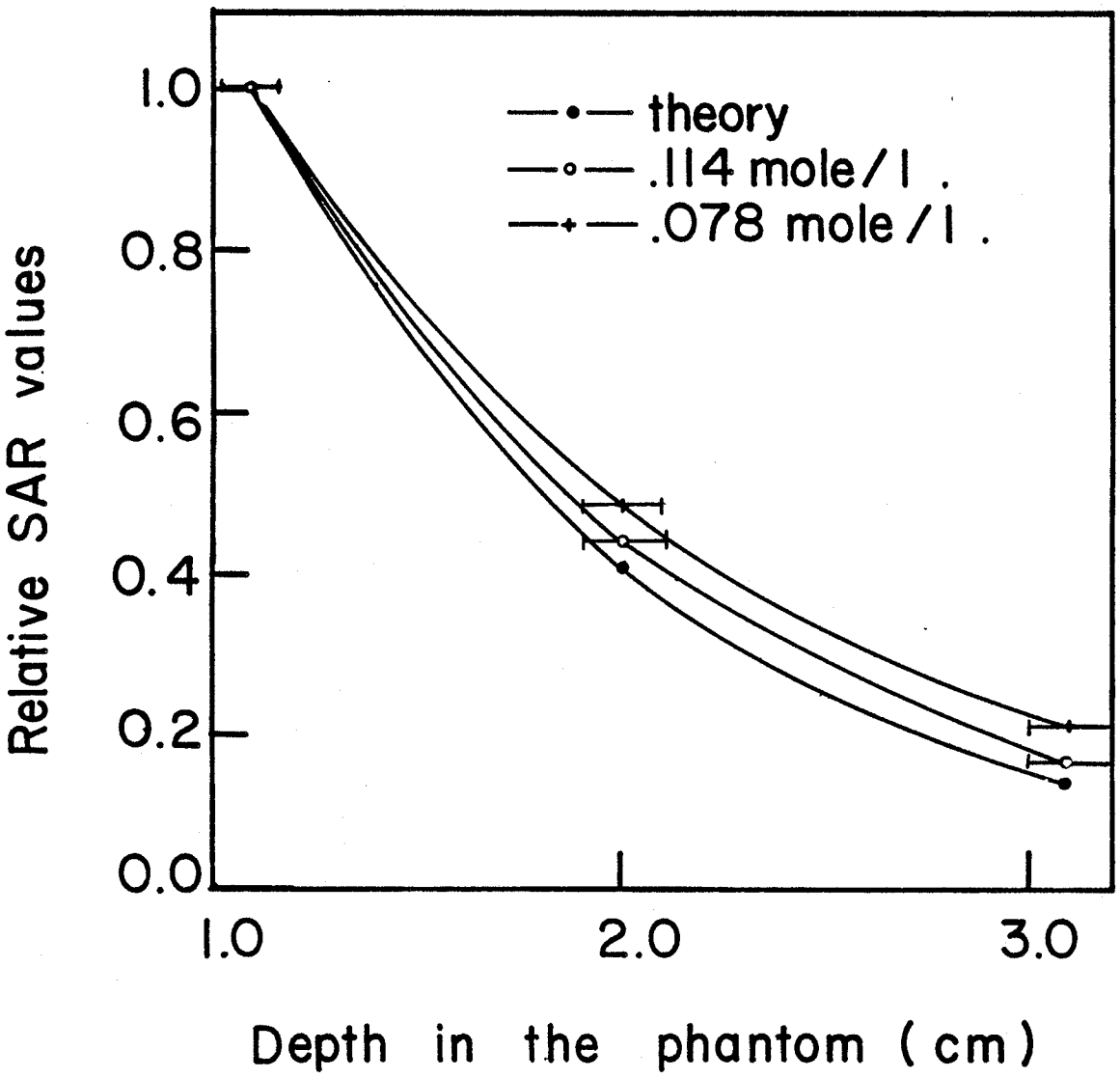
1.0
0.8
0.6
0.4
0.2
0.0
Relative SAR values
theory
.114 mole/l .
.078 mole/l .
1.0
2.0
3.0
Depth in the phantom (cm)

repeated and the value obtained was in agreement with the experimental value of d at the original NaCl concentration (C = .114 moles/liter; d = 2.1 cm).

The above measurements and calculations indicate that it is required to test the NaCl content on a weekly basis an d replenish whatever amount is lost, in order to be able to work under the assumed simulation standards.

5.1 INTRODUCTION

5.1.1 THE ROLE OF BLOOD FLOW IN THE DETERMINATION OF HYPERTHERMIA EFFECTIVENESS

Blood flow is the major factor in determining the heat dissipation in live tissues and therefore, it is of major importance to be able to predict it theoretically or measure it experimentally and eventually apply this knowledge to hyperthermia studies. There have been numerous documentations of normal or tumor tissue blood flow with respect to hyperthermia applications by various researchers.[100,101,102,103] However, these data cannot be directly applied to clinical hyperthermia treatments due to the fact that they resulted from observations of implanted tumors rather than spontaneously occurring ones and there might be a difference in their respective blood flows. Furthermore, there have not been any experiments concerning the regional blood flow of spontaneously occurring tumors exposed to fractionated hyperthermia.

These types of measurements are therefore valuable for qualitative comparisons to the clinical reality.

The temperature of a tissue subjected to hyperthermia is a function mainly of its blood flow and the heat input as long as the tissue is relatively insulated from external temperatures. This is because surface temperature not only depends on the blood flow but also on the tissue thermal conductivity, the evaporation rate, radiation and air convection effects.[104] It is therefore advised in blood flow studies to consider measurements that are recorded at a depth that can ensure the independence from such effects (i.e. 1 to

1.5 cm below the surface).

It has been indicated[105,26,28] that when normal tissues are subjected to hyperthermia they respond by an increase in their regional blood flow in order to dissipate the damaging heat from the heated volume. The regional blood flow continues to increase until a maximum blood flow is reached and after that it might be caused to decrease, if the heat load is too large and lasts too long, due to vascular occlusion.[106] Experimental data show that the induction time, ie the time for inducing maximum increase in blood flow, decreases with increasing treatment temperatures.[107] Manipulation of this tissue behavior in clinical applications can result in maximum effectiveness of hyperthermia in the treatment of tumors, while normal tissue is effectively protected from thermal damage. In this manner, an increased therapeutic ratio is achieved without any permanent impairment of normal tissue blood flow, since it returns to its normal flow rate within a few hours post-heating.[79,105,108]

5.1.2 THE THEORY

Through the years there have been many heat clearance measurements and theoretical models that were developed with various degrees of success (Gibbs 1933, Grayson 1952, Chaloner 1972, McCaffrey and McCook 1975, Castellana et. al. 1984, Milligan et. al. 1983 and 1985)[104] including the recent work by Shandhu (1986).[109]

Of relative importance in this study are the models and measurements developed by Milligan et al and Sandhu since the case under consideration is the study of thermal clearance for the

prediction of blood flow conditions under relatively small temperature gradients. In this case the study of blood flow conditions can be expressed by a simple exponential and exclude any conduction effects. A means for describing the temperature distribution inside the living tissue, theoretically, is through the so called bioheat equation which is the following:

$$m * \rho * c * \frac{\partial T}{\partial t} = \Delta \cdot (k\Delta t) + Q_b + Q_m \qquad (5.1)$$

where ρ = tissue density; c = tissue specific heat

m = mass of tissue; T = tissue temperature

Δ = gradient operator; k = thermal conductivity of tissue

Q_b = rate of heat exchange with blood;

Q_m = rate of metabolic heat generation

The experimental measurements are designed to record the blood flow effect on the temperature distribution during and after (thermal washout) the specific heat application. It is assumed that any changes are due to the blood flow rather than the thermal conductivity. Several researchers[110,70,111] have determined that the heat is eliminated through, mainly, the blood flow and that the thermal conductivity has a minimal effect in the bioheat equation regarding heat elimination, under conditions of low temperature gradients. However, when the temperature gradients become steeper it has been assumed that the conduction effects become considerable, but this is not the case in this study.[109] By exclusion of the k term in the bioheat equation it is obtained: $m\rho c\,(\partial T/\partial t) = Q_b + Q_m$ (5.2)

Considerations on the effects of metabolic heat generation show that the metabolic heat is relatively small compared to heat removal by blood flow and it can also be neglected; thus obtaining:

$$m\rho c\ \partial T/\partial t = Q_b \qquad (5.3)$$

According to Jain et. al.[70] who used the following simplification for the case when the tissue is subject to heat:

$$Q_b = w\rho_b c_b\ (T_a - T) \qquad (5.4)$$

where: w = effective perfusion rate; ρ_b = density of blood; c_b = specific heat of blood; T_a = arterial blood flow temperature.

By substitution of eqn (5.4) into (5.3) and assuming $\rho \simeq \rho_b$ and $c \simeq c_b$ the following expression is derived: $\partial T/\partial t = -w\Delta T$ (5.5) where $\Delta T = T_a - T$.

Since w is a constant through a particular washout period equation (5.5) is solved and results in:

$$\Delta T = \Delta T_o e^{-wt} \qquad (5.6)$$

It has been shown that equation (5.6) does not entirely describe the situation of heat transfer between real tissue and regional blood flow. For the purposes of the dynamic phantom however, equation (5.6) suffices, in order to describe the thermal clearance, since there is no increase in the blood flow rate during heating; the blood flow rate remains constant throughout the hyperthermia application.

5.2 EXPERIMENTAL MEASUREMENTS

5.2.1 MATERIALS AND METHODS

Thermal clearance measurements were performed on the dynamic phantom in order to determine a relation of the blood flow rate and the temperature fields originating at different flow rates. All measurements were performed at 1 cm depth inside the phantom on the central axis of the microwave field distribution area. Thermal

clearance data were obtained for 1 min after a steady state temperature was reached at a temperature rise of ΔT_o = 3° C from the ambient temperature of the phantom. Data were obtained for three thermocouple configurations regarding the medium surrounding the copper-constantan leads; that is, no medium (bare), the protective plastic tube casing (normal), and finally the clinical configuration of the thermocouple (normal in a plastic tube filled with air). Temperatures were recorded using the program "COOL" at half a second periods. During the course of the treatment, the thermocouple was left in place for avoiding any positioning variations since the effect of the metallic probe in the vicinity of the field resulted in minimal distortion of the data (see Chapter 3).

Phantom tissue was heated using the 2450 MHZ generator equipped with an approximately circularly polarized round applicator. The power input was controlled to achieve the desired rise in temperature in a minimum amount of time, but never exceeding the 30 W power input. The time of heating was relative to the flow rate used, the higher the flow rate the longer the time needed to achieve a steady state temperature. Treatment times ranged from a few minutes to an allowable maximum of 15 minutes, in order to avoid a temperature rise of the whole phantom system rather than the treated area only. There were three different flow rates used for these measurements i.e. 33 ml/min, 44 ml/min, 53 ml/min. The choice of these values was based on the values reported in the literature for human muscle and the limitations of the supporting equipment (i.e. pump). The values of the flow rates stated above were calculated with respect to the linear velocities and the cross section of the area considered [i.e. a

rectangular of (10 x 1) cm^2] The thermal clearance curves were constructed from the data collected and analyzed for the 1 minute period data collection.

The determination of the perfusion constant was achieved and the effects of the various experimental parameters (thermocouple configuration, blood flow rate, positioning) on this value were studied. During the experimental process, it was observed that the temperature of the phantom would increase without any administration of heat. This heating was linked with the heating of the pumping system. To study the effect of the pump induced heating on the overall temperature distribution of the phantom, the temperature was monitored on the central axis for time intervals of 15 minutes (time allowed for the system to stabilize) and 20 minutes. Several trials were performed to monitor the temperature of the system while no external heating was applied. The heating due to the pump varied with flow rates, resulting in a 20% increase of the step rise in temperature (ΔT) at high flows (i.e. about .150 cm/sec), and an 8% increase of ΔT at low flow rates (i.e. of about .055 cm/sec). Further trials were performed on the effects of the pump heating combined with microwaves applied for 20 minutes. The pump was operated for 15 minutes for the purpose of allowing the flow to attain uniformity throughout the system and the temperatures were recorded during this period at 5 minute intervals. Microwave heating of 23 W power input was then applied for 20 minutes and the measurements were recorded in the same manner. In Figure 5.1 the temperature rise is plotted against time for the two different types of trials. The lower part of the figure indicates the temperature rise due to pump heating when it

Figure 5.1: The temperature rise of the phantom system due to the pump (solid lines) alone and due to the pump plus 20 min of microwaves (slashed lines). A plot of the rise in temperature against the time of effect.

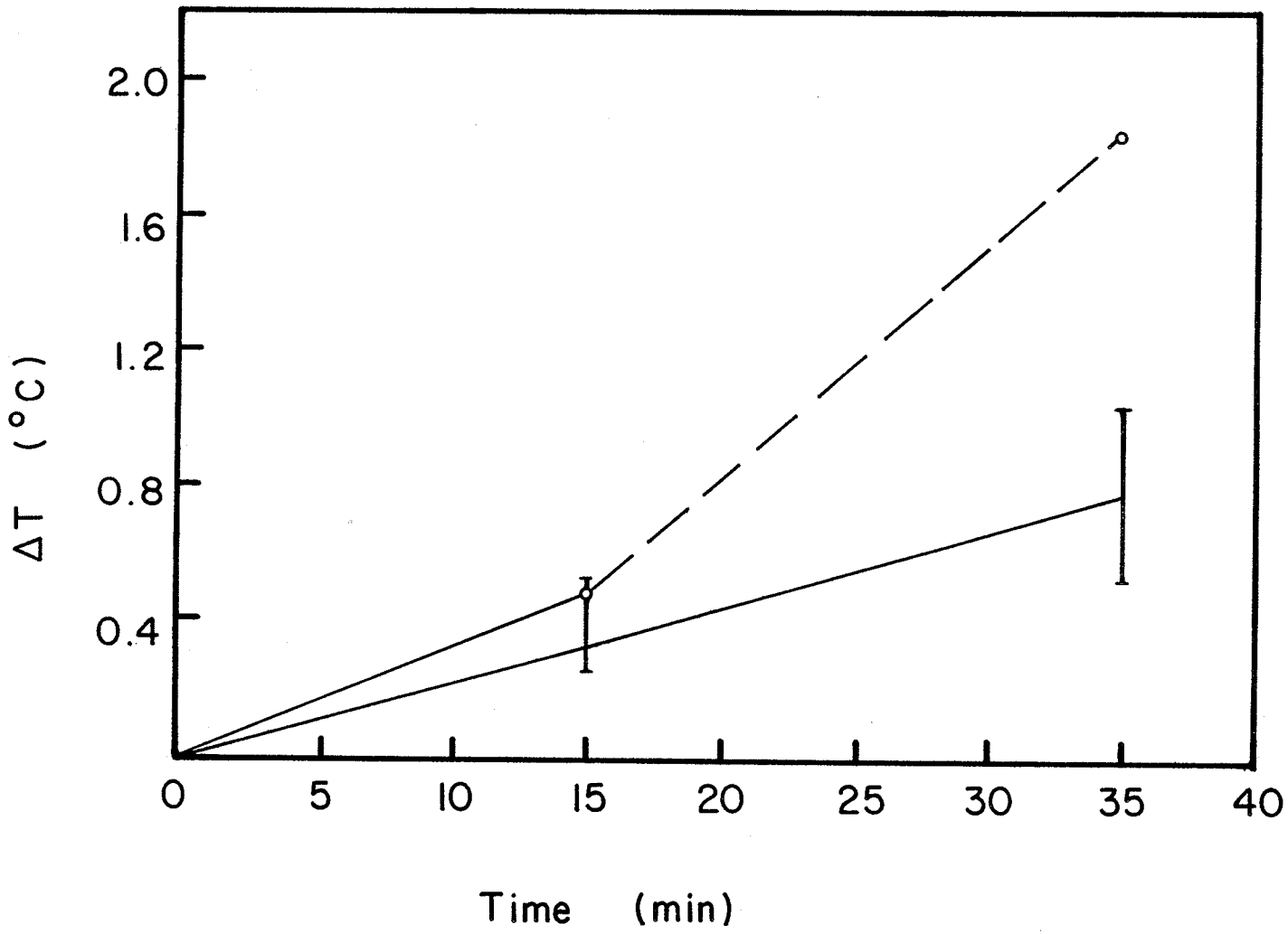
2.0
1.6
1.2
0.8
0.4
ΔT (°C)
0
5
10
15
20
25
30
35
40
Time (min)

is operated at different flow rates. At higher flow rates the increase in temperature due to pump heat is on the higher part of the variation interval while, when at the lower flow rates, the temperature rise in on the lower part of the variation interval. In the upper part of the figure the pump-microwave combination is shown when the pump is operated at high flow rate (i.e. .15 cm/sec). The average rate of rise in the temperature of the phantom due to the pump alone was found equal to .02° C/min and for the pump-microwave combination equal to .1° C/min and in this case the contribution to the temperature rise due to the pump alone is not insignificant. However, the contribution of the pump to the overall temperature of the heated area is not considered to have any major effect on the thermal clearance process. This is because the thermal washout is recorded for 1 min after the field is off and its effects on the temperature recording device have subsided, and during this interval the temperature changes are much larger than 1° C/min. (See Section 5.3) and therefore the contributions of the pump heating in the temperature is of minor importance for the data collected, since it only amounts to a small percentage of the overall change (i.e. $\leq$ 1% of the temperature change).

5.3 EXPERIMENTAL RESULTS

5.3.1 DATA ANALYSIS

Experimental measurements were obtained for each thermocouple configuration at the point of higher temperature rise within the heat area (i.e. the center of the heated area of 6.5 cm radius) and at flow rates of 33 ml/min, 44 ml/min, 53ml/min. All data were fitted

Figure 5.2: Thermal clearance data as obtained using the thermocouple configuration "normal", at the three flow rates used.

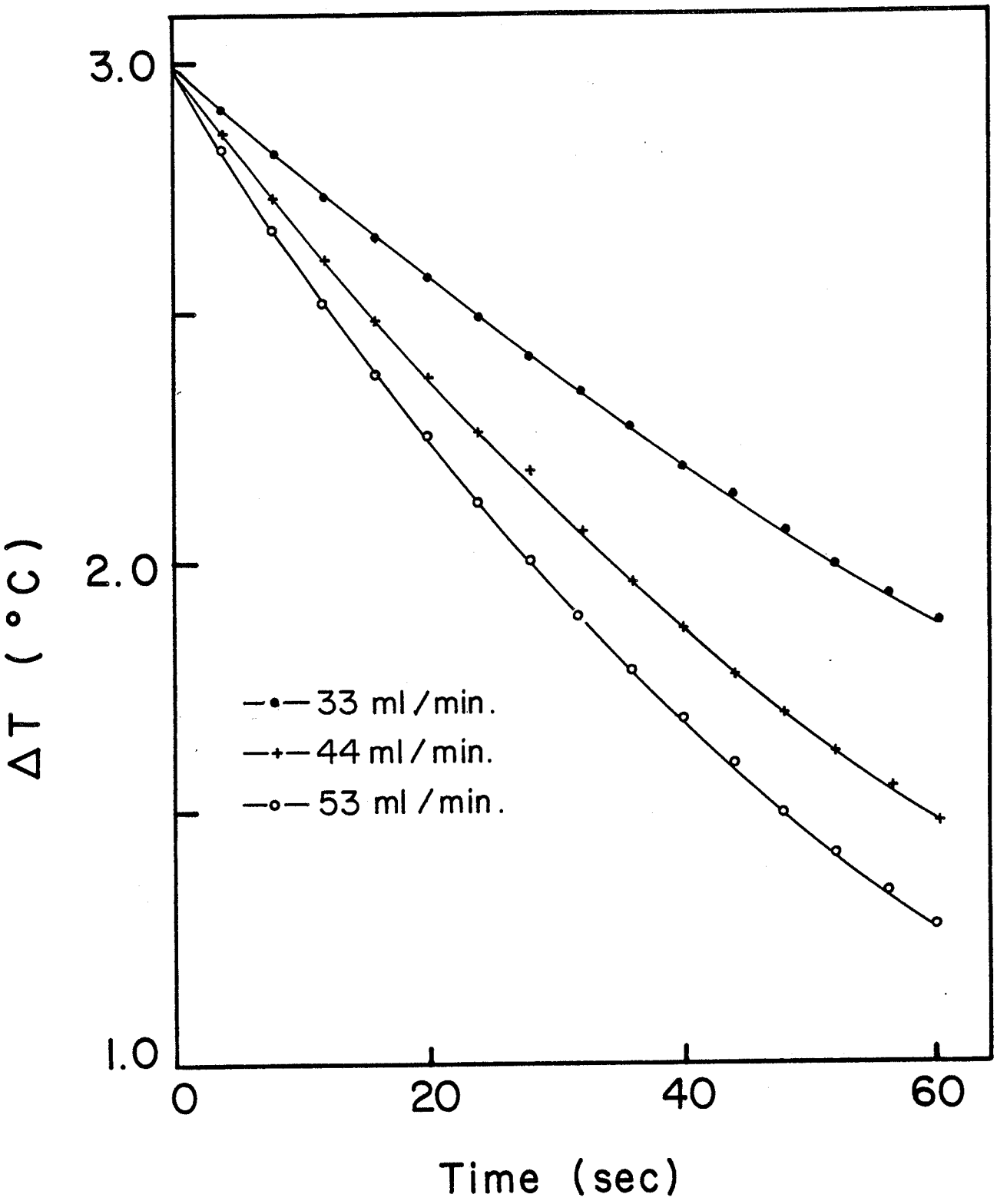
3.0
2.0
1.0
ΔT (°C)
0
20
40
60
Time (sec)
—•— 33 ml / min.
—+— 44 ml / min.
—∘— 53 ml / min.

through a multiple regression. In Figure 5.2 the data obtained are plotted as they were after the multiple regression fit. Multiple regression fits were applied on the data obtained using the "bare", "normal", and "normal plus extra tube" thermocouple configurations. By performing the multiple regression fits the perfusion time constant was also calculated for each case. As was mentioned before, the thermocouple was left in place during the whole treatment period and, in each case, the data considered were those obtained after the certain number of time constants required for each thermocouple configuration. The circular applicator was positioned at 1 cm above the phantom's surface to ensure better coupling. In Figure 5.3 the perfusion time constants calculated for each thermocouple configuration are plotted against the flow rates used. The perfusion time constants calculated for each probe at the same flow rate should be, if not the same, at least equal to within a small percent variation, because the perfusion time constant of the probe is small in comparison. This statement agrees with the values reported for the "normal" and "normal + extra tube" configurations. However, the values obtained using the bare thermocouple configuration overestimate the value of the perfusion time constant. The fact that the bare thermocouple has the shortest time constant might be one of the reasons for this overestimation. But, there are more serious structural set-backs to be considered for the explanations of this irregularity. First, the miniature metallic leads of the temperature sensor are exposed to the microwave field without any protecting coating to ensure their position with respect to the field configuration. As was mentioned previously, the thermocouple should

Figure 5.3: The perfusion time constant calculated as a function of flow rate for the three configurations of the probe.

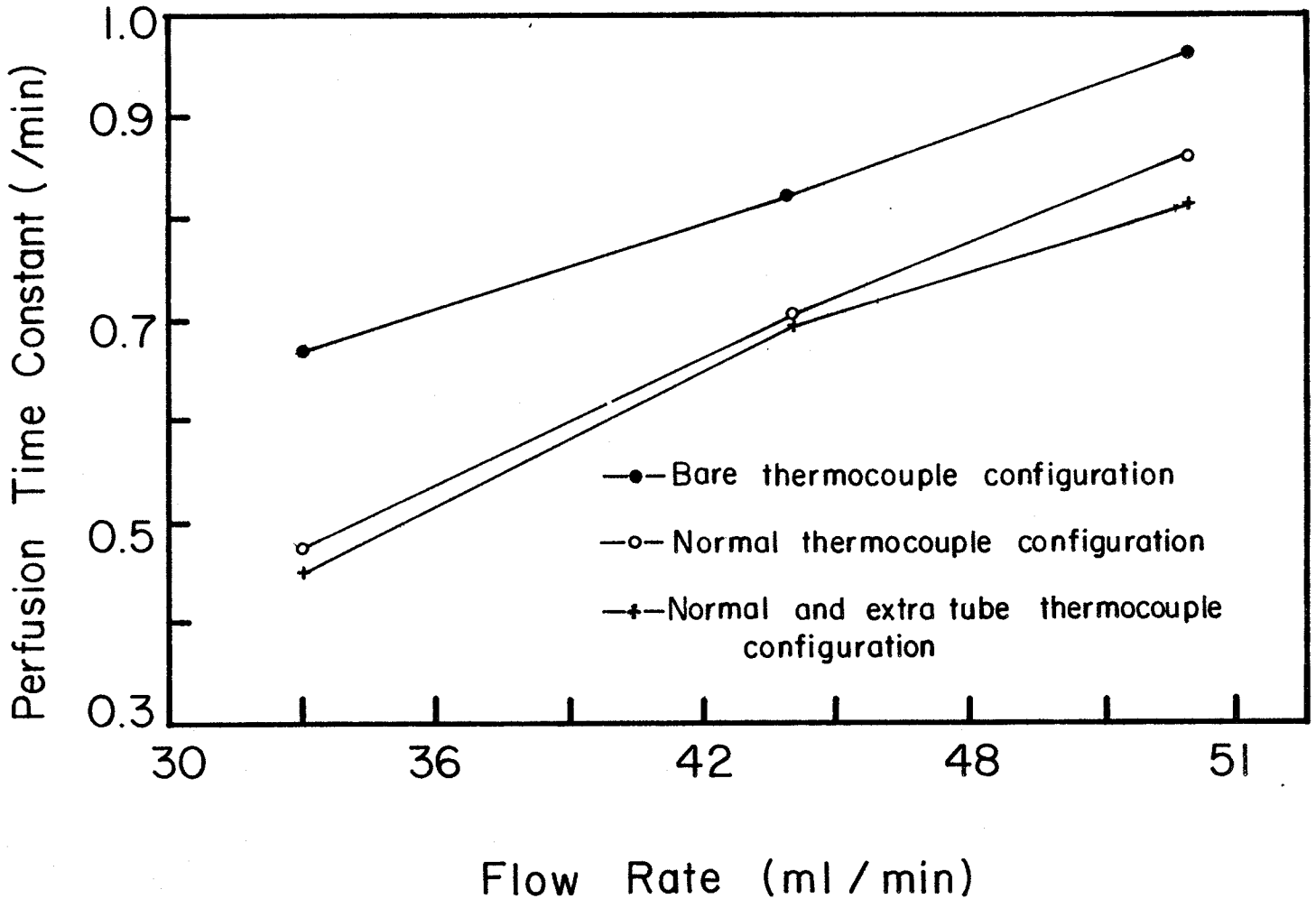
1.0
0.9
0.7
0.5
0.3
Perfusion Time Constant (/min)
30
36
42
48
51
Flow Rate (ml / min)
—●— Bare thermocouple configuration
—o— Normal thermocouple configuration
—+— Normal and extra tube thermocouple configuration

be perpendicular to the EM fields to avoid artifacts; however, the fine leads of the bare thermocouple can be bent or change position with the smallest force acting on them. Therefore, their position relative to the field cannot be ensured with absolute certainty: Second, the lack of any protection of the thermocouple could result in loosening of the soldered junction and therefore, incorrect data. Most of the above stated reasons for the behavior of the bare thermocouple could have been applied as well to the other two configurations. However, the construction and formation of the bare thermocouple enhances the possibility of such set backs. There is one other likely cause of this overestimation that is related to the bare thermocouple positioning inside the phantom. The site of measurement taking in the central axis was prepared to accommodate all three thermocouples, which means that the opening was very large in comparison with the bare thermocouple's diameter (i.e. ~ 2*50 μm); thus causing the local flow rate to be perturbed and eventually causing the overestimation of the perfusion time constant.

Another factor that was considered with respect to the accuracy of the treatment performance and for the purpose of comparing the resulting data, was the reproducibility of a heating treatment. Four trials were performed on four consecutive days in order to test the degree of reproducibility of a treatment. All the parameters involved were kept the same throughout the trails. That is the flow rate (33 ml/min), thermocouple configuration (normal, positioning of the applicator relative to the phantom surface and finally power input (27 Watts). The perfusion time constants calculated in these trials are shown in Table 5.1. These calculated values are in agreement to

Table 5.1: The perfusion time constants calculated for the reproducibility trials

Trial #	Flow Rate (ml/min)	Perfusion Time Constant(/min) [w/min]	Standard Deviation σ_w
1	33	.47	$5.54 * 10^{-7}$
2	33	.52	$6.89 * 10^{-7}$
3	33	.54	$7.4 * 10^{-7}$
4	33	.52	$6.9 * 10^{-7}$

Figure 5.4: Trials for the reproducibility of a heat treatment. The thermal washout data are plotted against the time of recording.

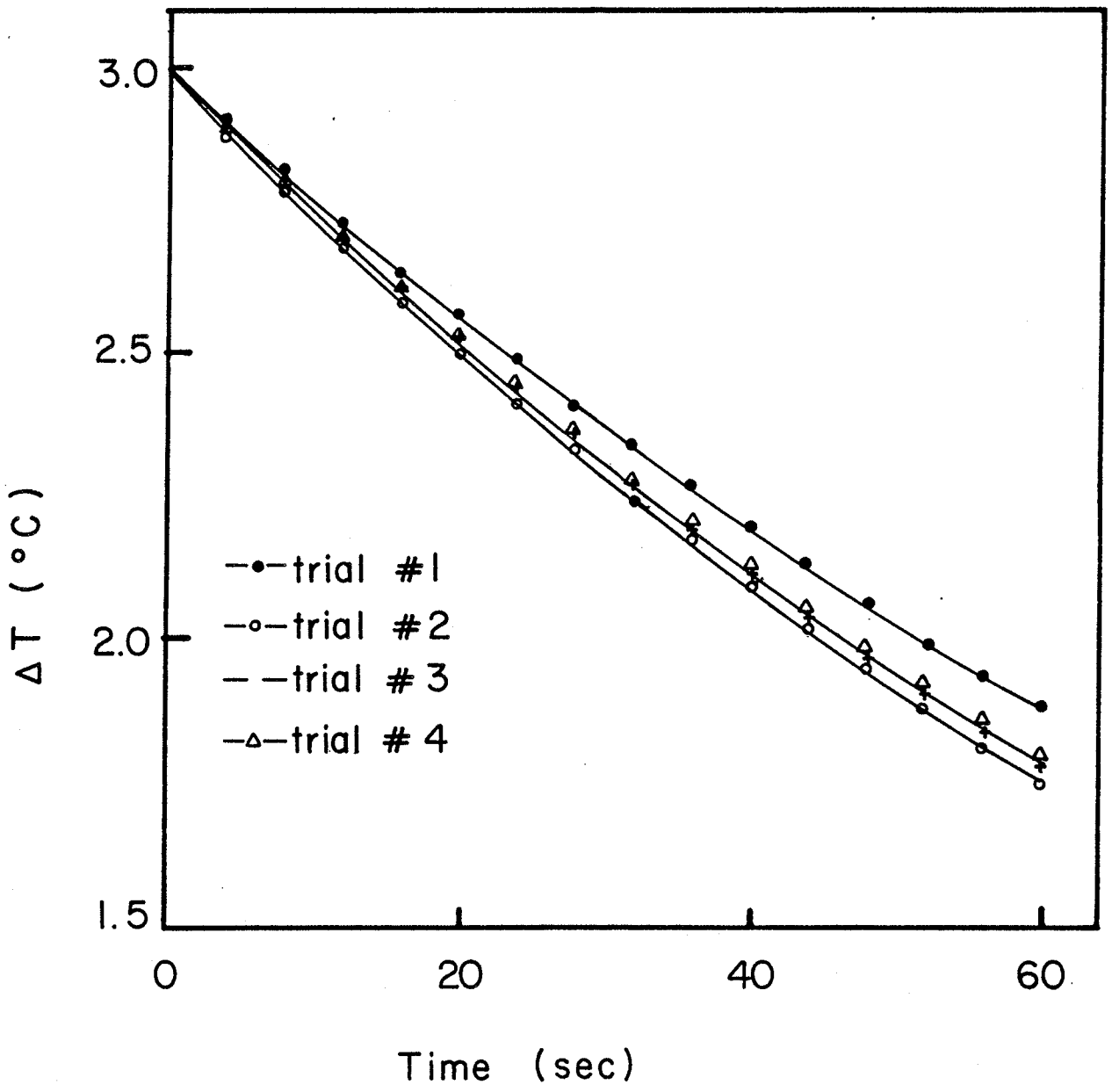
3.0
2.5
2.0
1.5
ΔT (°C)
—•—trial #1
—o—trial #2
— —trial #3
—△—trial #4
0
20
40
60
Time (sec)

within 10%, which is an acceptable variation in our results regarding the relative uncertainty of some experimental parameters, such as the positioning of the applicator relative to the phantom's surface (a slight change in the field configuration can result in a different rate of heating and eventually different temperature distributions).

In Figure 5.4 the rate of change of temperature during the thermal washout period is plotted as obtained from the multiple regression fit performed on the data obtained during the reproducibility trials.

Since the choice of the magnitude of the temperature rise (ΔT_o) was relatively arbitrary a set of measurements was undertaken for thermal clearance data at various temperature increases (ΔT_o = 1, 2, 3, 4°C). The measurements of the thermal washout for the different steady state ΔT_o were obtained at the flow rate of 33 ml/min. This particular flow rate was chosen for the trials because it requires less power input for achieving the desired ΔT_o and therefore, it is more unlikely to encounter any field disturbance problems due to metallic probes and eventually distortion in the data collected. In these measurements the normal thermocouple was also used. Analysis of these data showed that by changing the steady state ΔT_o the only resulting consequence is that the (ΔT vs time) plot is changing by moving upwards or downwards depending whether the steady state ΔT_o is a higher or a lower value. This means that the response of the phantom system during thermal washout is the same (i.e. w/min remains constant), regardless of the value of ΔT_o, as long as the flow rate is the same and ΔT_o is a low value, since in the case of steep gradients the handling of this case becomes more complicated with the addition

of the conductive effects along with the convective effects of blood flow.

There is one point to stress here, that is the perfusion time constant is exclusive for a specific blood flow and that, as long as it is tabulated relative to the blood flow values, they can be used as reference tables during clinical hyperthermia applications for the approximation of the regional blood flow change during heating and thus contribute in the prevention of damaging normal tissue due to extensive heating. It can further be used as a means of determining the blood flow of tumor and to take advantage of their inefficient flow rates.

A theoretical model for the blood flow prediction from the thermal washout data was developed by T. Constable (thesis work 1986) which calculates the blood flow rates under different steady state conditions.

5.4 DISCUSSION

The changes occurring in the blood flow of normal and tumor tissue during a hyperthermia application are very important in the determination of the optimum treatment time so as to cause minimal normal tissue damage and maximum tumor cell killing and/or radiosensitizing.

The measurements performed on the dynamic phantom regarding the association of regional blood flow and thermal washout are similar to those performed on live animals but ony in terms of procedure rather than in the response of the respective volumes.[109] Furthermore, they

cannot be compared to each other because of the different units used in the two studies to express the flow rate (animal flow rate is ml/100g-min; phantom flow rate is ml/min).

It has been reported in the literature[108] that hyperthermia application can result into tumor blood flow occlusion when applied for an optimum length of time, without causing any damage to the normal tissue found in the area of treatment. Therefore, if this blood flow prediction from the thermal washout method is refined and proven adequate for clinical applications, there will be a tremendous effectiveness of the hyperthermia application in the killing of tumor cells or in sensitizing them to either radiotherapy or chemotherapy.

The data obtained from these experiments, however not entirely conclusive, can be used as a guide for further experimental studies in refining the method of predicting the blood flow rates of hyperthermia treated tissues and thus enable the most effective use of clinical hyperthermia in the treatment of cancer.

6. CONCLUSIONS

The work presented in this report was undertaken in an effort to better understand the processes of microwave hyperthermia in relation to biological tissues. It was reported in the preceding chapters that dynamic or perfused phantoms are a closer approximation of biological tissue because of the blood flow incorporation in the simulation, however simple it might be. The design of the dynamic phantom discussed above was a successful simulation of the dielectric behavior of human muscle tissue as well as of a simple form of blood flow. The advantage of incorporating this simple form of unidirectional flow was that a steady state could be achieved in the temperature distribution during the heat treatments. The short useful life of the dynamic phantom in comparison with the static phantom studied (Appendix A) is not considered to be a disadvantage since the lost amounts of NaCl and H_2O can be replenished without any difficulty or uncertainty regarding the respective amounts needed. The blood flow studies which were performed as a function of thermal washout have shown that the effect of perfusion is quite dominating during thermal clearance when the temperature step rise is low and that the whole process can be expressed with a simple exponential.

However, recent studies[109] indicate that at steep temperature gradients the conduction effects are just as important as the blood flow in the expression of temperature decay. It is also indicated in these studies that the simple exponential approach, that is to ignore thermal conduction, can result in error in estimation of the blood flow values, even at the low temperature gradients, and that the

method of predicting the blood flow rate from the temperature decay curves is in general of limited value. The dynamic phantom blood flow-temperature decay studies at low temperature gradients have shown the convective effects to be of major importance. Therefore, it would be necessary to study the phenomenon at high temperature gradients in order to see the temperature decay curves as a function of both thermal conduction and convection. This could be an expansion of the dynamic phantom use for in vitro hyperthermia. Additional experimental work using the dynamic muscle phantom could be performed in the following areas:

1. Perfusion.

The addition of a constant temperature bath in the phantom-pump system (the bath to be added after the pump's outlet and before the phantom's inlet) would facilitate longer heat treatments by preventing any rise in the temperature of the saline entering the phantom. It would also eliminate the rise in the temperature of the phantom due to pump heating.

2. Composition.

a. Introduction of other layers of tissue simulating materials such as fat (as per P. Nilsson)[62] could provide information on the effects of the thickness of the subcutaneous fat in the microwave power absorption.

b. Introduction of a tumor simulating volume, which would provide information about the temperature distribution in and around a tumor volume.

In conclusion, there should be stressed the fact that hyperthermia is a promising means for the treatment of cancer alone or

in combination with other conventional methods and that there is still very much to be learned about the hyperthermia interactions with tissue. The understanding of the hyperthermia processes will be achieved through continuous efforts, like the one described above, which will provide the information relative to the biological, physical and physiological functions of human tissue when exposed to electromagnetic radiation.

A.1 STATIC PHANTOMS

A.1.1 MANUFACTURE OF A GUY TYPE STATIC PHANTOM

In this work, the basic muscle phantom recipe developed by Guy[61,70,85] was used to construct a static phantom and study it in terms of its dielectric behavior, its applicability to our hyperthermia in vitro work and in general to get a base start in hyperthermia phantom studies.

The recipe used to construct the static muscle phantom was that reported in the original publication by Guy[85] and is shown in Table 1.A along with the properties of the simulated muscle phantom resulting from this composition, and as measured by Guy. The muscle phantom has the form of a moist jellied plastic after the mixing of the constituents.

The mixing of the phantom constituents presented the problem of inhomogeneity throughout its volume, especially in terms of the powdered polyethylene constituent. However, the results of several trials showed that the most homogeneous model resulted for the following process: The appropriate quantities of H_2O and NaCl are mixed initially, followed by the slow addition of the TX-150 agent and finally powdered polyethylene which is introduced in small amounts while the whole mixture is thoroughly stirred. The stirring continues until the mixture thickens and all the air bubbles are eliminated from the material. The microwave phantom is then transferred into a supporting box of size relative to the size of the applicator used in order to avoid any wall interference during the microwave applications. The phantom's surface is covered with a layer of thin

Table 1.A: The muscle phantom composition reported by Guy[85]

Simulated Material	Percent Weight Composition	Dielectric Permittivity	Electrical Conductivity	Specific Heat	Density
Muscle	76.5% Saline solution $\frac{12\text{ g NaCl}}{1\text{ liter } H_2O}$				
	15.2% Powedered Polyethylene	49 - 58	1.13 - 2.72	0.86	1.0
	8.4% Jelling Agent (TX-150)				

(Note: The values for the electrical conductivity are read off the graph in Reference 85 and are therefore subject to error.)

plastic (i.e. clear plastic wrap) to avoid excess evaporation of the water.

However, the loss of H_2O from the phantom is a linear function of time. This was the reason that led to the study of the useful lifetime of such a phantom in terms of its water content and its effect on the dielectric and thermal behavior of the material for in vitro hyperthermia work.

A.2 EXPERIMENTAL WORK

A.2.1. MEASUREMENTS AND CALCULATIONS

Two muscle phantoms were constructed for this purpose of identical weight, composition and shape. One of them was kept in an air tight container, to prevent any H_2O evaporation, and the other was kept under the conditions that phantoms are usually kept during the experimental trials ie. covered with a clear plastic wrap.

Over the period of 15 days the two sample phantoms were kept at room temperature, [i.e. $(23 \pm 1.5)^\circ$ C], and had their weights recorded on a daily basis. In Figure 1.A the change of the water content of the test phantom relative to the control phantom is plotted against time in days.

The effect of this water loss in the test phantom in terms of its dielectric and thermal behavior were investigated by calculating the change in the electrical conductivity (σ), the depth of penetration (d) and the specific heat (c_{mp}) values, as a function of the H_2O content of the phantom over the trial period. The calculations of σ were performed according to the following formula:[112]

Figure 1A: The change of percent H_2O content of the test phantom as a function of time, in relation to the control phantom's percent H_2O content over the same period of time.

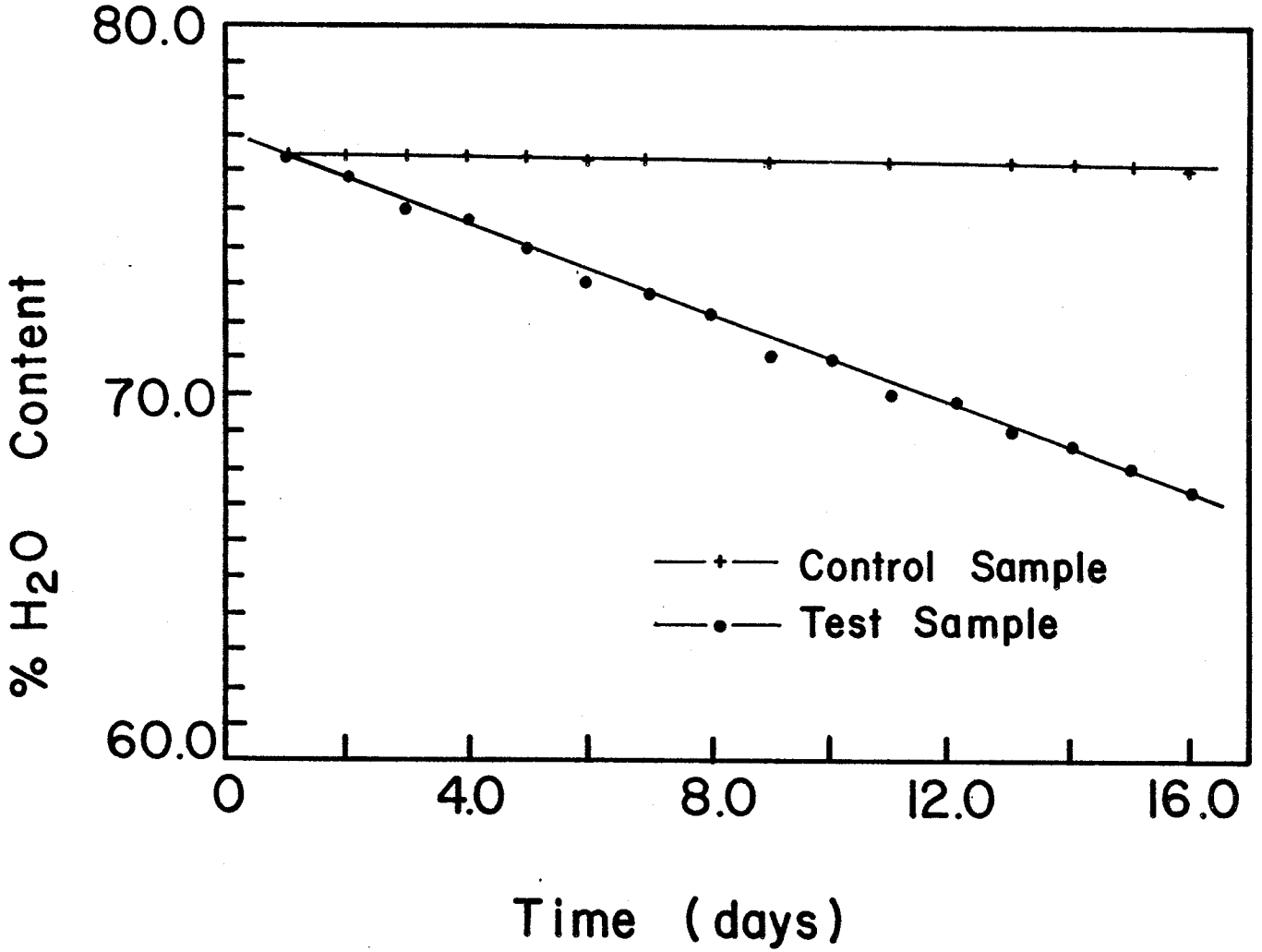
80.0
70.0
60.0
% H_2O Content
0
4.0
8.0
12.0
16.0
Time (days)
Control Sample
Test Sample

$$\sigma = \sigma_o + \frac{(\%H_2O - 30)\ \ (f^3/7.2 * 10^5)}{1 + (f/20)^2} \qquad \text{A.1}$$

where σ_o = 18.9 mmho/cm static conductivity of muscle at 20° C.[112]

f = microwave frequency of 2450 MHZ

$\%H_2O$ = percent weight of the H_2O constituent

The depth of penetration was calculated as a function of σ according to the following formula:[113]

$$d = \frac{\sqrt{\lambda\rho}}{17} \text{ for } 60\ \lambda\ >\ \varepsilon * \rho \qquad \text{A.2}$$

where λ = wavelength of the microwaves inside muscle tissue = 1.76 cm at 2450 MHZ.[61]

ρ = resistivity = $1/\sigma$

The specific heat for the different water content values was calculated according to eqn. (3.16) [Chapter 3]

The results from the above calculations are shown in figures 2.A, 3.A, and 4.A respectively.

From the depth of penetration change calculations, we see that, as was expected, d increases with the decrease in the H_2O content of the phantom material, due to the fact that the power absorption decreases thus enabling the field to penetrate further into the muscle phantom. The overall maximum change in the d value over the trial period is .07 mm, i.e. a .4% variation, which is a very small error and it is not vitally affecting the static phantom's behavior as a substitute for human muscle. Similarly small is the change in the value of the electrical conductivity, $\Delta\sigma$, which designates a decrease in the σ value of the phantom due to the loss of water (.91% decrease in σ over the trial period). The decreased σ value causes the

Figure 2A: The change in the depth of penetration as a function of the percent H_2O content of the static muscle phantom over the trial period. (Note: The pairs of dots indicate that the value of d was the same for two consecutive measurements).

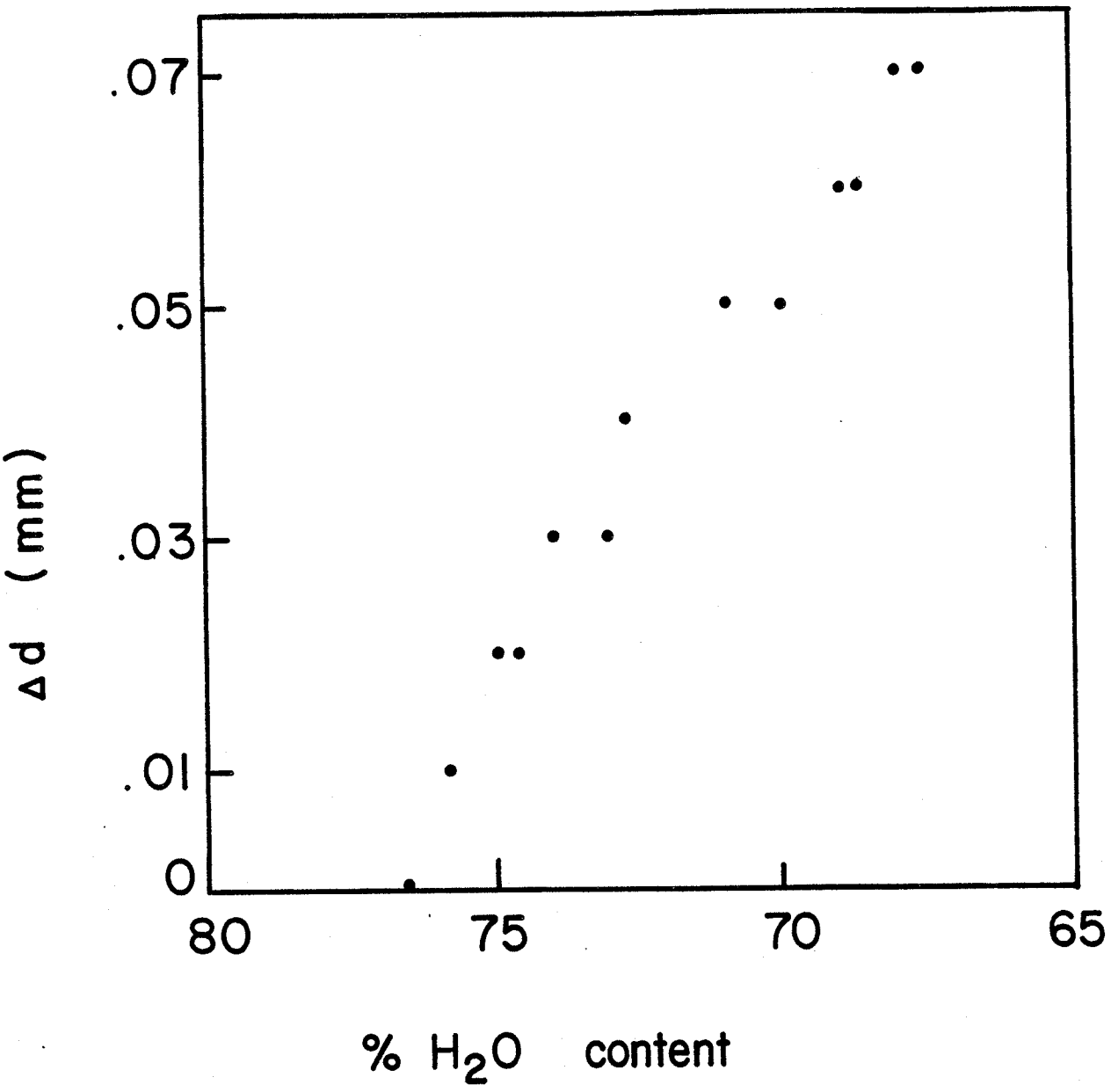
.07
.05
.03
.01
0
Δd (mm)
80
75
70
65
% H2O content

Figure 3A: The change in the electrical conductivity as a function of the percent H_2O content of the static muscle phantom over the trial period.

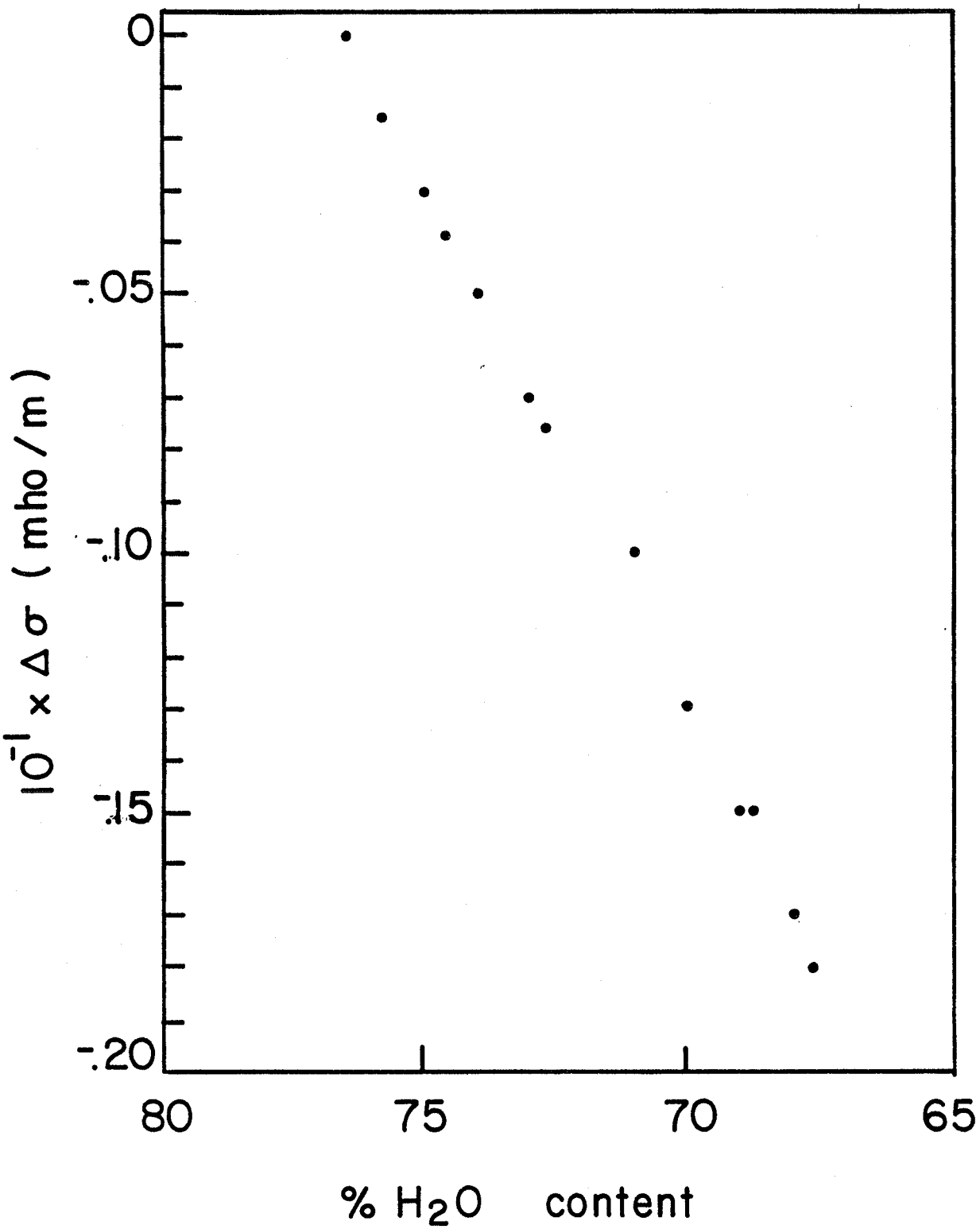
0
-.05
-.10
-.15
-.20
$10^{-1} \times \Delta\sigma$ (mho/m)
80
75
70
65
% H_2O content

Figure 4A: The specific heat values of the static muscle phantom as they were recorded over the trial period.

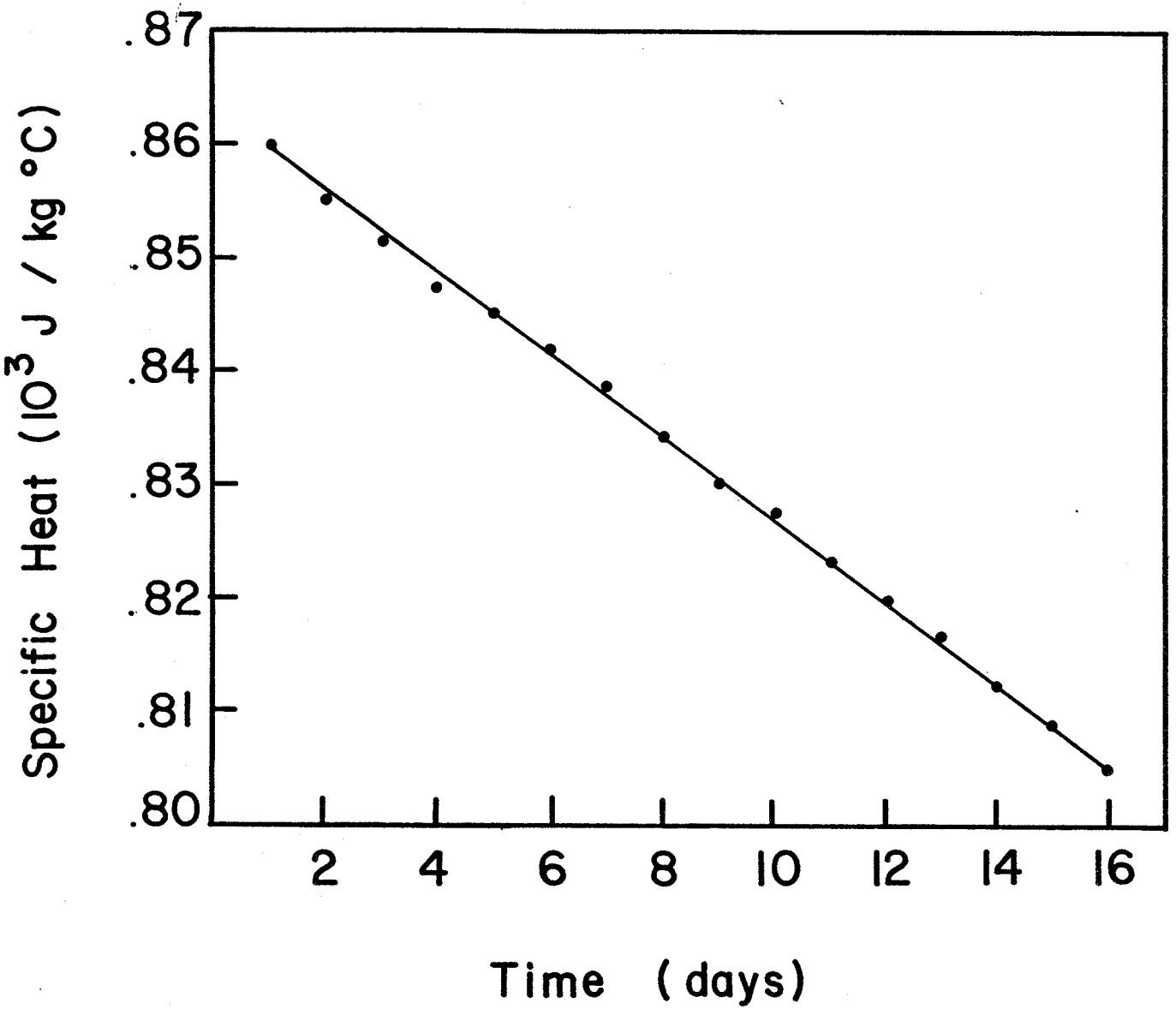
.87
.86
.85
.84
.83
.82
.81
.80
Specific Heat (10^3 J / kg °C)
2
4
6
8
10
12
14
16
Time (days)

conductive behavior of the material to change; it becomes less conductive, and this eventually leads to a lower ability to dissipate the power input, thus causing deeper penetration of the EM wave (ie greater depth of penetration).

A change of 6.4% in the value of the specific heat of the phantom was calculated in relation to the H_2O content of the material during the trial period.

In general, the variations calculated from the water content values measured over the trial period indicate that they all are within the 10% error range that is accepted during hyperthermia phantom studies. The accepted error range (i.e. 10%) has been determined from the variations that exist in the measurements of the dielectric and thermal properties of biological tissues. In conclusion a static phantom of the Guy type has an experimentally useful life span of about 15 to 20 days when it is kept at room temperature with minimal coverage. However, its useful life can be extended by appropriate coverage and/or refrigeration after the experiments.

The next step in the static phantom studies was to optimize the applicator setting relative to the phantom's surface. (Applicator: circularly polarized, 13 cm inner diameter).[7] The applicator was positioned at different distances over the phantom's surface and the values of the temperature rise, the time of application and the net power input were recorded. In Figure 5.A the rate of change of temperature over the net power input, i.e. [($\Delta T/dt$)/Net Power] is plotted against the specific distances of the applicator relative to the phantom. The net power is the power that results from the total

Figure 5A: The applicator optimum positioning relative to the phantom's surface for obtaining the least possible reflections of the microwave field (i.e. maximum $\Delta T/dt$).

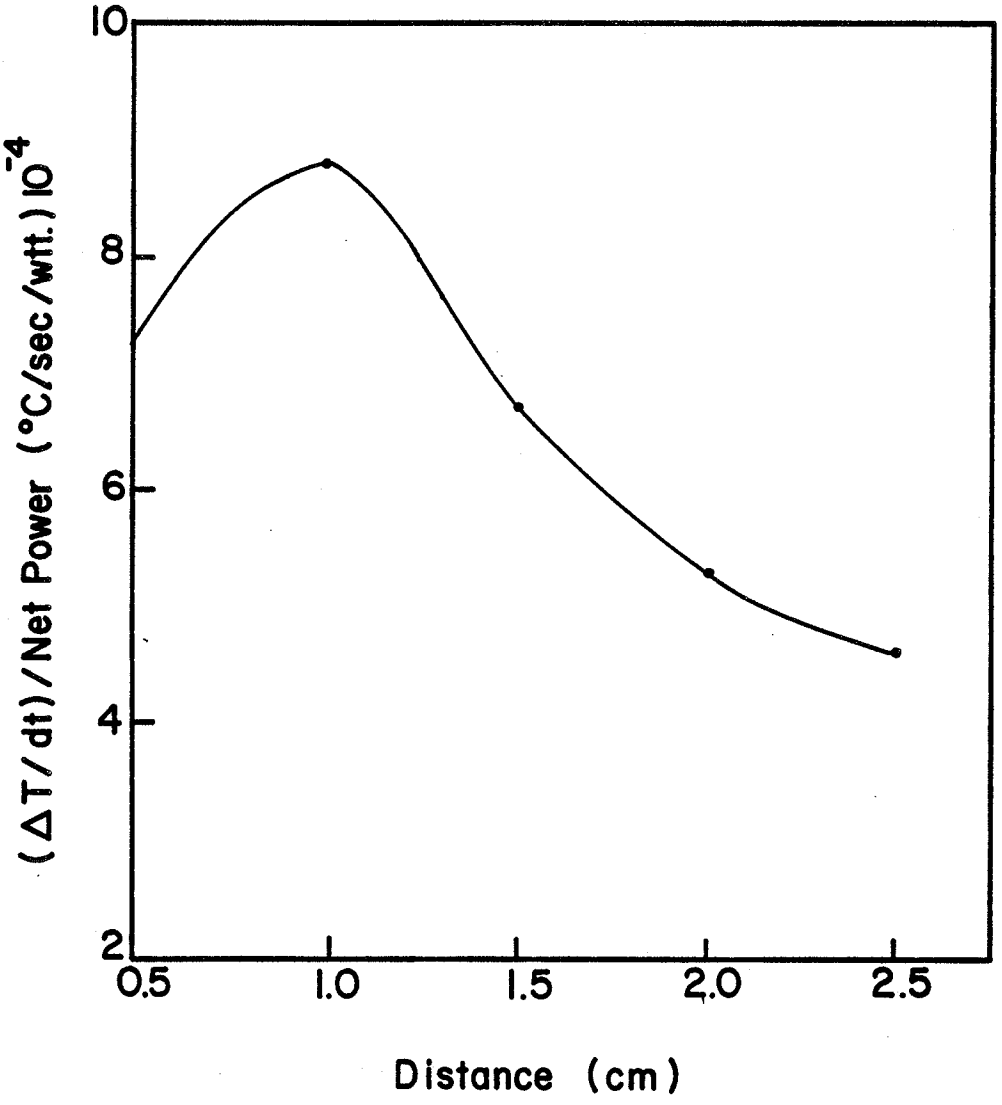
10
8
6
4
2
0.5
1.0
1.5
2.0
2.5
(ΔT/dt)/Net Power (°C/sec/wtt.) 10^-4
Distance (cm)

power input minus the reflected power, as indicated by the generator control panels. For all the positions tested the total power input was the same i.e. 15 Watts and it was applied on the phantom for as long as it was necessary to raise its temperature at 1 cm depth by 2° C (ie. $\Delta T = 2°$ C). That is, the time required is dependent on each position of the applicator. It can be seen from Figure 5.A that the optimum distance, the one at which the 2° C rise is achieved in the shortest time interval, is when the applicator is placed at 1 cm above the phantom surface.

After establishing the applicator positioning relative to the phantoms surface, several temperature measurements were taken with respect to time and the thermocouple position across the microwave field, posed by the applicator, and inside the phantom up to a depth of 3 cm. These temperature measurements were used for the calculation of the Specific Absorption Rate values ($SAR = c\ \Delta T/dt$). For the temperature recording two thermocouple arrays of four junctions each were used and the temperatures were measured at two perpendicular axes (x and y) along the phantom surface and within the area defined by the EM field (i.e. an area of radius equal to 8 cm) of the applicator. In Figure 6A the calculated SAR values, normalized to 100, are plotted against the distance (in cm) on the x and y axis; each line corresponds to a different depth inside the phantom i.e., surface, 1 cm, 2 cm, and 3 cm below the surface.

All these measurements were performed at a total power input of (45 ± 1) Watts applied for 60 seconds each time the phantom was exposed to microwaves. SAR values cannot be considered absolutely accurate due to the several error factors associated with the

Figure 6A: The percent Specific Absorption Rate distribution along the two perpendicular axes of the temperature distribution field.

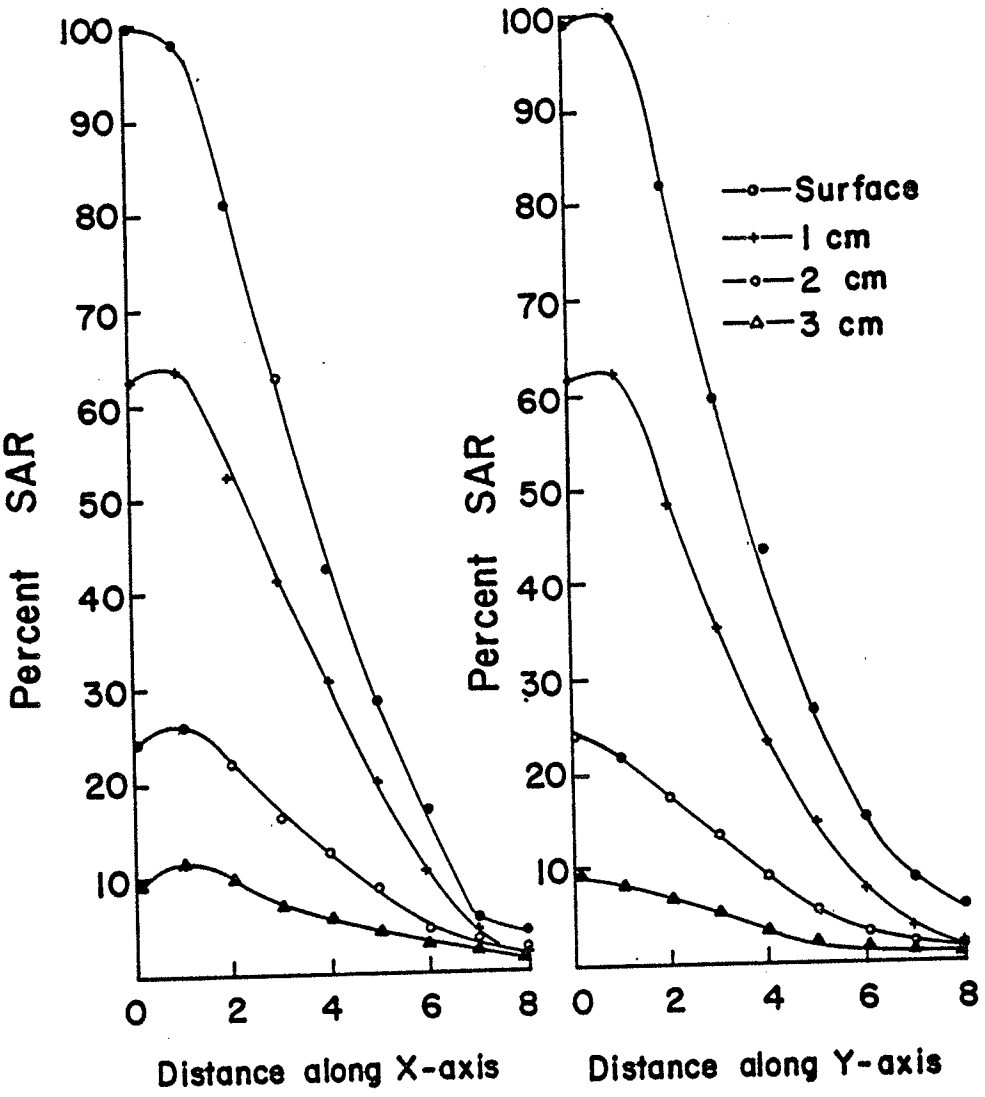
100
90
80
70
60
50
40
30
20
10
Percent SAR
0
2
4
6
8
Distance along X-axis
Distance along Y-axis
Surface
1 cm
2 cm
3 cm

temperature measurements. There were random errors arising from the thermocouple positioning inside the phantom, the thermocouple itself due to its encapsulation into a metallic needle, thus resulting in temperature errors, and from the time, in terms of temperature recording timing etc. Systematic errors resulted from cooling during and after heating and also from the thermal behavior change (i.e. specific heat change) due to the gradual loss of H_2O from the phantom. Nevertheless, these SAR plots indicate qualitatively the temperature distribution throughout the heated volume of the static phantom, that is the distribution of the power that is absorbed inside the heated volume.

The work described above was initiated for the purpose of understanding the use of hyperthermia phantoms and the processes involved in acquiring useful information that could be applied to clinical applications of hyperthermia. Furthermore, the errors involved with such measurements were determined in terms of error initiation factors, thus providing the required experience as to avoid them in the dynamic phantom studies.

APPENDIX B: CLINICAL HYPERTHERMIA PROGRAMS

The calibration of the thermometry system and the experimental measurements were performed using the following computer hyperthermia programs (written by J. McLellan): 1) Calibration; 2) Main prog more D; 3) Data Search and 4) COOL.

In the "Calibration" program it is assumed a linear Voltage (V) - Temperature (T) response curve in order to produce the factors for a Voltage-Temperature equation. Initially the user is instructed to immerse the thermocouples (thermometry probes) in a low temperature bath and to enter the temperature of the bath in the computer. The same procedure is followed in the high temperature bath also. With the low and high temperature bath inputs the calibration factors of the thermometry probe pair are calculated and displayed on the screen.

The "Main prog more D" program collects and stores the temperature data for each heat treatment. The readings are taken, displayed and stored on the disk every 15 seconds. When the data collection is complete (when "S" is pressed or 60 minutes have passed) the program exits and the recording process is stopped.

The "Data Search" program retrieves the temperature data stored on the disk and prints the data out in a tabular form with the output sent either to the screen of the computer or to the printer.

The program "COOL" records the temperature of only one junction in the thermocouple array that can be chosen when the program is started. With this program data are ready every .5 seconds and are sent directly to the printer instead of being displayed or stored on the disk.

There were some other programs used for the calculation of the wave parameters and the SAR values, which were written according to the theoretical formulae (Chapter 2) by the author of this report. (see following pages)

```
2 OPEN 4,4
3 CMD 4
4 REM ************************************
5 REM CALCULATION OF REFLECTION COEFF.*
6 REM ************************************
10 FOR I= 1 TO 6
20 INPUT E1(I),E2(I),E3(I),E4(I)
30 A=E1(I)↑2+E2(I)↑2
40 B=E3(I)↑2+E4(I)↑2
50 AS=SQR(A)
60 BS=SQR(B)
70 C=0.5*(E1(I)+AS)
80 D=0.5*(E3(I)+BS)
90 CS=SQR(C)
100 DS=SQR(D)
110 Z1=0.5*E2(I)*(1/CS)
120 Z2=0.5*E4(I)*(1/DS)
130 PRINT"SQUARE ROOTS OF COMPLEX NOS:"
135 PRINT"X1=";CS,"Y1=";Z1
140 PRINT"X2=";DS,"Y2=";Z2
150 GOSUB 1000
160 PRINT"COMPLEX  NO FROM SUBTRACTION"
165 PRINT U(0);" , ";U(1)
170 GOSUB 2000
175 PRINT
180 PRINT"COMPLEX NO FROM ADDITION"
185 PRINT W(0);" , ";W(1)
190 GOSUB 3000
195 PRINT
200 PRINT"COMPLEX NO FROM DIVISION"
205 PRINT Z(0);" , ";Z(1)
210 R=Z(0)↑2+Z(1)↑2
220 RS=SQR(R)
230 PC=Z(0)/RS
240 PS=Z(1)/RS
250 PRINT"COS(PHI)=";PC,"SIN(PHI)=";PS
276 PRINT
280 PRINT"THE MAGNITUDE OF RHO=";RS
281 PRINT
290 NEXT I
291 FOR S=1TO1000:NEXT S
292 PRINT#4
293 CLOSE 4
300 END
999 REM ********************************
1000 REM SUBTRACTION OF COMPLEX NOS.*
1005 REM ********************************
1010 U(0)=CS-DS
1020 U(1)=Z1-Z2
1030 RETURN
1040 PRINT
1041 REM ***************************
2000 REM ADDITION OF COMPLEX NOS.*
2005 REM ***************************
2010 W(0)=CS+DS
2020 W(1)=Z1+Z2
2030 RETURN
2040 PRINT
2041 REM ***************************
3000 REM DIVISION OF COMPLEX NOS.*
3005 REM ***************************
3010 DE=W(0)*W(0)+W(1)*W(1)
3020 Z(0)=(U(0)*W(0)+U(1)*W(1))/DE
3030 Z(1)=(U(1)*W(0)-U(0)*W(1))/DE
3040 RETURN
```

```
2 OPEN4,4
3 CMD4
4 REM ************************************
5 REM CALCULATION OF: LAMDA,DELTA,BETA,*
6 REM ALPHA                              *
7 REM NAME:CALCULATIONS                  *
8 REM ************************************
10 FOR I=1 TO 6
20 INPUT E1(I),E2(I),F(I)
30 GOSUB 1000
40 PRINT "X=";X:REM REAL PART OF CMPLX
50 GOSUB 2000
60 PRINT "Y=";Y:REM IMAGINARY PART
70 LAMDA=(3E8)/(F(I)*X)
75 PRINT
80 PRINT "THE WAVELENGTH=";LAMDA:REM(M)
90 GOSUB 3000
100 DELTA=(3E8)/(OM*Y)
105 PRINT
110 PRINT "DEPTH OF PENETRATION:";DELTA
120 BETA=2*π/LAMDA
130 ALPHA=1/DELTA
140 PRINT
150 PRINT"BETA=";BETA
160 PRINT
170 PRINT"ATTENUATION COEFF.=";ALPHA
171 PRINT
175 NEXT I
176 FOR S=1TO1000:NEXT S
177 PRINT#4
178 CLOSE 4
180 END
999 REM ************************
1000 REM CALCULATION OF X      *
1005 REM ************************
1010 A=E1(I)↑2+E2(I)↑2
1020 AS=SQR(A)
1030 X1=0.5*(E1(I)+AS)
1040 X=SQR(X1)
1050 RETURN
1051 REM ************************
2000 REM CALCULATION OF Y       *
2005 REM ************************
2010 Y=0.5*E2(I)*(1/X)
2020 RETURN
2021 REM ************************
3000 REM CALCULATION OF OMEGA   *
3005 REM ************************
3010 OM=2*π*F(I)
3020 RETURN
```

```
2 OPEN 4,4
3 CMD 4
4 REM ************************************
5 REM SPECIFIC ABORPTION RATE VALUES  *
6 REM NAME:P.A.2:AT THE FAT/MUSCLE INT*
7 REM ************************************
10 FOR I=1 TO 6
20 INPUT CE(I),R(I),AL(I),B(I),PH(I)
30 FOR J=0 TO 3 STEP 0.5
40 Z=J:PRINT"Z=";Z:PRINT
50 G=2*AL(I)*Z:PRINT"G=";G
60 GI=EXP(-G)+R(I)↑2*EXP(G)
70 PRINT:PRINT"GI=";GI
71 GOSUB 1000
72 PRINT
73 PRINT"COS=";CS
80 F=GI+2*R(I)*CS:PRINT:PRINT"F=";F
90 PO=0.5*CE(I)*100*F:PRINT
100 PRINT"REL.ABS.POWER DENSITY=";PO
101 SA=((10↑-3)/.937)*PO:PRINT
102 PRINT"SAR(W/KG) =";SA
120 NEXT J
130 NEXT I
131 FOR X=1TO1000:NEXT X
132 PRINT#4
133 CLOSE 4
140 END
141 REM **********************
1000 REM CALCULATION OF COS*
1005 REM **********************
1010 A=(((2*B(I)*Z*(180/3.1416))+PH(I))*π/180)
1020 CS=COS(A)
1030 RETURN
```

REFERENCES

1. Hall, E.J.: Radiology for the Radiologist (2nd ed.), Harper and Row, Hagerstown, MD, (1978)
2. Field S.B., Bleehen N.M.: Cancer Treatment Reviews (1979) 6, 63-94
3. Stewart J.R., Gibbs F.A. Jr.: Syllabus for the ASTR Refresher Course #303 (1983) Los Angeles, California
4. Emami B., Song C.W.: Int. J. Radiation Oncology Biol. Phys., (1984) 10,289-295
5. Henderson M.A., Pettigrew R.: Lancet (1971) 1, 275-277
6. Herman T.S., Zukoski C.F., Anderson R.M.: (Abstr.) Proceedings of the 3rd International Symposium on Cancer Therapy by Hyperthermia Drugs and Radiation: National Cancer Inst. (1980), p. 112.
7. Dunscombe P.B., McLellan, J., Malaker K.: Heat Production in Microwave Irradiated Thermocouples (submitted for publication 1986).
8. Warters, R.L., Roti Roti J.L.: Radiation Research (1982) 92, 458-462
9. Dewey W.C., Hopwood L.E., Sapareto S.A., Gerweck L.E.: Radiology (1977) 123, 463-474
10. Eddy H.A., Sutherland R.M., Chmielemski G.: (abstr.) J. Radiation Oncology Biol. Phys. (1980) 6, 1385-1386
11. Mondovi B., Agro A.F., Rotillio G. Storm R., Moricca G., Fanelli A.R.: Eur. J. Cancer (1969) 5, 137-146
12. Cavaliere R., Ciocatto E.C., . . ., Rossi-Fanelli A.: Cancer (1967) 20, 1351,1363
13. Mondovi B., Storm R., Rotillio G. Argo A.F., Moricca G., Fanelli A.R.: Eur. J. Cancer (1969) 5, 129-136
14. Perez C.A., Emami B., Nussbaum G., Sapareto S.: Refresher Course #19, Amer. Society of Therapeutic Radiologists (1983), 25th Annual Meeting
15. Cress A.E., Culver P.S., Gerner E.W.: Cancer Res. (1982) 42, 1716-1721

16. Overgaard J.: Cancer Therapy by Hyperthermia and Radiation, Proc. of the 2nd International Symposium, Essen (1977), C. Streffer ed. Munich, Urban and Schwarzenberg (1978), 49-61
17. Raapharst G.P., Romano S.L., Mitchell J.B., Bedford J.S., Dewey W.C.: Cancer Res. (1979) 39, 396-401
18. Song C.W.: In Physical Aspects of Hyperthermia (1982.) Nussbaum G. ed,. AAPM Med Phys. Monog. #8, pp 43-62
19. Song C.W.: J. Natl. Cancer Inst (1978) 60; 3, 711-713
20. Emami B, Nunbaum G.H., Tenttaken R., Hughes, W.: Radiology (1980) 137, 805-809
21. Harisiadis L., Hall E.J., Kraljevic U., Borek C.: Radiation Biol. (1975) 117, 447-452
22. Song, C.W., Rhee J.G., Levitt S.H.: Int. Journal Radiation Oncology Biol. Phys (1982) 8, 851-856
23. Goldin E.M., Leeper D.B.: Radiology (1981) 141, 505-508
24. Gerweck L.E.: Rad. Res. (1977) 70, 224-235
25. Gerweck L.E., Rottinger E.: Rad. Res. (1976) 67, 508-511
26. Song C.W., Kang M.S., Rhee J.G., Levitt S.H.: Radiology (1980) 137, 795-803
27. Bicher H.I., Hetzel F.W., . . ., O'Brien T.: Radiology 91980) 137, 523-530
28. Song C.W., Kang M.S., Rhee J.G., Levitt S.H.: Annals NYAS (1980) 335, 35-47
29. Urano M., Rice L.C., Montoya V.: Int. J. Radiation Oncology Biol. Phys. 91984) 8, 227-233
30. Field S.B., Anderson R.L.: Natl. Cancer Inst. Monograph (1980) 61, 193-201
31. Meyer J.L., Kersen N., Becker B., Hahn G.M.: Int. J. Rad. Oncology Biol Phys (1985) 11, 973-981
32. Urano M., Kahn J.: Int. J. Radiation Oncology Biol Phys. (1986) 12, 89-93
33. Leeper D.B., Karamuz J.E., Henle K.J.: Proceed. Am. Assoc. Cancer Res. (1977) 18, 139
34. Hahn G.M., Shiu E.C.: Int. J. Radiation Oncology Biol Phys (1985) 11, 159-164
35. Henle K.J., Dethlefsen L.A.: Cancer Res. (1978) 38, 1843-1851

36. Sapareto S.A., Hopwood L.E., Dewey W.C., Mundundi R.R., Gray J.W.: Cancer Res. (1978) 38, 393-400
37. Connor W.G., Gerner E.W., Miller R.C., Boone M.L.M.: Radiology (1977), 123, 497-503
38. Westra A., Dewey W.C.: Int. J. Radiation Biology (1971) 19, 467-477
39. Robinson J.E., Wizenberg M.J., McCready W.A.: Radiology (1974) 113, 195-198
40. Thrall D.E., Gillette E.L., Dewey W.C.: Radiation Res. (1975) 63, 363-377
41. Freeman M.L., Holahan E.V., . . .,Dewey W.C.: Int. J. Radiation Oncology Biol. Phys. (1981) 7, 211-216
42. Sapareto S.A., Raaphorst G.P., Dewey W.C.: Int. J. Radiation Oncology (1979) 5, 343-347
43. Hill S.A., Denekamp J.: British J. Radiology (1979) 52, 209-218
44. Dewey W.C., Westra A., Miller H.H., Nagasawa H.: Int. J. Radiat. Biol. Phys. (1971) 20, 505-520
45. Urano M., Rice L., Maher J., Kahn J.: (Abstr.) Proc. of the 22nd Annual ASTR Meeting
46. Arcangeli G., Barni E., . . ., Tabocchini A.: int. J. Radiation Oncology Biol. Phys. (1980) 6, 143-148
47. Bicher H.I., Sandhu T.S., Hetzel F.W.: Int. J. Radiation Oncology Biol. Phys. (1980) 6, 867-870
48. Hahn G.M.: Cancer Res. (1979) 39, 2264-2268
49. Cetas T.C., Connor W.G.: Medical Phys. (1978) 5(2), 79-91
50. Dike, P.H., Schwan H.P.: Ch. 2 and Ch.3 from Therapeutic Heat, Sidney Light ed., New Haven, Conn. (1958)
51. Togawa T.: Clin. Phys. Physiol. Meas. (1985) 6(2), 83-103
52. Sapozink M.D., Gibbs F.A. Jr., Sandhu T.S.: Int. J. Radiation Oncology Biol. Phys. (1985) 11, 555-560
53. Dewhirst M.W., Sim D.A., Sapareto S., Connor W.G.: Cancer Res. 91984) 44, 43-50
54. Henle K.J., Roti. Roti J.L.: Radiat. Res. (1980) 82, 138-145
55. Sapareto S.A., Dewey W.C.: Int. J. Radiat. Oncology Biol. Phys (1984) 10, 775,786
56. Perez C.A., Sapareto S.A.: Cancer Res. (Suppl.) [1984] 44, 48185-48255

57. Sapareto S.A., Dewey W.C.: Int. J. Radiation Oncology Biol. Phys. (1984) 10, 787-800
58. Iskander M.F.: In Physical Aspects of Hyperthermia (1982) Nussbaum G. ed., AAPM Med. Phys Monog. #8, 151-208
59. Guy A.W., Lehmann J.F., Stonebridge J.B.: Proc. IEEE (1974) G2(1), 55-75
60. Microwaves and Cancer, Hahn G.M. ed., Plenum Press, New York, London, (1982)
61. Johnson C.C., Guy A.W.: Proc. IEEE (1972) 60(6), 692-718
62. Nilsson P.: PhD Thesis (1984) Lund Sweden
63. Therapeutic Heat and Cold (3rd ed), J. Lehmann ed., Wiley and Wiley Pub., Baltimore, London, (1982)
64. Schwan H.P., Piersol G.M.: Amer. J. of Physical Med (1954) 33, 371-404
65. Stuchly M.A., Stuchly S.S.: J. of MW Power (1980) 15(1), 19-26
66. Shepps J.L., Foster K.R.: Phys. Med. Biol (1980) 25(6), 1149-1159
67. Hey-Shipton G.L. Matthews P.A., McStay J.: Phys. Med. Biol (1982) 27(8), 1067-1071
68. Smith, S.R., Foster K.R.: Phys. Med. Biol (1985) 30(9), 965-973
69. Rejou-Michel A., Henry F., deVillardi M., Delmotte M: Phys. Med. Biol (1985) 30(8), 831-837
70. Hyperthermia in Cancer Therapy, Storm, F.K., ed, G.K. Hall Medical Publishers, Bostom, Mass. (1983), 285
71. Steel M.C., Sheppard R.J.: Phys. Med. Biol (1985) 30(7), 621-630
72. Emulsion Science, Sherman P. Ed., New York, Accademic, (1969), Ch. 5
73. Stuchly M.A., Kraszewskit, Stuchly S.S., Smith A.M.: Phys. Med. Biol. (1982) 27(7), 927-936
74. Schwan H.P., Foster, K.R.: Proc. IEEE (1980) 68(1), 104-113
75. Balasubramaniam T.A., Browman H.F.: Trans. of the ASME (1977) Aug., 148-154
76. Bowman H.F.: In Physical Aspects of Hyp. (1982) Nussbaum G. ed., AAPM Med. Phys. Monog. #8, 511-548
77. Song C.W., Rhee J.G., Levitt S.H.: J. Natl. Cancer Inst. (1980) 64(1), 119-124

78. LeVeen H.H., Wapnick S., Piccone V., Falk A.G., Ahmed N.: JAMA (1976) 235, 2198-2200
79. Patterson J., Strang R.: int. J. Radiation Oncology Biol Phys. (1979) 5, 235-241
80. Song C.W.: Cancer Res. (suppl.) (1984) 44, 47215-47305
81. Song C.W.: Natl. Cancer inst. Monog 61 (1982), 169-176
82. Van Der Berg-Block A.E., Reinhold H.S.: Int. J. Radiation Oncology Biol. Phys. (1984) 10, 737-740
83. Mellander S., Johansson B.: Pharmacol. Rev. (1968) 20, 117-196
84. Mantyla M., Kuikka J., Reconen A.: Biol. J. Radial. (1978) 49, 335-338
85. Guy A.W.: IEEE Trans. MTT (1971) 19(2), 204-214
86. Bini M.G., Ignesti A., . . ., Vanni R.: IEEE Trans BME (1984) 31(3), 317-322
87. Lagendijk J.J.W., Nilsson P.: Phys. Med. Biol (1985) 30(7), 709-712
88. Baish J.W., Foster K.R., Ayyaswamy P.S.: Perfused Phantom Models of Microwave Irradiated Tissue (July 1985)
89. Sandhu T.S.: Natl Cancer Inst. Monog. 61 (1980), 513-515
90. Lee D.J., O'Neill M.J., Lam W.C., Lam K.S., Partowmah M.: A Practical Steady State Phantom for the Calibration of Microwave Applicators (paper handout at the AAPM meeting 1984)
91. Dielectric and Electronic Properties of Biological Materials, Pethig R. (1979); J. Wiley and Sons Publishers
92. Emulsion Science, P. Sherman ed. (1969), Academic, New York
93. Handbook of Electrochemical Constants, R. Parsons (1959).
94. Leonard J.B., Foster K.R., Athey T.W.: IEEE Trans BME (1984) 31(7), 533-536
95. Handbook of Chemistry and Physics, CRC, (3rd ed.)
96. Stogryn A.: IEEE Trans. MTT (1971) 19, 733-736
97. Handbook of Mathematical Tables, CRC suppl. to Handbook of Chem and Phys. (2nd ed)
98. Constable R.T., Dunscombe P, Tsoukatos A., Malaker K: Perturbation of the temp. Distribution in MW irradiated tissue due to the presence of metallic thermometers, (submitted to Med. Physics).

99. Waterman F.M.: Med. Physics (1985) 12(3), 368-372
100. Milligan A.J., Parjehpour M.: Int. J. Radiation Oncology Biol. Phys. 91985) 11, 1679-1684
101. Strang, Patterson J.: Int. J. Radiation Oncology Biol. Phys. (1980) 6(6), 729-735
102. Joines W.T. Jirtle R.L., Rafal M.D., Schaefer D.J.: Int. J. Radiation Oncology Biol. Phys (1980) 6, 681-687
103. Schwan H.P.: In Advances in Biological and Medical Physics (1957) V, Academic Press Inc., New York
104. Nitzan M., Anteby S.O., Mahler Y.: Phys. Med. Biol. (1985) 30(6), 557-563
105. Kang M.S., Song C.W., Levitt S.H.: Cancer Res (1980) 40, 1130-1155
106. Jain R.: Annals NYAS (1980) 335, 48-66
107. Milligan A.J., Conran P.B. . . .Dobelbower R.R.: Int. J. Radiation Oncology Biol Phys. (1983) 9, 1335-1343
108. Kim J.H., Hahn E.W.: Cancer Res (1979) 39:2258-2251
109. Sandhu T.S.: Int. J. Radiation Oncology Biol. Phys. (1986) 12, 001-006
110. Vorhees W.D., Babbs C.F.: Proc AAMI 16th Ann. Meeting (1981) Arlington, 105
111. Eberhard R.C., Shitzer A., Hernandez E.J.: Annals NYAS (1980) 336, 107-132
112. Cheung A.Y., Koopman D.W.: IEEE Trans. MTT (1978) 24, 669-673
113. Schwan H.P.: IEEE Trans. MTT (1971) 19(2), 146-152